Novel Adsorbents and Electrocoagulation in Arsenate Removal from Water

by Thi Thuc Quyen Nguyen

Thesis submitted in fulfilment of the requirements for
the degree of Doctor of Philosophy

under the supervision of

Principal supervisor	: **Dr. Tien Vinh Nguyen**
Co-supervisor	: **Prof. Saravanamuthu Vigneswaran**
Co-supervisor	: **Prof. Huu Hao Ngo**

University of Technology Sydney
Faculty of Engineering and Information Technology

January 2021

CERTIFICATE OF ORIGINAL AUTHORSHIP

I, Thi Thuc Quyen Nguyen declare that this thesis is submitted in fulfilment of the requirements for the award of Doctor of Philosophy, in the Faculty of Engineering and Information Technology at the University of Technology Sydney.

This thesis is wholly my own work unless otherwise referenced or acknowledged. In addition, I certify that all information sources and literature used are indicated in the thesis.

This document has not been submitted for qualifications at any other academic institution.

This research is supported by the Australian Government Research Training Program.

Production Note:
Signature removed prior to publication.

Thi Thuc Quyen Nguyen
January 2021

ACKNOWLEDGEMENT

By this thesis, I wish to thank all the people whose assistance was an important milestone in the completion of my study.

I wish to express my sincere appreciation to my principal supervisor, **Dr. Tien Vinh Nguyen**, and co-supervisor, **Professor Saravanamuthu Vigneswaran** who have guided, encouraged, and supported me on the tough road of scientific research. Without their support, sometimes, I think I could not overcome obstacles on this pathway. I also wish to show my gratitude to my co-supervisor, **Professor Huu Hao Ngo** for the invaluable assistance that he provided during my study.

I wish to show my gratitude to **Assoc. Prof. Paripurnanda Loganathan** for his great support and guidance throughout my study, who spent a lot of time on each of my works.

I am indebted to **the manager and staff at Environmental Lab and Tech Lab** for their useful help in carrying out my experiments.

My special thanks approve to **Dr. Leonard Tijing** and **Dr. Gayathri Danasamy**. Their valuable comments and caring were help me improving my study in time.

I would like to thank the Australian Government Department of Foreign Affairs and Trade's (DFAT) innovationXchange (iXc) and Aus4Innovation programs for the financial support for my research.

I wish to acknowledge my family for their substantial financial support during my study, especially **my parents Nguyen Dinh Khanh - Nguyen Thi Be, my husband Cao Anh Tuan, my older sister and brother-in-law Thuc Doan – Tien Dung.** Particularly, I would like to thank my loved husband and my beloved daughter **Khanh An**. Together, we

spent the most difficult and arduous days in this strange land. Without them, I think I could not overcome every challenge from study to daily life.

Finally, I would like to give special thanks to my friends at UTS, especially the Vietnamese friends and Ms. Van Le - School Academic Officer in FEIT. They gave me many unforgettable memories in school time.

With love, I wish that all of you would always be happy and successful in your life.

DEDICATION

This thesis is deeply dedicated to the following people:

To My Lovely Parents ***Nguyen Dinh Khanh - Nguyen Thi Be***

To My Lovely Husband ***Cao Anh Tuan*** *and My Lovely Daughter* ***Cao Khanh An***

To My Brothers, Sister, Brother-In-Law

Hoai Vuong – Tien Dung – Thuc Doan – Hoai Van – Hoai Vu

My Nieces and Nephews

Khanh Vy – Khanh Dang – Khanh Diep

To My Family - In – Law

Parents: ***Tran Anh Dung – Cao Thi Nguyen***

Family of My Sister – In – Law: ***Trong Le – Anh Tu – Nhat Anh***

ACHIEVEMENTS

A. PUBLICATIONS

Nguyen, T.T.Q., Loganathan, P., Nguyen, T.V., Vigneswaran, S. 2020, Removing arsenic from water with an original and modified natural manganese oxide ore: batch kinetic and equilibrium adsorption studies, *Environmental Science and Pollution Research*, vol. 27, no. 5, pp. 5490-502.

Nguyen, T.T.Q., Loganathan, P., Nguyen, T.V., Vigneswaran, S., Ngo, H.H. 2020, Iron and zirconium modified *luffa* fibre as an effective bioadsorbent to remove arsenic from drinking water, *Chemosphere*, p. 127370.

Nguyen, T.T.Q., Loganathan, P., Nguyen, T.V. & Vigneswaran, S. 2020, 'Removing arsenate from water using modified manganese oxide ore: column adsorption and waste management', *Journal of Environmental Chemical Engineering*, p. 104491.

Nguyen, T.T.Q., Loganathan, P., Dinh, B.K., Nguyen, T.V. Vigneswaran, S., Ngo, H.H., 2020, Removing arsenate from water using batch and continuous-flow electrocoagulation with diverse power sources (submitted to *Journal of Environmental Chemical Engineeringl*).

B. CONFERENCES, SHOWCASES, AND SCHOLARSHIPS

N**guyen, T.T.Q.**, Loganathan, P., Nguyen, T.V., Vigneswaran, S., Ngo, H.H., Arsenate removal from water using *luffa* fibre, *'Technology and Innovation Research Showcase'* organised by the Consulate General of the Socialist and Repulic of Vietnam in Sydney - Australia, Science and Technology Representative Office, September 2018.

N**guyen, T.T.Q.**, Loganathan, P., Nguyen, T.V., Vigneswaran, S., Arsenate removal from water using novel adsorbents and electrocoagulation process, The 2020 FEIT 3MT Faculty Heat, video presentation, July 2020.

N**guyen, T.T.Q.**, Loganathan, P., Nguyen, T.V., Vigneswaran, S., Novel green method for arsenate removal for drinking water, UTS Visualise Your Thesis Competition 2020, 60s video presentation, August 2020.

N**guyen, T.T.Q.**, Loganathan, P., Nguyen, T.V., Vigneswaran, S., Ngo, H.H., Arsenate removal from groundwater using dried *luffa* plant coating iron, 9th International Summit on Global Warming and Environmental Science, Stockholm, Sweeden, oral presentation (webinar), 10th - 11th August 2020.

Faculty of Engineering and Information Technology Scholarship (Google DFAT Project)

TABLE OF CONTENTS

LIST OF FIGURE

LIST OF TABLE

NOMENCLATURE/ABBREVIATION

As	Arsenic
As(III)	Arsenite
As(V)	Arsenate
A_T	Temkin isotherm equilibrium binding constant (L/g)
B	Constant related to heat of sorption (J/mol)
BET	Brunauer-Emmett-Teller nitrogen adsorption
BJH	Barrett-Joyner-Halenda method
b_T	Temkin isotherm constant
BV	Bed volume
C_e	Equilibrium concentration of arsenate (V) (mg/L)
$C_{electrode}$	Electrode consumption concentration (mg/L)
C_o	Initial concentration of arsenate (mg/L)
CO_3^{2-}	Bicarbonate
C_t	As(V) concentration in effluent at time t (mg/L)
C_{WHO}	WHO guideline concentration
DC	Direct current
E	Arsenic removal efficiency (%)
EC	electrocoagulation
EDS	Energy-dispersive X-ray spectroscopy
EIL	Ecological investigation level
Fe	Iron
Fe^a-VMO	Iron coating Vietnamese manganese oxide ore

FLF-3	Iron grafting *luffa* fibre
FTIR	Fourier transform infrared
h	hour
H	Bed-height (cm)
HNO_3	Nitric acid
HRT	Hydraulic retention time (min)
I	Current intensity (A)
k_1	Rate constant of pseudo-first order adsorption (L/h)
k_2	Rate constant of pseudo-second order (g/mg.h)
k_f	Freundlich constant related to adsorption capacity (L/g)
k_L	Langmuir isotherm constant (L/mg)
KOH	Potassium hydroxide
k_p	Intra-particle diffusion rate constant (mg/g. $h^{1/2}$)
K_{Th}	Thomas rate constant (L/h/mg)
LEAF	Leaching Environmental Assessment Framework
LF	*Luffa* fibre
m	Mass of adsorbent (g)
m_{Fe}	Mass of Fe generated (mg)
min	minute
Mn	Manganese
n	Heterogeneity factor, dimensionless
$NaNO_3$	Sodium nitrate
NaOH	Sodium hydroxide
PFO	Pseudo-first order

PO_4^{3-}	Phosphate
PSO	pseudo-second order
Q	Flow velocity (L/h)
q_e	Amount of As adsorbed per unit mass of adsorbent (mg/g)
q_{exp}	Experimental As
q_m	maximum amount of the As adsorbed per unit mass of the adsorbent (mg/g)
q_t	Amount of As adsorbed at time t (mg/g)
q_T	Thomas model adsorption capacity (mg/g).
R	Universal gas constant (8.314 J/mol/K)
RCPT	Rapid chloride penetrability test
R_L	Equilibrium parameter
rpm	Revolutions per minute
S/S	Solidification/stabilisation
SEM	Scanning electron microscopy
SiO_3^{2-}	Silicate
SO_4^{2-}	Sulphate
T	Temperature (^{o})
t	Time (h) or (min)
TCLP	Toxicity characteristic leaching procedure
U	Voltage (V)
USEPA	The United States Environmental Protection Agency
V	Volume of solution (L)
VMO	Vietnamese manganese oxide ore
VPV	Volume of permeable voids

WHO	World Health Organisation
XRD	X-ray diffraction
XRF	X-ray fluorescence
ZLF-3	Zirconium grafting *luffa* fibre
ZPC	Zero point of charges
Zr	Zirconium
Zr^a-VMO	Zirconium coating Vietnamese manganese oxide ore
α	Initial adsorption rate (mg/g.min)

ABSTRACT

Arsenic (As) is one of the most dangerous substances and especially when it exists in its inorganic form in water, wastewater, air, and food. Elevated concentrations of inorganic As have been discovered in groundwater sources in many places worldwide, particularly Bangladesh, India, Nepal, Cambodia, Vietnam, and some areas of Australia. In many developing countries, As-contaminated groundwater is used as the primary drinking water source. Its concentration can reach as high as 1,000 μg/L, which is much larger than the WHO recommended standard of 10 μg/L. Inorganic As can lead to a number of diseases such as gastrointestinal symptoms, severe disturbances of the cardiovascular system, central nervous systems, and cancer. In natural aqueous systems, the most toxic species of As are trivalent arsenite (As(III)) and pentavalent arsenate (As(V)). As(III) is more toxic than As(V) and can be oxidized to As(V).

Research on As removal, particularly As(V), began several decades ago, and many treatment technologies have been devised and implemented. However, the high treatment cost and complicated nature of As treatment systems present the main challenges in applying these technologies, especially at a decentralised scale and in rural or isolated areas. Consequently, the main objective of this research is to develop novel and cost-effective methods that can be applied widely to remove As (V), particularly for vulnerable groups of people. Cost-effective adsorption based on novel adsorbents and electrocoagulation with solar energy was the focus of this study. Simplicity and cost-efficiency during design and operation were the main topics analysed here.

In the first part of this research, **two novel adsorbents** were developed and used to adsorb As(V) from water. A low-cost **manganese oxide ore** from Vietnam (VMO) (containing 25.6% Mn and 16.1% Fe mainly in the forms of cryptomelane and goethite

minerals) was firstly evaluated for its performance in As(V) removal from water. VMO was then modified by grafting with iron oxide and zirconium oxide to improve its adsorption capacity. Results show that the Langmuir maximum adsorption capacity of new modified VMO, namely Fe^a-VMO and Zr^a-VMO were 2.19 mg/g and 1.94 mg/g, respectively, nearly 20 times higher than that of the original VMO (0.11 mg/L). These adsorbents were used in a column study to remove As(V) from synthetic contaminated water under various conditions. Column adsorption data fitted well to the Thomas model and the predicted adsorption capacities followed the same order as that observed in the batch experiment for these three adsorbents: Fe^a-VMO > Zr^a-VMO > VMO. At an influent concentration of 0.25 mg As(V)/L, and flow velocity of 0.15 L/h, the Thomas model adsorption capacities of VMO, Fe^a-VMO, and Zr^a-VMO were 0.151, 1.145, and 0.925 mg/g, respectively.

Other novel adsorbents, namely FLF-3 and ZLF-3 have also been produced from a popular agricultural by-product, ***luffa* plant fibre** (LF), by grafting LF with iron oxide and zirconium oxide. This is the first time a *luffa* plant, an agricultural by-product, was used to treat As(V) from water. The Langmuir adsorption capacity of LF, at the influent As(V) concentration of 0.5 mg/L and pH 7, was found to be only 0.035 mg/g. Although the adsorption capacity of LF was poor, it improved remarkably after modification, in fact up to 2.55 mg/g for FLF-3 and 2.89 mg/g for ZLF-3. The adsorption capacities of FLF-3 and ZLF-3 are comparable or higher than those of many other chemically modified bio-adsorbents. In the column study, the experimental data also fitted well to the Thomas model and the As(V) adsorption capacity of ZLF-3 proved to be the highest (2.7 mg/g at initial As(V) concentration of 0.1 mg/L), followed by FLF-3 (1.26 mg/g) and LF (0.06 mg/g).

In the second part of this research, **a novel electrocoagulation** method using different power sources (including new renewable energy - solar panel or rechargeable battery) was applied to remove As(V) in water. This method can be applied to remove As(V) in rural and isolated areas because of its capability of operating without electricity. For an initial As(V) concentration of 0.1 mg/L, an operational time of 5 min, an electrical potential difference of 7.5 V, and electrodes distance of 1 cm were identified as optimal conditions for removing As(V). In the batch study using a 9 V rechargeable battery and 12 V solar panel, the electrocoagulation reactor could remove 93 and 98% of As(V), respectively, from 0.1 mg As(V)/L solution. As(V) concentration in treated water was smaller than that of the WHO drinking water guidelines. In the continuous study, a small, cost-effective system (cost $15AUD) using DC electrical power or a small solar panel of 12V could successfully treat 12L contaminated water per hour (similar flow rate as many commercial household filters). During 4 hours of continuous testing, the As(V) removal efficiency maintained at more than 91% for DC electrical system and 96% for the solar energy system, respectively

Finally, **the third part of this research** focused on **managing the toxic waste** resulting from the adsorption process. Solidification/stabilisation method (for VMO and modified VMOs) and phytoremediation method (by *Pityrogramma calomelanos* (fern plant) for LF and modified LFs) were investigated. The quality tests of concrete used for solidification (compressive strength, rapid chloride penetrability test, and volume of permeable voids) and leaching tests confirm that the concrete produced from the solidification/stabilisation can be safely disposed of or used as a structural construction material for driveways or pavements. To manage the exhausted LF and modified LFs, phytoremediation results show that As(V) could be well transferred from waste

adsorbents to plants and diffused to all parts of the plants. As(V) concentration from the mixing of soil and exhausted LFs reduced significantly from 38.56 mg/kg to 9.92 – 10.20 mg/kg, much lower than the permissible level of the United States Environmental Protection Agency (USEPA) (24 mg/kg) and the ecological investigation level (EIL) limit of As in soil in Australia (20 mg/kg).

In summary, this study successfully developed two novel adsorbents and a novel electrocoagulation process for removing As(V) in water. The new adsorbents and treatment process includes features that favour As(V) removal such as cost-effectiveness, high removal efficiency, environmental friendliness and simple application. The exhausted adsorbents can be safely disposed into the environment once the treatment process is completed. The novel electrocoagulation process using renewable energy is also a promising approach. The most important feature of this approach is its independence from power, which allows its application in the rural and isolated areas with poor infrastructure.

CHAPTER 1

Introduction

Chapter 1. Introduction

1.1 Background of research

Nowadays, more and more people are suffering from the impact of environmental pollution. Regardless of the efforts of many countries, organisations, and communities to relieve the effect of environmental degradation, it remains a serious issue. Besides human activities, some pollution sources come from nature. For arsenic (As), it occurs in water because of both natural geologic processes and anthropogenic activities. In nature, As could be found in minerals and hydrothermal veins (Søgaard, 2014), which upon weathering release As to surface and ground waters and sediments. The popular artificial sources of As pollution are mining, smelting of non-ferrous metals, combustion of fossil fuels, and groundwater exploitation (Søgaard, 2014). As contamination in drinking water is related to many human health problems, primarily causing cancer in the skin, lungs, kidneys, and bladder and elevating the risk of non-cancerous pathologies such as diabetes, skin lesions and metabolic dysregulation (Jochem et al. 2019; Mandal et al. 2016). A recent study by Singh (2017) shows that currently more than 200 million people in the world are exposed to As. Most of them live in rural areas with poor infrastructure conditions and the required resources. Therefore, the demand for an appropriate, simple, and cost-effective As treatment method is extremely important.

Historically, many technologies have been applied to remove As, for instance, oxidisation, precipitation, coagulation, adsorption, ion-exchange, and membrane. Each method has its own advantages and disadvantages. However, not all of them can meet treatment requirements, including treatment efficiency and economic aspects. Adsorption

is a popular method in As treatment at the decentralised scale due to its simple implementation, low-cost, high efficiency, and low waste production. It could be deemed an appropriate technique to remove As in contaminated regions.

A low-cost manganese oxide ore (VMO) derived from the mining process in Vietnam contains mainly Mn and Fe. Hence, it can be used as an adsorbent for removing As(V). It can be modified by grafting with Fe and Zr to improve As adsorption capacity. The exhausted media can be managed by the solidification/stabilisation method so that it is safe to dispose of into the environment.

Another medium is known as porous *luffa* fibre, an agricultural by-product. This material is very environmentally friendly, easy to prepare, locally available, and extremely cheap. The prominent characteristics of *luffa* fibre are that it is very porous and durable in an aqueous environment. To achieve higher adsorption capacity, original *luffa* fibre can also be chemically modified. By grafting with Fe and Zr, the adsorption capacity of this material can improve considerably. The saturated adsorbents from this process can be managed by the phytoremediation method safely.

Besides adsorption, electrocoagulation (EC) recently has emerged as a promising approach to remove As(V) from water. The new EC system can be operated with energy supplied by both an electricity source and a renewable energy source like solar energy. For this reason, it can be applied at a decentralised scale in remote and isolated areas without electricity. The advantages of this method are that it avoids chemical use, minimum solid waste, low-cost while still obtaining high As removal efficiency.

1.2 Objectives and scope

This research aims to investigate and evaluate the arsenate (As(V)) removal efficiency of the adsorption method using two novel types of low-cost absorbents (manganese oxide ore and *luffa* fibre with and without modification) and a new electrocoagulation process (which can be run continuously with renewable energy source) to remove As(V) from water. The treatment targets the treatment of As(V) in the water source to meet the WHO drinking water guidelines.

The specific objectives of this dissertation are:

- Developing the novel adsorbents from manganese oxide ore (Chapter 3) and *luffa* fibre (Chapter 4) by applying appropriate modification methods.
- Investigating and evaluating the adsorption capacity of the original media (including manganese oxide ore and *luffa* fibre) and their modified forms (Chapter 3, Chapter 4).
- Modelling the performance of these adsorbents in batch equilibrium and kinetics adsorption and continuous adsorption studies (Chapter 3, Chapter 4).
- Evaluating the influence of pH, coexisting anions, As(V) initial concentration on the adsorption capacity (Chapter 3, Chapter 4).
- Managing the waste from the adsorption process (Chapter 5).
- Investigating new electrocoagulation using stainless steel electrodes to remove As(V) from water (Chapter 6).
- Replacing an electricity source with solar energy in an electrocoagulation system to evaluate the applicability of this process in remote and isolated areas (Chapter 6).

1.3 Thesis structure

This dissertation includes seven chapters and four appendices. They are briefly described below:

Chapter 1: This introduces the topic and basic information about the research problems and solutions. This chapter includes details about the objectives and scope of the research covered here.

Chapter 2 (*Literature review*): This chapter presents a comprehensive review on As pollution problems, including: (i) source and distribution of As compounds, (ii) As species and behaviour in the aqueous environment, (iii) effect on human health, (iv) limitation of As in drinking water, (v) As removal technologies, (vi) an overview of the adsorption method, (vii) an overview of the electrocoagulation method, and (viii) As-contained waste management.

Chapter 3: Investigated and evaluated here are the As(V) adsorption ability of original and modified manganese oxide ore in batch and column studies. The effect of influential factors such as pH, coexisting anions, As(V), and initial concentration on the adsorption performance together with a series of models, are discussed in detail.

Chapter 4: This chapter describes the As(V) treatment utilising the adsorption method with raw and modified *luffa* fibre forms. The experimental data from both batch and fluidised-bed adsorption studies are discussed in detail.

Chapter 5: Two methods of solid waste management, namely solidification/stabilisation (for modified and unmodified manganese oxide ore) and phytoremediation (for grafted and ungrated *luffa* fibre) are described in this chapter. In

this chapter, relevant experiments and analyses are carried out to evaluate the safety of waste disposal.

Chapter 6: This chapter presents a new electrocoagulation process's efficiency in removing As(V) using both electrical source and solar energy in batch and continuous studies. The applicability of the new electrocoagulation system at the decentralised scale, including cost calculation, is discussed.

Chapter 7: The last chapter of this study summarises the key findings and provides recommendations for future analyses to explore.

CHAPTER 2

Literature review

Chapter 2. Literature review

2.1 Source and occurrence of As compounds

Arsenic (As) is the 33rd chemical element in Mendeleev's periodic table. It is a metalloid but is usually classified as heavy metal (Järup 2003). It is one of the world's most toxic elements and causes many cancerous and non-cancerous diseases. The United States Environmental Protection Agency (US EPA) has categorised As as a group A carcinogen (Singh 2017). In regard to its abundance, As is the 52nd most common element in the earth's crust, 20th in nature, 14th in seawater and 12th in the human body (Gupta & Chatterjee 2017). In nature, As exists within more than 300 minerals and its approximate concentration on the earth is 5 mg/L (Nazari et al. 2017). The most common As-contained minerals are arsenopyrite (FeAsS), niccolite (NiAs), realgar (AsS/As_4S_4), orpiment (As_2S_3), cobaltite (CoAsS), and the secondary minerals formed by oxidation of these minerals (Sogaard 2014).

Historically, As was discovered in the fourth century BC by the Greek philosopher Aristotle (Gupta & Chatterjee 2017). The first study on As contamination was reported in Germany in 1885. In 1983, the first study in As-contaminated groundwater was carried out in four As-affected districts in West Bengal, India. In 2008, the As-affected districts in this area increased to nine, which indicated the mobility of As in water (Gupta & Chatterjee 2017).

As can be derived from both natural and anthropogenic sources (Fig. 2.1). As from geological origin can be released into groundwater, surface water, and sediments through weathering the As-contained minerals and hydrothermal veins (Sogaard 2014). In

particular, As in groundwater was mostly generated as a result of the resilient effect of water-rock interfaces. The As natural geological origin was found to be connected in a complex manner with groundwater flow regime and aquifer geometry (Gupta & Chatterjee 2017). The physical and geochemical conditions of the aquifer also affect the mobilisation, concentration, and accumulation of As in groundwater. Anthropogenic sources of As appeared decades ago, mainly in the groundwater exploitation, agricultural and industrial processes. These processes include mining, smelting, producing and using biocides, pesticides, fertilisers and wood preservatives, fossil fuel combustion, municipal wastes, military activities, medicinal uses, waste treatment, etc. (Gupta & Chatterjee 2017; Sogaard 2014). In the past, As was even utilised to improve the complexion of women and for feeding horses (Singh & Stern 2017). From the late 1990s, farmers in many countries used some As-contained products for crops as a pest control method, including monosodium methane arsenate, disodium methane arsenate, cacodylic acid. As a result, the concentration of As in this raw food increased, leading to an uptake of As in plants, animals and humans (Gupta & Chatterjee 2017). In Australia, a number of workers suffered chronic As poisoning before 1970 due to the indiscriminate use of As-contained pesticides (Gupta & Chatterjee 2017).

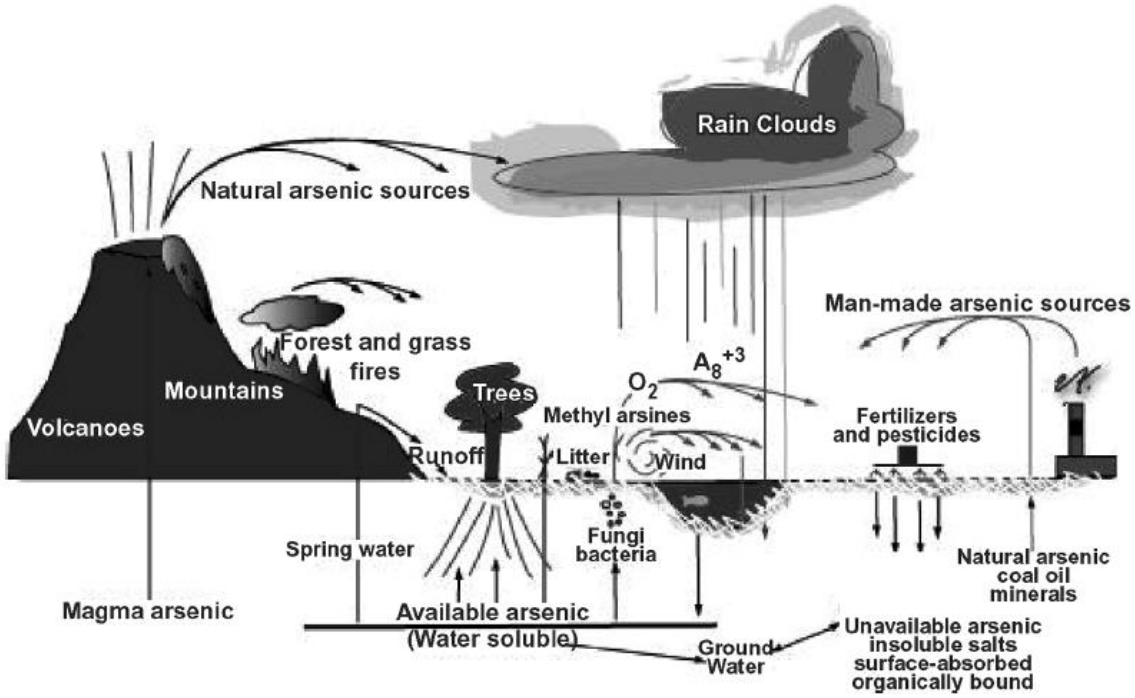

Fig. 2.1. Natural cycling of As (Jones 2007)

Many places around the world are reported to be harmfully affected by As contaminated groundwater. In 2008, Amini et al. (2008) modelled the global probability of geogenic As contamination in groundwater (Figure 2.2). The maps illustrate the distribution of As under two conditions: (a) highly reducing aquifers where As predominantly presented in its reduced state, and (b) high-pH aquifers where As is relatively soluble in its oxidised state. The concentration of As in both cases was measured to be as high as 5,000 µg/L. It also introduces that the most As-contaminated regions are Bangladesh, Cambodia, Vietnam, Taiwan, India, China, Mexico, Chile and southwest America (Amini et al. 2008). Therein, the As pollution statement in Asia, particularly Bangladesh, is worse than other regions of the world with more than 120 million people exposed to As, followed by America and Africa with 48 million and 24 million people, respectively (Singh & Stern 2017).

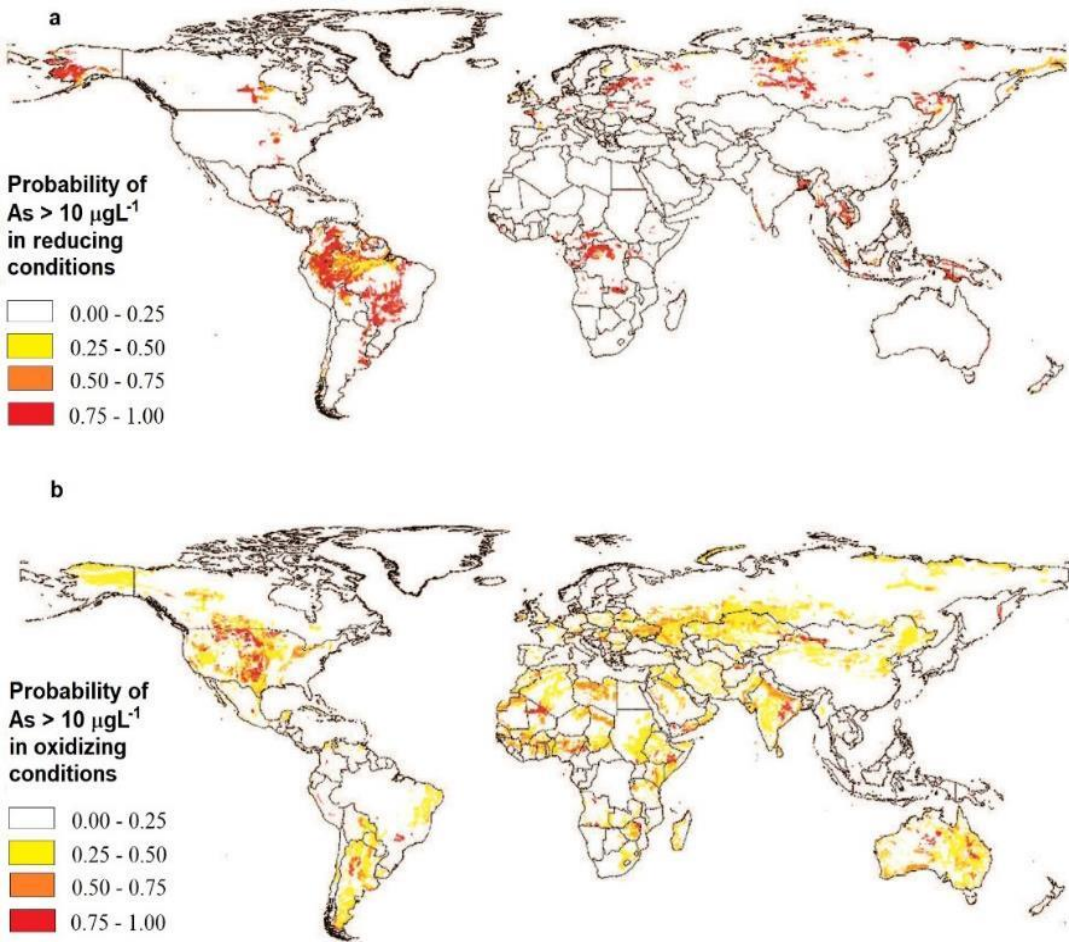

Fig. 2.2. Modelled global probability of geogenic arsenic contamination in groundwater (Amini et al. 2008)

2.2 As species and behavior

As is present in both organic and inorganic forms in the water environment. The occurrence of As species depends on the pH and potential condition of water (Thirunavukkarasu et al. 2002). In nature, the most common inorganic As compounds are arsenite (As(III)) and arsenate (As(V)), while the popular organic As species are monomethylarsonate (MMA) and dimethylarsinate (DMA). Their toxicity order is as

follows: As(III) > As(V) > MMA > DMA. Due to the high toxicity of inorganic As, most of the studies conducted on As removal usually focuses on this species.

Generally, As(III) and As(V) exist in two opposite redox conditions (Fig. 2.3). As(III) exists under a reductive environment with the non-ionised form (H_3AsO_3) at pH < 9 while the ionised form ($HAsO_3^{2-}$) appears at pH > 9. As(V) mainly occurs in oxidising conditions with the ionised form ($H_2AsO_4^-$, $HAsO_4^{2-}$, AsO_4^{3-}) at most values of pH (pH 2 – 14) (Nguyen et al. 2020b, Sogaard 2014). Another basic difference between them is their solubility. The solubility of As(V) is 66 g/100 mL water, much higher than that of As(III), which is only 10.1 g/100 mL (Sogaard 2014).

In groundwater, the inorganic As species varies at different regions. The ratio of As(V) and As(III) also changes frequently due to many factors, such as the variations in the availability of redox active solids, the activity of microorganisms, and the extent of convection and diffusion of oxygen from the atmosphere. Based on global As measurement of about twenty thousand samples, Amini et al. (2008) reported that 77% of As variation in reducing areas and 68% of As variation in oxidising areas. In some well-known As-contaminated regions, such as Bangladesh, Vietnam, and Taiwan (where 35.4, 15.8 and 8.2% areas are contaminated with As at concentration of above 0.75 µg/L, respectively), the predominant As species in groundwater is As(III) (Amini et al. 2008; Guo et al. 2014; Jiang et al. 2013; Postma et al. 2007). In the United States, which 8.2% area having As contaminated in groundwater, a national research program stated that 48% of well water across the country had As(V), 44% had As(III) and 8% had both species (Sorg, Chen & Wang 2014).

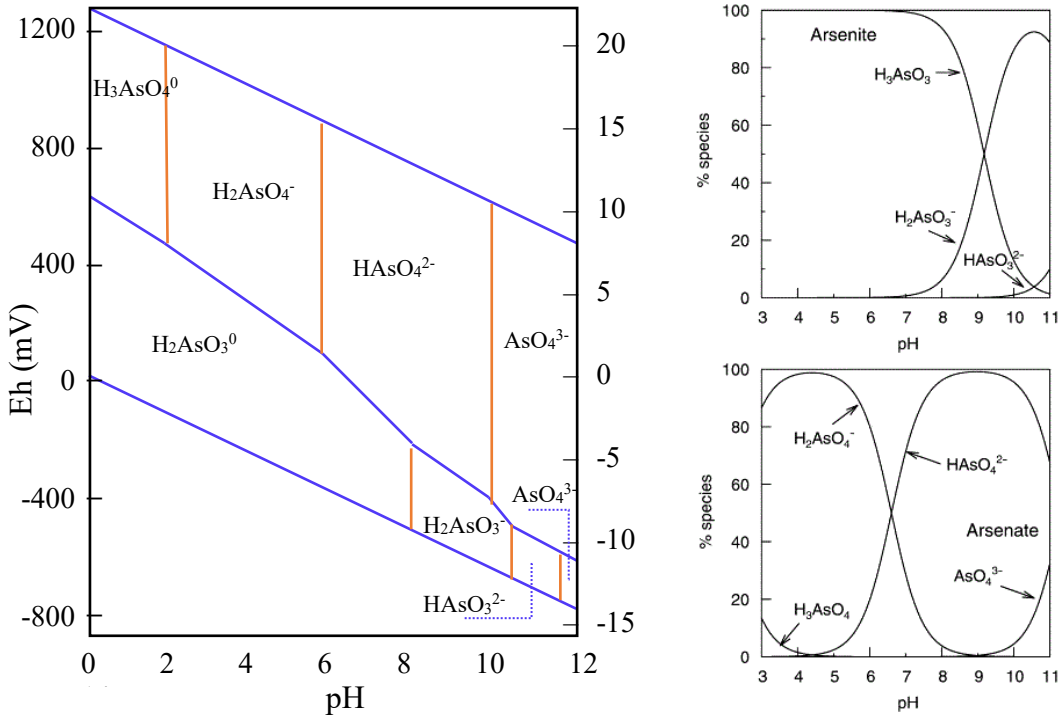

(a) (b)

Fig. 2.3. (a) Eh-pH diagram for As species in water at 25 °C and 1 bar and (b) As(III) and As(V) speciation as a function of pH (ionic strength 0.01 M) (Smedley & Kinniburgh 2002b).

2.3 Effect on human health

As was named “the king of poisons” (Gupta & Chatterjee 2017). It can cause poisoning to humans by a natural pathway, or it can be used as a poison in high doses. Two of the most famous As poison events were of two contemporaries - Napoleon Bonaparte, the Emperor of France, and King George III of the United Kingdom. After their deaths, elevated concentrations of As were found in strands of their hair (Sogaard 2014).

Naturally, humans are affected by As mainly through As-contaminated drinking water and these health effects are called arsenicosis. According to Singh (2017), approximately 202 million people in 100 countries have been affected by drinking As polluted water. Due to its high toxicity even at low concentrations, As contamination in drinking water becomes a global health concern (Sogaard 2014). The evaluation conducted by WHO states that As poisoning through drinking water can cause lungs, kidneys, bladder, and skin cancer at an As concentrations of about 0.1 mg/L (WHO 2001). Scientists have demonstrated that large quantities of inorganic As come into human body can lead to gastrointestinal symptoms, severe disturbances of the cardiovascular and central nervous systems, and eventually death (Järup 2003). Bone marrow depression, hemolysis, hepatomegaly, melanosis, polyneuropathy, and encephalopathy can be observed in others. There are many neurological complications when people are exposed to As also to be confirmed (impaired memory, poor concentration, Parkinson's disease, Guillain-Barre-like neuropathy, verbal comprehension, encephalopathy, and peripheral neuropathy) (Brinkel, Khan & Kraemer 2009; Yadav et al. 2010). Sogaard (2014) presented data on As accumulation in the human body in his research. This research shows that after entering the human body, As mostly accumulates in nails (1.30 – 52.03 mg/kg) and hairs (0.1 – 83.4 mg/kg). A smaller amount of As can be found in urine (0.025 – 9.420 mg/L).

2.4 Limit of As in drinking water

As a critically dangerous element even at a very low concentration, As limitation in drinking water is rigorous. The As standard does vary between countries throughout the world. Generally, As limitation in drinking water in the developed countries is

relatively lower than that of the developing countries (Table 2.1) (Sogaard 2014). The first guideline of As set by WHO in 1958 was 200 µg/L. However, they then realised that this value was not suitable because of emerging evidence of chronic As toxicity (Fisher et al. 2017). They reduced this limitation twice, down to 50 µg/L in 1963 and to 10 µg/L, the current guideline since 1993 (Fisher et al. 2017). Most countries adjusted their As standard to be similar to the WHO guidelines. Denmark even set the maximum contaminant level of As in drinking water to 5 µg/L. However, some countries such as Bangladesh, Mexico, India, Brazil, and Chile have delayed this adaptation. Their national As standard remains in the 25 – 50 µg/L range (Sogaard 2014).

Table 2.1. As concentration in various countries' regions with their As limitation in drinking water (Siddique et al. 2020)

Country	Tested region	As concentration (µg/L)	Permissible limit (µg/L)
Afghanistan	Ghazni	10 – 500	10
Bangladesh	Noakhali	<1 – 4730	50
Brazil	Minas Gerais	0.4 – 350	10
Cambodia	Prey Veng, Kandal-Mekong delta	1610	10
Canada	Nova Scotia (Halifax county)	1.5 – 4440	10
China	-	17 – 4440	50
Finland	Southwest Finland	17 – 980	10
India	West Bengal, Uttar Pradesh	10 – 3200	50
Japan	Fukuoka Prefecture	1 – 293	10
Mexico	Lagunera	8 – 620	25
Nepal	Rupandehi	2620	50
Pakistan	Muza_argarh	906	50
Taiwan	-	10 – 1820	10
Thailand	Ron Phibun	1 – 5000	10
USA	Tulare Lake	2600	10
Vietnam	Red River Delta, Mekong Delta	<1 – 3050	10

2.5 As removal technologies

Due to its toxicity, As removal from contaminated water is always an essential issue. However, As and their compounds cannot be destroyed. They can only change their forms and phases, making them able to be attached or separated from particles or decrease their solubility in water (Pichhode & Gaherwal 2019). As can be removed from water using many technologies. To date, oxidation, coagulation/precipitation, adsorption, ion exchange, and membrane technologies are recognised as the most effective and popular As removal methods (Sogaard 2014). Many approaches have been studied in order to improve the efficiency in removing As. The selection and implementation of As removal technology is based on many aspects such as water characteristics, treatment capacity, treatment cost, and operational and maintained requirements.

2.5.1 Oxidation

Oxidation is a simple As treatment process. It results in the transformation of As species, from As (III) to As (V). However, this process alone cannot effectively remove As. It usually is combined with other methods like adsorption, ion exchange, and coagulation (Nicomel et al. 2016). Therefore, oxidation is normally used as a pre-treatment step in an As treatment system. Natural and chemical oxidation agents are often utilised, such as ozone, free chlorine, hypochlorite, permanganate, hydrogen peroxide, and fulton's reagent, etc. As oxidation reactions with various agents are displayed in reactions [2.1 – 2.8] (Sharma et al. 2007).

$$H_3AsO_3 + HOCl \rightarrow AsO_4^{3-} + Cl^- + 4H^+ \quad [2.1]$$

$$H_3AsO_3 + 2ClO_2 \rightarrow AsO_4^{3-} + 2ClO_2^- + 5H^+ \quad [2.2]$$

$$5H_3AsO_3 + 2ClO_2 + H_2O \rightarrow 5AsO_4^{3-} + 2Cl^- + 17H^+ \quad [2.3]$$

$$H_3AsO_3 + NH_2Cl + H_2O \rightarrow AsO_4^{3-} + NH_4^+ + Cl^- + 3H^+ \quad [2.4]$$

$$H_3AsO_3 + H_2O_2 \rightarrow As_4^{3-} + H_2O + 3H^+ \quad [2.5]$$

$$H_3AsO_3 + O_3 \rightarrow AsO_4^{3-} + O_2 + 3H^+ \quad [2.6]$$

$$2H_3AsO_3 + 2MnO_4^- \rightarrow 3AsO_4^{3-} + 2MnO_2 + 7H^+ + H_2O \quad [2.7]$$

$$H_3AsO_3 + FeO_4^{2-} + H_2O \rightarrow 3AsO_4^{3-} + 2Fe(OH)_3 + 5H^+ \quad [2.8]$$

In many developing countries, the natural oxidation process is widely applied to remove As partly. The practical application of natural oxidation includes passive sedimentation, in-situ oxidation, and solar oxidation. A case study in Bangladesh shows that the method's As removal efficiency was below 50% and As concentration in treated water did not meet the As limitation in drinking water (Ahmed 2001). Here, As was mostly removed by the oxidation of dissolved oxygen and ferrous iron in water. The application of chemical oxidation agents usually generates better oxidation efficiency compared to natural oxidation. In recent research, more than 93% of As(III) was oxidised to As(V) by δ-MnO_2 modified activated carbon, resulting in more than 90% of As removed by subsequent adsorption process (Wang et al. 2020). In electrocoagulation, the oxidation process plays an important role in oxidising As(III) to As(V) and releasing/oxidising metal ions at the anode determined the efficiency of As treatment (Kobya et al. 2020).

In some research, some bacterium species, such as *Bacillus arsenoxydans, Pseudomomas arsenoxydans, Xanthomonas arsenoxydans, Achromobacter rsenoxydans, Alcaligenes faecalis,* etc., were able to oxidise As (III) to As (V) (Sogaard 2014). The reaction is presented in reaction 2.9:

$$H_3AsO_3 + \frac{1}{2}O_2 \xrightarrow{Bacteria} H_3AsO_4 \qquad [2.9]$$

For drinking water treatment, only some bacteria are suitable when considering the impact on human health. The main factors that dominate the benefit of bacteria for the water treatment process are nutrient supply and autotrophic ability, oxidised ability, temperature and As concentration (Sogaard 2014).

2.5.2 Coagulation/Co-precipitation

The traditional coagulation process is chemical coagulation, which uses chemicals as coagulants. The popular coagulants such as aluminium sulphate $Al_2(SO_4)_3$, ferric chloride $FeCl_3$, and ferric sulphate $Fe_2(SO_4)_3$ are effective in removing As from water (Sogaard 2014). In the chemical coagulation process, the coagulant is added to water and it quickly forms aluminium or ferric hydroxide micro-flocs. These micro-flocs then agglomerate to form larger flocs that are settable. During this flocculation process, the negatively charged As ions are attached to the flocs by electrostatic attachment and settle with the flocs, which are then separated from the water by filtration or settlement (Nidheesh & Singh 2017). Although this method has been evaluated as one of the most effective As removal strategies, it still has some drawbacks such as requiring a lot of chemicals and high treatment cost, producing a large amount of As-contaminated sludge.

Table 2.2 presents the As removal efficiency of different coagulants. Results from previous studies show that treatment efficiency of As(III) was generally lower and less dependent on solution pH than that of As(V).

Table 2.2. The As removal efficiency of several coagulants

Coagulant	Coagulant dosage (mg/L)	pH	Type of water	As concen-tration (µg/L)	As removal efficiency		Reference
					As(III)	As(V)	
Ferric nitrate	6	8.2	Agriculture wastewater	73.9	80 (As total)		Qiu et al. (2019)
Ferric chloride	40	7.0	Municipal wastewater	8.6	-	78	Ge et al. (2020)
Aluminium chloride	40	7.0	Municipal wastewater	8.6	-	84	Ge et al. (2020)
Ferric chloride	15	7.0 – 8.0	Synthetic groundwater	300	51	60	Jahin et al. (2017)
Aluminium chloride	20	6.5 – 7.5	Synthetic groundwater	300	43	56	Jahin et al. (2017)

Recently, electrocoagulation (EC) has emerged as a promising technology to remove As from water. It can eliminate some disadvantages of other traditional water treatment techniques, particularly chemical coagulation (Kalaruban et al. 2017). Some advantages of EC are that it only requires simple equipment, is easy to operate, reduces chemical use, and produces less sludge. However, this method strongly depends on the operational conditions such as the type of electrodes and electrical source, which can be expensive or unavailable in some rural areas. The removal efficiency of the EC technique

can range from 75 to 99% when iron, aluminium, copper, titanium, and zinc served as the electrodes (Nidheesh & Singh 2017).

2.5.3 Adsorption technique

Amongst a large number of water treatment technologies for As removal, adsorption is considered to be the best technology for the decentralised context because of its high removal efficiency, low-cost features, and simple implementation and operation (Fu & Wang 2011; Jiuhui 2008; Mohan & Pittman Jr 2007). The selection of an appropriate adsorbent and its adsorption capacity depends on the As concentrations, the existing co-ions, pH, etc. For example, activated alumina is often efficient at pH values around 6, lower than the ones encountered in natural groundwater (Lescano et al. 2015). Many natural and synthetic media have been examined for As removal from the water, such as activated alumina, activated carbon, iron, manganese coated sand, kaolinite clay, hydrated ferric oxide, activated bauxite, titanium oxide, silicium oxide (Nicomel et al. 2016). Mohan & Pittman Jr (2007) comprehensively reviewed the properties and adsorption capacity of many absorbents. In general, some low-cost adsorbents originated from agricultural by-products or industrial wastes such as treated slags, char carbons, coconut husk carbons, goethite, and commercial adsorbents such as activated carbon (AC), granular ferric hydroxide have high As adsorption capacities. In addition, some adsorbents have been pre-treated or modified to improve the adsorption capacity (Mohan & Pittman Jr 2007). For example, in the case of AC, the As(V) adsorption capacity of AC after modification by zirconium and iron were 73 - 78 times higher than that of original AC (Darco 12 × 20 carbon), respectively. In their study, Nicomel et al. (2016) recommended that most conventional adsorbents have irregular pore structures and low

specific surface areas, leading to low adsorption capacities. Therefore, in many cases, pre-treatment and modification of adsorbents for improving the surface areas and pore structures are the key factors to improve the As adsorption capacity of adsorbents.

2.5.4 Ion exchange

The As removal mechanism of ion exchange is similar to that of the adsorption process, but ion exchange resin – a synthetic product is utilised instead of an adsorbent. The ion exchange capacity (meq/mL) depends on the number of exchange sites and the competition of anions. Here, some anions in the water source can compete with As ions to occupy the exchange sites, leading to a reduction in ion exchange capacity. The general ion-exchange process with As(V) is described in the followed reactions (Mohanty 2017):

As exchange: $2R - Cl + HAsO_4^{2-} \rightarrow R_2HASO_4 + 2Cl^-$ [2.10]

Regeneration: $R_2HAsO_4 + 2Na^+ + 2Cl^- \rightarrow 2R - Cl + HAsO_4^{2-} + 2Na^+$ [2.11]

where R is the polymetric unit of ion-exchange resin.

There are four types of resins, strong acid (e.g. sulphonate, $-SO_3^-$), weak acid (e.g. carboxylate, -COO-), strong base (e.g. quaternary amine, $-N^+(CH_3)_3$), and weak base (e.g. tertiary amine, $-N(CH_3)_2$). Within these types, the strong base resin is usually used to treat As(V). However, As(III) almost cannot be eliminated by this method and must be oxidised to As(V) in the pre-treatment step. Chloride ions are reported to be one of the most effective anions present in ion exchange resins that can exchange with As(V), along with bromide and acetate ions. Some strong base anion-exchange resins like Purolite A-505 and Relite-A-490 were able to remove 99% of As(V) from drinking water (Mohanty 2017).

2.5.5 Membrane techniques

Membrane filtration is one of the advanced technologies in water treatment. The pore structure of the membrane acts as a selective barrier that does not allow some constituents of the water to pass through. The advantages of membrane technology are its simplicity and versatility, no chemical addition, high efficiency, and commercial availability. However, the prominent disadvantages of the membrane include its high-cost, high-energy consumption and membrane fouling. In addition, its requirement for input water is free from suspended solids and oxidising agents because they can block or damage the membrane (Criscuoli & Figoli 2019). Due to these disadvantages, membrane technology is only applied as one of the last steps in the water treatment system.

The most popular membrane filtrations are microfiltration (MF), ultrafiltration (UF), nanofiltration (NF) and reverse osmosis (RO). Due to the larger size of the membrane pore (> 2 nm), MF and UF are not effective in removing As alone. They are usually combined with other processes. For example, coagulation using ferric salts as coagulants was applied before MF. The coagulation increases the particle size of As-bearing species, leading to an increase in As removal efficiency by MF (Han et al. 2002). However, the efficiency of this method was affected by pH and the occurrence of other ions in water.

In comparison with MF and UF, both NF and RO are more effective at removing As from water because of their very small pore size (< 2nm). NF90-4040, a commercial NF was found able to remove 94% and 90% of As(V) and As(III) from drinking water, respectively (Harfoush et al. 2018). The commercial RO product, namely XLE, BW30 could remove more than 97% of both As(III) and As(V) from drinking water (Elcik et al. 2016). However, as presented before, the cost of the commercial membrane is still quite

high, makes it become a high-cost method, and is not appropriate to rural areas in developing countries.

Generally, the cost of As treatment method is very difficult to identify precisely. There were no much studies reported the treatment cost. The relevant cos of only some As treatment systems used the commercial products such as ion exchange, membrane, could be estimated appropriately. Other processes, for example, adsorption using waste materials/by-products from the industry or agriculture as adsorbents, or EC using waste metals as the electrodes, were seldom calculated in the literature (Mohan & Pittman Jr 2007). The cost of each applied water treatment system depends on many factors, such as local availability, operation conditions, initial As concentration. Therefore, the cost evaluation of each process employed in this study is estimated in details basing on these aspects. Then, these costs are compared with the literature to evaluate the feasibility.

In summary, a comparison among current As removal technologies is presented in Table 2.3. It shows different aspects of As removal technologies, including efficiency, economy, and applicability. Basing on the demand of As contaminated regions, especially in the rural and isolated areas in developing countries, the simple, low-cost and high-efficiency technologies are generally the priority choice. Adsorption is one of the most appropriate methods would be selected. With most of the prominent features as introduced before, developing new cost effective adsorbents of good performance is necessary. Besides that, electrocoagulation also emerges as a new technology of many good features. In order to reduce the disadvantages of this technology, focusing on reducing the power dependence and optimising the operation conditions are the essential requirement. In addition, due to the unequal distribution of residents in the As-contaminated areas, particularly in rural and isolated areas, development of suitable

decentralised water treatment systems is a priority option. Adsorption and electrocoagulation in the decentralised scale are focused of this study.

Table 2.3. A comparison among several common As removal technologies (adapted from Sogaard (2014) and Mohanty (2017))

Technology	Advantages (+)/ Disadvantages (-)	Removal efficiency	
		As(III)	As(V)
Oxidation	(+) Relatively simple, low-cost; Oxidizes other impurities and kills microbes (-) Slow process; Cannot alone remove As, must be coupled with other processes.	+++	++
Coagulation	(+) Effective over a wider range of pH; Common chemicals are commercially available (-) Produces toxic sludge; Pre-oxidation, readjustment of pH, and additional filtration required	+	+++
Electro-coagulation	(+) Less space requirement; Sustainable technology (-) Sludge production; Electrode replacement required; High energy consumption	++	+++
Adsorption	(+) Low cost; Ease of operation; Adsorbent can be regenerated (-) pH, surface area, and the nature of the adsorbent: need to be maintained; adsorbent replacement required	++	+++
Ion exchange	(+) Well-defined medium and capacity; Less dependent on pH of water; Exclusive ion-specific resin to remove As (-) High-cost medium; Regeneration creates a sludge disposal problem	+	+++
Membrane	(+) Well defined and high removal efficiency; No toxic solid wastes is produced (-) High capital cost; Pre-treatment; High water rejection;	+	+++

+ very low efficiency, ++ average efficiency, +++ very high efficiency

2.6 Overview of adsorption technology

2.6.1 Basic concepts and definitions

Adsorption is a phase transfer process that transfers chemical species from liquid or gas phases onto the surface of a solid. In water treatment, molecules or ions of contaminants in the aqueous solution are removed by adsorption onto solid surfaces (Worch 2012).

According to adsorption theory, the solid material that provides the surface for adsorption is called an adsorbent. The contaminant that will be adsorbed is referred to as adsorbate. The reverse process of adsorption, which changes the properties of the liquid phase and releases the adsorbed species, is known as desorption (Fig. 2.4) (Worch 2012). The major mechanisms in the adsorption process are Van der Waals force, ion exchange, hydrogen bonding, ligand exchange, surface precipitation, and diffusion (Kalaruban 2017).

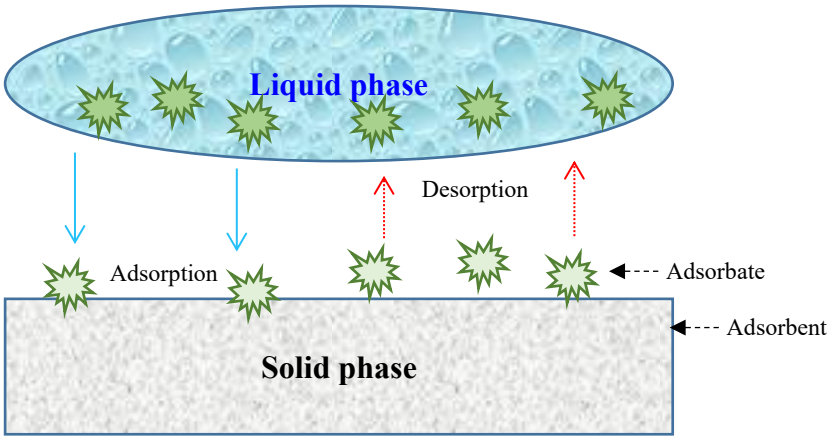

Fig. 2.4. The terms used in the adsorption process (adapted from Worch (2012))

Since adsorption is a surface process, the adsorbate uptake by the adsorbent surface should be expressed by surface concentration. However, because determining the surface area of adsorbent is more difficult than that of adsorbent mass, in practice, the mass-related adsorbed amount, q (mg/g), is typically used instead of the surface concentration and is calculated by the following equation:

$$q = \frac{n_a}{m_A} \qquad [2.12]$$

where n_a is adsorbed amount (mg), and m_A is the adsorbent mass (g).

Given the practical application of adsorption, three crucial factors that must be investigated in order to identify the dependencies of the adsorbed amount on the characteristic process parameters are the adsorption equilibrium, adsorption kinetics, and adsorption dynamics (Fig. 2.5) (Worch 2012). The adsorption equilibrium describes the dependence of the adsorbed amount on the adsorbate concentration (c) and temperature (T), which is usually considered constant, so q =f(c). The adsorption kinetics describe the time dependence of the adsorption process, q =f(t) and c =f(t). The adsorption dynamics or column dynamics depict the dependence of the adsorption process on time (t) and space (z), q =f(t,z) and c =f(t,z).

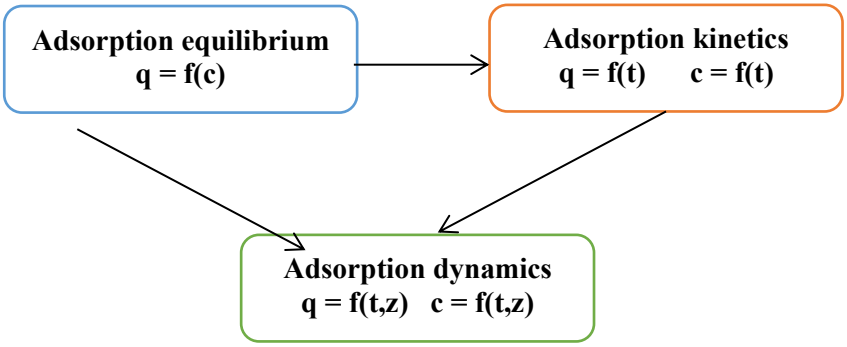

Fig. 2.5. Key aspects of adsorption theory (Worch 2012)

2.6.2 Adsorption modelling

a. Equilibrium adsorption models

Several models are used to describe the equilibrium adsorption in water treatment. Langmuir and Freundlich isotherm are the two most popular models. The Langmuir model is developed with the assumption that one molecule is adsorbed at each adsorbent's surface site, and the modules do not interact with each other. In other words, it is described as monolayer adsorption at specific homogenous sites. In contrast, the Freundlich model is described as the adsorption characteristics for the heterogeneous surface with multilayer adsorption. The Temkin model is another empirical model used to describe the equilibrium adsorption data. It assumes that the heat of adsorption of all molecules in the adsorbent layer will decrease linearly rather than in a logarithmic pattern with coverage (Ayawei et al. 2017). The equilibrium adsorption models are displayed in Table 2.4.

Table 2.4. The equilibrium adsorption models (Ayawei, 2017)

Model	Equation	Parameter
Langmuir	$q_e = \frac{q_m . k_L . C_e}{(1 + k_L . C_e)}$ $R_L = \frac{1}{1 + (1 + k_L . C_0)}$	▪ q_e : the amount of adsorbate adsorbed per unit mass of adsorbent (mg/g) ▪ q_m : the maximum amount of adsorbate adsorbed per unit mass of the adsorbent (mg/g) ▪ C_e : concentration of adsorbate at equilibrium (mg/L) ▪ C_o : initial concentration of adsorbate (mg/L) ▪ k_L : Langmuir isotherm constant (L/mg) ▪ R_L : Equilibrium parameter
Freundlich	$q_e = k_f . C_e^{1/n}$	▪ k_f : Freundlich constant related to adsorption capacity (L/g) ▪ n : heterogeneity factor, dimensionless
Temkin	$q_e = \frac{RT}{b_T} . \ln (A_T . C_e)$ $B = \frac{RT}{b_T}$	▪ A_T : Temkin isotherm equilibrium binding constant (L/g) ▪ b_T : Temkin isotherm constant, dimensionless ▪ R: universal gas constant (8.314 J/mol/K) ▪ T: room temperature at 298 ^oK ▪ B : constant related to heat of sorption (J/mol)

b. Kinetic adsorption models

Popular models commonly used to describe kinetic adsorption include pseudo-first order (PFO), pseudo-second order (PSO), Weber and Morris, and Elovich models. The PFO model is often used to describe the kinetic process under un-equilibrium conditions (Guo & Wang 2019), while it has been demonstrated PSO is suitable for the adsorption of lower molecular-weight adsorbates on smaller adsorbent particles (Wu et al. 2009).

The Elovich model assumes that the nature of active sites of the sorbent is heterogeneous and leading to a difference in activation energies for chemisorption. The Weber and Morris model is used to investigate the rate of diffusion of the adsorbate into the adsorbent through these pores/channels (Kalaruban et al. 2019). The equations of these kinetic adsorption models are shown in Table 2.5.

Table 2.5. The kinetic adsorption models (Kalaruban et al. 2019)

Model	Equation	Parameter
PFO	$\frac{dq_t}{dt} = k_1(q_e - q_t)$	▪ q_e : the amount of adsorbate adsorbed at equilibrium (mg/g) ▪ q_t : the amount of adsorbate adsorbed at time t (mg/g) ▪ k_1 : the rate constant of the PFO model (1/h) ▪ t : adsorption time (h)
PSO	$\frac{dq_t}{dt} = k_2(q_e - q_t)^2$	▪ k_2 : the rate constant of the PSO model (g/mg.h)
Elovich	$\frac{dq_t}{dt} = \alpha e^{-\beta q_t}$	▪ α : the initial adsorption rate (mg/g.min) ▪ β : the desorption constant, related to the affinity of adsorbate to adsorbent (g/mg)
Weber and Morris	$q_t = k_p\sqrt{t} + B$	▪ k_p : intra-particle diffusion rate constant (mg/g. $h^{1/2}$) ▪ B : a constant which provides a measure of the boundary layer thickness (mg/g)

c. Column adsorption models

In the column study, the Thomas model is most popular model for analysing the adsorption capacity in column adsorption experiments and predicting the breakthrough curve. The Thomas model is theoretically suitable for the adsorption process where the external and internal diffusion limitations are absent (Aksu & Gönen 2004; Padmesh et al. 2005). The equation of this model is described in the below table.

Table 2.6. The column adsorption models (Hammud et al. 2014)

Model	Equation	Parameter
Thomas	$\frac{C_t}{C_o} = \frac{1}{1 + \exp\left(\frac{K_{Th} q_T m}{Q} - K_{Th} C_o t\right)}$	▪ C_o : initial concentration of adsorbate (mg/L) ▪ C_t : concentration of adsorbate at time t (mg/L) ▪ t : flow time (h) ▪ k_{Th} : Thomas rate constant [L/(h.mg)] ▪ m : the amount of adsorbent in the column (g) ▪ q_T : the Thomas model adsorption capacity (mg/g) ▪ Q : the volumetric flow rate (L/h)

2.6.3 Adsorbents

Adsorbent is the main factor of the adsorption process. It can originate from natural or industrial products. In general, adsorbents can be classified into two groups: natural absorbent and engineered adsorbent. The typical natural adsorbents are clay minerals,

natural zeolites, oxides, or biopolymers. Some prominent engineered adsorbents for As removal are carbonaceous adsorbents (e.g., activated carbon), oxidic adsorbents (including solid hydroxides, hydrated oxides, and oxides mainly originated from aluminium and iron materials), and synthetic zeolites (Worch 2012). Low-cost and environmentally friendly adsorbents originated from natural products or agricultural waste such as dry plants, bioadsorbents, red mud, fly ash, zeolites, blast furnace slags, hydrotalcite, and hydroxides. These have attracted a lot of attention due to their competitive cost and abundance (Chiban et al. 2012; Worch 2012). Additionally, many studies are focusing on adsorbent modification in order to improve the adsorption capacity of the adsorbents. Some modification methods have been applied effectively to modified As adsorbents and they include protonation, chemical modification (metal and metal oxides impregnation, acid treatment) and heat treatment (Mohan & Pittman Jr 2007). This section focuses on modifying adsorbents by iron oxide and zirconium oxide.

Granular activated carbon (GAC) is a well-known adsorbent. Although it possesses a very high surface area (800 - 1200 m^2/g), its As adsorption capacity is relatively low because of the surface's negative charge (Hao et al. 2018). Several studies chose iron as an effective modification agent to enhance the As adsorption capacity of GAC. Kalaruban et al. (2019) used 500 mL 0.1 M ferrous chloride ($FeCl_2$) to incorporate with 20 mg of GAC at pH 4.2 – 4.5, 25 ^oC within 24 h to produce Fe-GAC. The modification slightly improved the As(V) adsorption capacity from 1.01 of original GAC to 1.43 mg/g of Fe-GAC at As(V) initial concentration of 1 mg/L. Sigrist et al. (2014) employed iron tri-chloride to impregnate GAC. The Fe-GAC products, namely P-2 and P-3 obtained the equilibrium As(V) adsorption of 3.38 and 3.30 mg/g, respectively, at a solution pH of 3.3 - 3.4, initial As(V) concentration of 0.337 - 0.362 mg/L.

The As adsorption capacity of biocomposite materials is generally low. However, their As adsorption capacity was considerably enhanced after iron modification. The iron oxy-hydroxides doped biocomposite adsorbents were considered to be promising media because of their high-effective, low-cost, and eco-friendly nature (Hao et al. 2018). Biochar, a product of pyrolysis derived from agricultural wastes, is also said to be an effective and low-cost adsorbent after being modified by iron. Biochar produced from dried hickory chips was prepared through direct hydrolysis of iron salt $Fe(NO_3)_3$ to create a Fe-impregnated biochar, and subsequently applied to remove As(V) from synthetic water at As(V) initial concentration of 0.1 – 55 mg/L. The Langmuir adsorption capacity of this modified biochar was 2.16 mg As(V)/g, which was much higher than that of the pristine biochar, obtained below 0.01 mg As(V)/g (Hu et al. 2015). Some bioadsorbents and natural materials such as jute fibre, wheat straw, fungal biomass, chestnut shell, and sand were also successfully modified by iron. The As adsorption capacity of the modified products was generally much higher than that of original ones (Hao et al. 2018).

In addition to Fe, zirconium (Zr) has functioned to modify adsorbents. The advantages of Zr are high affinity of Zr oxides/hydroxides to As adsorption and it is safe in regard to human health. A D401-Zr created by loading hydrous Zr oxide onto the polymeric adsorbent D401 was found to increase the adsorption capacity up to 60% compared with the original D401 (Li et al. 2013). Zr was also used in modifying GAC. The Langmuir adsorption capacity of Zr-oxalate complexes loaded GAC with As(V) was 3.9 mg/g, 43% higher than that of the original GAC (Velazquez-Jimenez et al. 2018).

In summary, most of the natural adsorbents are low-cost but they also has low As adsorption capacity. They can be modified by many methods to improve their adsorption capacity. Fe and Zr are the common chemical agents chosen to modify the adsorbents.

This study focuses on adsorption using new low-cost and environmentally friendly natural adsorbents. The modification of these natural media by Fe and Zr is also implemented.

2.7 Overview of electrocoagulation method

2.7.1 Concept and mechanism

Electrocoagulation (EC) was first applied to treat wastewater in the 19th century in England. However, due to its high capital and operating costs, mostly related to power cost, its application was limited for a long time. Until recent decades, given the developments of the power industry and what it has produced, more attention has been given to applying EC for solving issues in water supply and wastewater treatment (Song et al. 2017). EC technology has been trialled in treating various contaminants in water and wastewater such as turbidity, hardness, phosphate, fluoride, oil and heavy metals (copper, mercury, lead, arsenic, chromium, etc.) even at a very high influent concentration (Song et al. 2017).

Similar to the chemical coagulation (CC), the EC process also removes contaminants by the coagulation. However, in the EC process, an in-situ coagulant generated by electrolytic oxidation of electrode is used instead of adding chemical coagulant in the CC. The EC process is operated based on three components: (1) electrochemical reactions, including anodic oxidation and cathodic reduction, (2) flotation, and (3) coagulation or adsorption. Fig. 2.6 displays the conceptual framework of the EC process as an overlapping of these components. Here the metals like Fe, Al, Zn, etc., are usually employed as electrodes of the EC system to generate the in-situ coagulant.

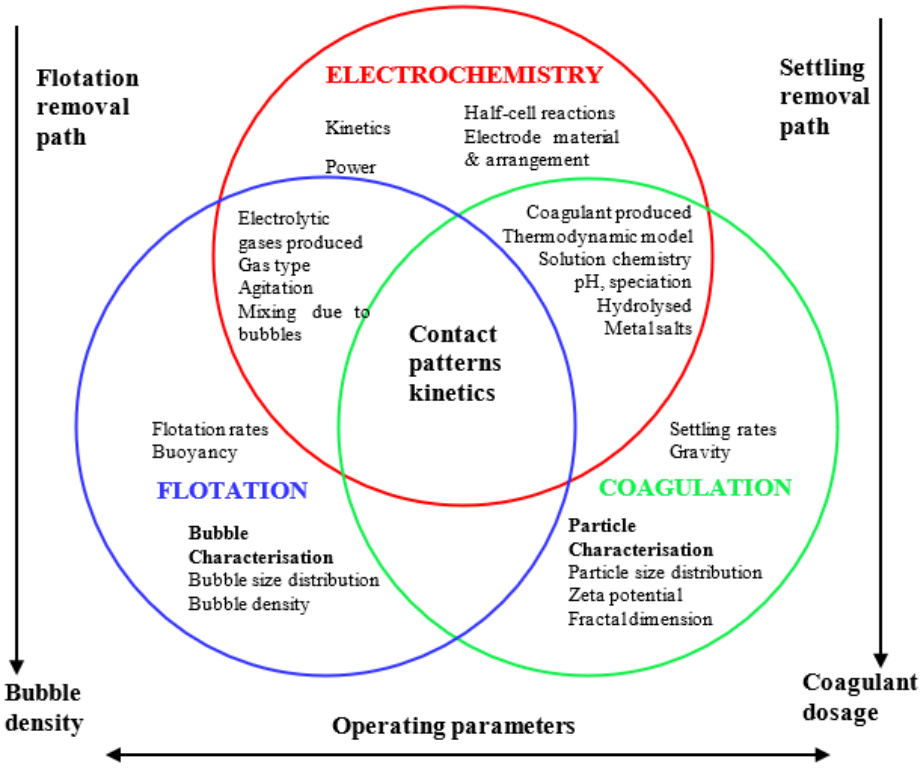

Fig. 2.6. A concept of EC process (Song et al. 2017)

The mechanism of EC is described in Fig. 2.7. It includes electrochemical reactions, which occur at both electrodes and in-situ production of flocs or coagulants. Nidheesh & Singh (2017) suggested that the general reactions possibly occurring within the EC reactor did so according to the below reactions [2.13 – 2.15].

At the anode:

$$M_{(s)} \rightarrow M^{n}_{(aq)} + ne^{-} \quad [2.13]$$

$$2H_2O \rightarrow 4H^{+}_{(aq)} + O_{2\,(g)} + 4e^{-} \quad [2.14]$$

At the cathode:

$$nH_2O + ne^{-} \rightarrow \left(\frac{n}{2}\right) H_{2(g)} + nOH^{-}_{(aq)} \quad [2.15]$$

When receiving a direct current, the oxidation occurs at the metallic anode and generates di- or trivalent metallic ions as well as releasing an equal amount of electrons. The aggregation occurs in the solution due to charge neutralisation between metallic ions and negatively charged ions. At the anode, the hydrogen ion and oxygen from water molecules are also released. At the cathode, the water molecules dissociate into hydrogen ions and hydroxide ions. The hydrogen ions in the EC system combine with each other and generate hydro gas. Meanwhile, the metallic ions at the anode combine with hydroxide ions at the cathode to generate metallic hydroxides. These metallic hydroxides work as an adsorbent to adsorb the pollutants in solution.

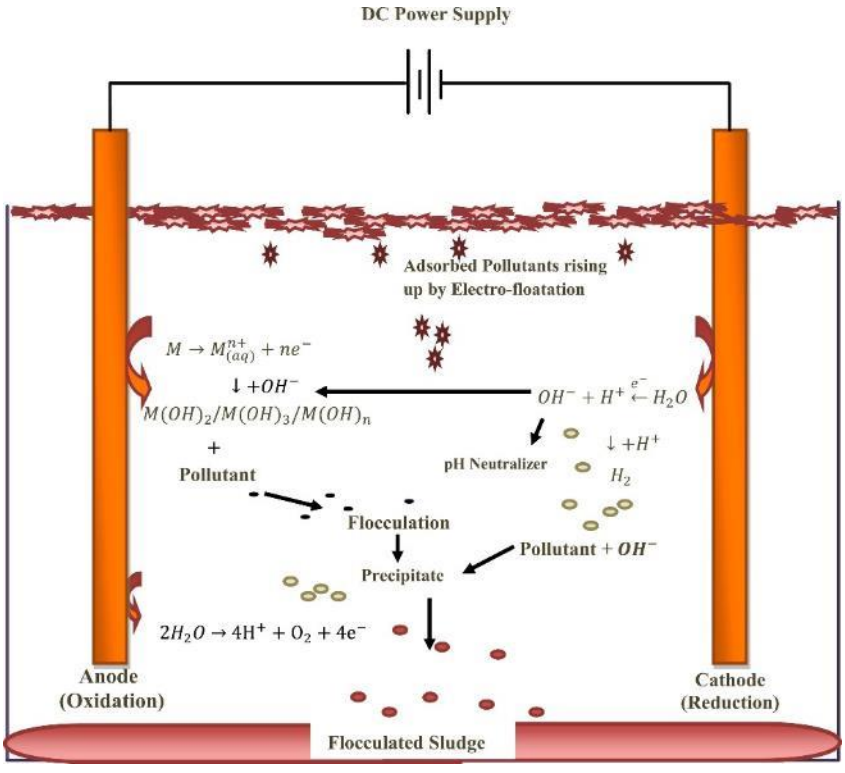

Fig 2.7. Mechanism of contaminant removal by EC process (Nidheesh & Singh 2017)

2.7.2 Arsenic removal by EC process

The common metal electrodes used in the EC system for As treatment are Fe, Al, stainless steel, Cu, Ti, and Zn (Nidheesh & Singh 2017). Among these, Fe and Al were used mostly because of good performance, low-cost, and easy availability. Besides this, the hybrid electrodes (e.g., Fe-Al) have also been trialled. Previous studies show that removing As with the EC process could be high and doing so depends on many factors. Ucar et al. (2013) reported that a batch study of EC process using Fe electrodes in monopolar parallel connection mode could remove 95% of As(V) from 0.5 mg/L synthetic water in 5 min, at pH 7 and current density of 4.5 mA/cm^2. Similarly, Kobya et al. (2016) also used Fe plate electrodes to remove 95% of As(V) from 0.15 mg/L synthetic water within 7.5 min at and pH 6.5 and electrical consumption of 2.5 mA/cm^2. In comparison between these studies, at the same electrodes material and connection mode but different in initial As(V) concentration, they were conducted under varied operating conditions such as pH, current density, and operation time to obtain an expected As(V) removal efficiency. Employing Al electrodes, Flores et al. (2014) removed 92% of As(V) from 50 µg/L ground water at a current density and flow velocity of 6 mA/cm^2 and 1.8 cm/s, respectively.

In the EC process, As(III) can be removed through two stages, including As(III) treatment/oxidation and As(V) removal. In the first stage, As(III) can be treated by adsorption directly onto metal hydroxides/oxyhydroxides (Lakshmanan et al. 2010) or by As(III) oxidation to As(V) followed with As(V) adsorption onto the metal hydroxides/oxyhydroxides (Wan et al. 2011). The As(V) removal capacity in the EC process is 3-20 times higher than that of As(III). Therefore, the conversion from As(III) to As(V) is a crucial stage that affects the EC system's efficiency in removing As (Song

et al. 2017). It is argued that the mechanism of As(III) oxidation occurs between three pathways: (1) As(III) oxidation in the EC process by the electrodes; (2) As(III) oxidation with DO in the EC process; and (3) As(III) oxidation with Cl_2 in the EC process (Song et al. 2017).

As(III) was oxidised to As(V) in the EC process by the electrodes or an intermediate. Wan et al. (2011) reported that at least 25% of As(III) was converted to As(V) during the EC process. They observed that the As(V) concentration firstly increased and then decreased with the operation time. It indicates that As(III) was firstly treated by converting to As(V) before completely removed by As(V) adsorption and precipitation processes (Kumar et al. 2004b). The same phenomenon was also observed in studies of Kumar et al. (2004b) and Meng et al. (2002). They also concluded that As(III) was oxidised to As(V) before being removed with As(V) in the solution.

The As(III) oxidation rate by the EC reactor was low and could be improved by increasing the DO and Cl_2 concentrations. DO can be produced from the anode or supplied by adding pure oxygen or air (Song et al. 2017). In their study, Song et al. (2014) stated that As(III) was favourably converted to As(V) with the increase of aeration intensity. When aeration intensity rose from 0.00 to 0.32 L/min, As(III) concentration decreased 60% while As(V) concentration increased about 50% and As(total) removal efficiency increased more than 30%. With the graphite anode, a small amount of Cl_2 was generated (2 – 5% of theoretical amount calculated by the Faraday's law) and helped to completely oxidise As(III) to As(V) in the solution of 0.05 mg/L of As(III) at the current of 0.025 – 0.15 A in 1 min.

In the second stage, As(V) can be removed by the ligand exchange mechanism. Here, As(V) replaces the hydroxyl group of hydroxides/oxyhydroxides. The reactions

[2.16 – 2.20] describes the possible reactions of As(V) in the EC system, which contains Al and Fe electrodes (Song et al. 2017):

$$2FeOOH_{(s)} + H_2AsO_4^- \rightarrow (FeO)_2HAsO_4^- + H_2O + OH^- \quad [2.16]$$

$$3FeOOH_{(s)} + HAsO_4^{2-} \rightarrow (FeO)_3HAsO_{4(s)} + H_2O + 2OH^- \quad [2.17]$$

$$mAl_{(aq)}^{3+} + (3m-n)OH^- + nHAsO_{4(aq)}^{2-} \rightarrow Al_m(OH)_{(3m-n)}(HAsO_4)_{n(s)} \quad [2.18]$$

$$\equiv Al-OH_{(s)} + HAsO_{4(aq)}^{2-} \rightarrow \equiv Al-OAs(O)_2(OH)_{(s)}^- + (OH)_{(aq)}^- \quad [2.19]$$

$$Al(OH)_{3(s)} + AsO_{4(aq)}^{3-} \rightarrow [Al(OH)_3AsO_4^{3-}]_s \quad [2.20]$$

In EC and adsorption technologies, several operating parameters can affect their performance. pH, influent concentration, co-existing ions, operation time, operating mode, and current density (for EC) are the most common factors that significantly impact efficiency in As removal. Therefore, in this study, detailed experiments were carried out to determine the impact of these factors as well as to identify the optimal operating conditions. Additionally, this study also focuses on solving the power dependence problem of the EC method, leading to a promising technology that could be implemented at all places, including isolated areas. The scale of EC reactor is also one of the important factors. This study focuses on the decentralised scale so that the new EC system can be applied at the household level.

2.8 As-contained waste management

Processes to remove As generate several types of wastes (Table 2.7). It is necessary that these wastes should be managed properly to prevent As being returned back to the

environment. The As contained wastes can be divided into two types, liquid and solid waste (Litter et al. 2019). The liquid waste includes brines of regeneration of ionic exchange resins, water reject of membrane systems and spent regenerants of adsorption media. Generally, the concentration of As in the liquid waste is high. Therefore, liquid waste must be treated, normally by precipitation or coagulation and filtration, before being discharged into the waterways. With semi-liquid wastes, they can be thickened and dewatered and then treated as solid waste.

Table 2.7. Wastes from As removal processes (Litter et al. 2019)

Process	Wastes	Type of wastes
Coagulation, adsorption, filtration	Solids deposited in a sedimentation tank Backwashing of filters	Very dilute semiliquid with 2 – 8% solids
Ionic exchange	Exhausted resins Regeneration agents	Solid and liquid
Membrane	Exhausted membranes Liquids from chemical cleanings	Solid-liquid from chemical cleanings
Activated alumina	Regeneration agents and exhausted adsorbents	Liquid and solid
Iron-based adsorbents	Washings Exhausted adsorbents	Liquid and solid

As-contained solid wastes could be treated by four methods: (1) desorption/regeneration, (2) concentration and containment, (3) dilution and dispersion, and (4) encapsulation of the material (Leist et al. 2000, Mandal et al. 2016, Mohan & Pittman 2007). The primary factors that dominate the applicability of these methods are treatment cost and safety. The first three methods are not considered as the best choice because they have problems regarding the safe storing, limited market demand and low purity of As. The decline in the quality of the products after desorption and regeneration is another obstacle of the first approach. Mohan & Pittman Jr (2007) stated that desorption/regeneration method is usually used for other metals and organics rather than for As. In the As desorption process, the most popular eluents used to desorb As are sodium hydroxide and strong acid, which are chosen basing on the adsorption mechanism and nature of adsorbents. Chiban et al. (2012) used 0.07 M NaOH to regenerate the used *W. frutescens* plant and recovered 92% of As(V). Similarly, 2M NaOH solution was employed to desorb bead cellulose loaded with iron oxyhydroxide and reused it for four cycles (Guo & Chen 2005). 0.5M HCl could recover more than 85% of As(III) from exhausted fungal biomass and this biomass could be regenerated up on 10 cycles. However, most studies concluded that desorption/regeneration is not an attractive option due to the difficulty in the storage of the concentrated As and the limited market value of the recovered As. Encapsulation through solidification/stabilisation (S/S) is selected as one of the most attractive methods in the literature. It is recognised as the Best Demonstrated Available Technology (BDAT) for the land disposal of hazardous elements by the U.S. Environmental Protection Agency (USEPA) (Yoon et al. 2010). The advantages of this method are cost-effectiveness and being safely disposed of in a secure landfill. The most popular agents used in S/S process are cement, cement mixed iron (II,

III), lime, fly ash, or silicate (Leist et al. 2000, Mandal et al. 2016), while a few studies also tried industrial slags and polymers (Nguyen et al. 2014). Many studies tested S/S products, mostly based on the toxicity characteristic leaching procedure (TCLP) of USEPA to identify the As concentration in leachates. The encapsulated material can be safely disposed of into the environment when the As concentration in leachate is below the regulation requirement, which is currently 5 mg/L in the United States and Australia (Lei et al. 2017; NSW EPA, 2014).

Liu et al. (2018) applied the S/S method to co-treat solid wastes produced by copper smelting. These wastes included flotation waste of copper slag, neutralisation sludge, and As-containing gypsum sludge, which are very difficult to dispose of. Firstly, they prepared the binder by a combination of 40% flotation waste of copper slag, 10% of neutralisation sludge, 50% cement clinker, and the ratio of water: binder was 1:4. After 28 days, the unconfined compressive strength of the binder was 43.24 MPa. The binder was also mixed with As-containing gypsum sludge at the ratio of 5:5 in the S/S process. As a result, the unconfined compressive strength of the S/S product after 28 days fell to 11.06 MPa but still met the required level of MU10 brick in China. In this mixing state, the leachate concentration was much lower than the limits of the China standard leaching test (CSLT) of 5 mg/L. Sludge containing As and heavy metals from the primary lead-zinc smelter was also successfully encapsulated with the binder at a mass ratio of 1:1. After 28 days, the As concentration in the leachate was lower than that in the current TCLP threshold limit (Li et al. 2016). The products from both studies were recommended for reuse as construction materials.

Sarntanayoot et al. (2019) stabilised/solidified the As-contained iron waste generated from tap water production at the Bangkhen Water Treatment Plant, Thailand

with cement. The waste from this treatment plant was dried at 100 °C overnight. Then, it was mixed with cement in four ratios of 4:6, 3:7, 2:8, and 1:9, and cast in a plastic cylindrical mould (40 ± 1 mm high and 43 ± 1 mm in diameter). After 14 days, only the solidification at a ratio of 4:6 passed the requirement of unconfined compressive strength test (USEPA) and was then used in the leaching test. The cumulative concentrations of As leached from the solidification sample were much lower than the USEPA's TCLP regulatory limit value of 5 mg/L after 64 days.

Mohapatra et al. (2008) noted another As-contained waste treatment approach, biological treatment. Here As bearing waste was mixed with cow dung. The As in the solid waste could be transferred into soluble and volatile species (trimethylarsine and arsine) by some microbial species such as *Clostridium collagenovorans, Desulfovibrio gigas, Desulfovibrio vulgaris, Methanothermobacter thermautotrophicus, Bacillus idriensis* and *Sphingomonas desiccabilis* (Liu et al. 2011; Michalke et al. 2000). However, the application of this method has been limited due to the generation of gaseous arsine, which is also an As toxic compound.

In addition, the phytoremediation method, which is usually applied to treat As-contaminated soils, also can be considered in managing As-contaminated solid waste. Some As-hyperaccumulating fern species were observed as being able to remove As from soil (Niazi et al. 2016). This method takes a longer time in comparison with the S/S method and more studies are needed to evaluate the possibility of managing As-contaminated waste by phytoremediation.

2.9 Conclusion

As is one of the most toxic elements in the world's water resources and seriously impacts human health in many countries. Using As-contaminated drinking water, even at

a low concentration, can cause cancerous and non-cancerous diseases. Efforts to remove As from drinking water have obtained many achievements, including investigation of various As treatment methods, such as oxidation, coagulation/precipitation, adsorption, ion exchange, and membrane technology. These approaches can be used individually or in combination to reduce As concentration in aqueous environments to the acceptable level. The appearance of As contamination in groundwater majorly affected the rural areas of developing countries, where groundwater is used as the primary drinking water source. Therefore, low-cost, highly effective water treatment system is the priority option for the affected areas. Within these treatment methods, adsorption and electrocoagulation are promising methods for decentralised scale systems, which can be implemented in rural and isolated areas. This study focuses on developing (i) two novel adsorbents fabricated by simple modification methods and (ii) a novel EC process that can be used with different energy sources. The continuous flow mode, which is more relevant to real treatment systems but not studied too much in literature, is also conducted in this study.

Moreover, the waste generated from the As removal process also needs to be well managed to prevent the generation of secondary pollutants. Solidification/stabilisation and phytoremediation, when employed in suitable conditions, can be applied to safely handle the As contaminated waste.

CHAPTER 3

Removing arsenic from water with an original and modified natural manganese oxide ore

Chapter 3. Removing arsenate from water with an original and modified natural manganese oxide ore

Summary

Chapter 3 presents the first research finding about a low-cost adsorbent, namely Vietnamese manganese oxide ore, and its modified forms, namely Fe^a-VMO and Zr^a-VMO in removing As(V) from water. The batch study was published in the Journal of Environmental Science and Pollution Research (Q2 journal, impact factor: 3.00) in 2020 as below.

Nguyen, T.T.Q., Loganathan, P., Nguyen, T.V. & Vigneswaran, S. 2020, 'Removing arsenic from water with an original and modified natural manganese oxide ore: batch kinetic and equilibrium adsorption studies', *Environmental Science and Pollution Research*, vol. 27, no. 5, pp. 5490-502.

The column study was published as the first part in the following paper in the Journal of Environmental Chemical Engineering (Q1 journal, impact factor: 4.02).

Nguyen, T.T.Q., Loganathan, P., Nguyen, T.V. & Vigneswaran, S. 2020, 'Removing arsenate from water using modified manganese oxide ore: column adsorption and waste management', *Journal of Environmental Chemical Engineering*, p. 104491.

The research findings in this work includes two novel and low-cost adsorbents for removing As(V) from water. In this chapter:

- Four different modification methods using Fe and Zr compounds were applied to produce modified VMO adsorbents which had better As(V) adsorption performance.
- Batch and column studies were conducted to identify the As(V) adsorption capacity and treatment cost.
- Evaluation of the effects of aqueous environmental conditions on the As(V) adsorption (e.g. pH, co-existing anions).
- Testing the adsorbent characteristics to determine the adsorption mechanism.

3.1 Introduction

Inorganic arsenic (As) is one of the most serious and challenging pollutants that must be removed from water sources because it is highly toxic in drinking water (Sogaard 2014). As contamination of water is prevalent in several countries because of natural geological processes and human activities such as mining, chemical industries, and groundwater exploitation (Järup 2003). The range of As concentration in water varies widely from below 0.001 mg/L up to 1.0 mg/L; in some places, it can even reach 3.0 mg/L or higher (Amini et al. 2008; Berg et al. 2001). These concentrations are much higher than the WHO recommended As concentration in drinking water of 0.01 mg/L. In some well-known contaminated regions in Asia, such as Bangladesh, India, Nepal and Vietnam, the common As concentration in the affected areas is 0.2 - 0.5 mg/L (Berg et al. 2007; Berg et al. 2001; Buschmann et al. 2007; Chakraborti et al. 2002; Polya et al. 2005; Smedley & Kinniburgh 2002a). The most common As species in groundwater are arsenate As(V) and arsenite As(III).

Several studies have demonstrated that various techniques can remove As, for example, coagulation, adsorption, ion exchange, and membrane separation (Maiti et al. 2010). Choosing the best appropriate As removal technology is based on many factors: water characteristics, treatment cost, treatment target, treatment efficiency, application conditions, etc. Removing As through adsorption technology has many advantages such as low-cost, simple implementation, high efficiency at a wide range of concentrations, and minimum waste production. It is also suitable for application in decentralized systems in affected areas, especially in developing countries where the As problem mostly occurs.

A wide range of materials, both natural and synthetic media, have been used as adsorbents for As removal. Some commercial and synthetic media such as activated

carbon, activated alumina and Zr resin have produced a very high As removal capacity, i.e., over 10 mg/g (Mohan & Pittman Jr 2007). Several natural materials or waste industrial/agricultural products (including sand, natural clay, kaolinite clay, bentonite, laterites, manganese ore, iron ore, dry plants, red mud, fly ash, etc.) have emerged as low-cost As removal options (Ahmed 2001; Chakravarty et al. 2002; Chiban et al. 2012). Unlike commercial products, some natural materials cannot reach As adsorption capacity higher than 1 mg/g. For example, the capacity of red mud is 0.514 mg/g, and kaolinite clay is below 0.23 mg/g (Altundoğan et al. 2002; Mohan & Pittman Jr 2007). In some cases, they could not even meet the As permissible limit for practical application (Kabir & Chowdhury 2017). However, when compared to the most popular and efficient As adsorbent, such as activated carbon, which has a high price and regeneration cost, the natural materials' advantages are cost-effectiveness, mechanical stability and local availability in many As affected areas (Chiban et al. 2012). This has encouraged researchers to promote the use of low-cost, locally available natural adsorbing materials.

Natural manganese oxide ore is a popular low-cost material that has been used to remove both As(III) and As(V) (Ahmed 2001; Chakravarty et al. 2002). However, the adsorption capacity of this ore is generally low (Chakravarty et al. 2002), and for this reason, it is difficult to use it widely and compete with other adsorbents having higher adsorption capacity. Chemical modifications can significantly improve the adsorption capacity of adsorbent media (Asere et al. 2019). For example, modification of clinoptilolite-Ca zeolite using manganese dioxide doubled the adsorption capacity of the unmodified zeolite (Camacho et al. 2011). The modification of biochar using magnetic gelatine also increased As adsorption capacity by about three times (Zhou et al. 2017).

Pokhrel & Viraraghavan (2008a) reported that iron oxide-coated biomass (IOCB) improved the efficiency significantly in removing As compared to uncoated materials.

Among the many chemicals used as modified agents, water-insoluble metal oxides are the best choice (Khan et al. 2013). Coating low-cost materials with iron (Fe) oxide and zirconium (Zr) oxide is considered an efficient method because of the high affinity of Fe and Zr towards As adsorption (Khan et al. 2013, Mohan & Pittman Jr 2007, Pokhrel & Viraraghavan 2008a).

In this study, a low-cost manganese oxide ore from Vietnam (VMO) with and without modification was tested as an adsorbent for As(V) removal from aqueous solution in batch kinetics and equilibrium adsorption studies. The modification was carried out by coating VMO with Fe oxide and Zr oxide under four different coating conditions and the modification that produced the highest adsorption capacity was chosen for detailed studies. These included testing the effects of pH and coexisting anions ($PO_4^{3-}, SiO_3^{2-}, SO_4^{2-}, CO_3^{2-}$) on adsorption as well as determining the mechanism of adsorption.

Based on the promising results obtained in batch studies, these adsorbents were used in a column study for removing As(V) from synthetic contaminated water under various experimental conditions. The column study is more relevant to practical conditions in water treatment plants than the batch study. The column study could mimic the decentralised scale system, the household water filtration system.

3.2 Material and Methods

3.2.1 Feed solution

In this study, 1 L synthetic stock solution was prepared by dissolving sodium arsenate ($Na_2HAsO_4 \cdot 7H_2O$) in Milli-Q water to obtain a concentration of 10 mg As(V)/L. This stock solution was then diluted to desired concentrations for use in the experiments. The solution's ionic strength was maintained at $1x10^{-3}$ M $NaNO_3$ and the solution pH was adjusted to 7.0 ± 0.2 by adding diluted nitric acid (0.1 M HNO_3) and sodium hydroxide (0.1 M NaOH).

3.2.2 Original adsorbent

A commercial Vietnamese manganese oxide (VMO) (particle size 0.1 – 3.0 mm), which is a mineral waste originating from the Tuyen Quang mine, and supplied by Phuong Nam Import-Export Trading and Service Joint Stock Company, Ha Noi, Vietnam, was used as an adsorbent for As. It is a low-cost material and employed locally as an adsorbent in water treatment systems. The VMO was ground and sieved into three different sizes - 0.3 – 0.6 mm, 0.6 – 1.0 mm and 1.0 – 2.0 mm - to study the effect of particle size on the VMO adsorption performance towards As. The sieved materials were washed by deionized distilled water and diluted nitric acid (0.1 M HNO_3) to remove any dirt and soluble compounds adhering to its surface. Then it was dried at 100 ^oC for 24 h to remove excess water and moisture before being stored in tightly closed plastic bags.

3.2.3. Modified adsorbents

Modified VMOs were produced from VMO with a particle size of 0.3-0.6 mm using four coating methods. Both Fe and Zr were used as coating agents. Below are the details of the modification processes:

- *Fe^a-VMO*: 200 g of VMO was poured into a mixture of 80 mL 2 M ferric nitrate nonahydrate ($Fe(NO_3)_3.9H_2O$) and 1 mL 10 M NaOH and shaken manually for 5 min. The mixture was heated at 110 ºC for 4 h and then at 550 ºC for 3 h for the first time. After cooling and washing the mixture, 100 g of this material was poured into a similar mixture as before and heated again at 110 ºC for 20 h. This modification procedure is an adaptation of the method used by Thirunavukkarasu et al. (2003) for preparing iron oxide coated sand (IOCS-2).
- *Fe^b-VMO*: VMO was modified again by impregnation of iron. 10 g VMO was mixed with 1 L ferric chloride hexahydrate $FeCl_3.6H_2O$ (2.0 g Fe^{3+}/L) and the mixture was shaken for 1 h at 120 rpm. Then, the pH of the mixed solution was adjusted to 8.0 by adding 1 M NaOH. After 3 h of continuous shaking, the shaking speed was reduced to 30 rpm and the suspension was intermittently mixed for 24 h. The material was then rinsed by Milli-Q water to remove unreacted Fe and dried at 45 ºC for 24 h (Kalaruban et al. 2016).
- *Fe^c-VMO*: This material was prepared by adding 10 g VMO to 150 mL solution of 0.1 M ferrous chloride tetrahydrate ($FeCl_2.4H_2O$) at pH 4.2 - 4.5 and agitated at 120 rpm for 24 h at room temperature (25±1 °C). This was followed by washing it with 200 mL Milli-Q water three times and drying at 80 °C for 4 h (Gu et al. 2005).

- *Fe^{d}-VMO*: The preparation procedure was similar to that of Fe^{c}-VMO. However, 20 mL sodium hypochlorite (13% NaClO) was added four times to the 150 mL solution during the shaking phase, each at intervals of 6 h. In this process, pH was maintained at 4.5 - 5.0 (Gu et al. 2005).
- Similarly, Zr^{a}, Zr^{b}, Zr^{c}, Zr^{d} were produced by mixing zirconyl chloride octahydrate ($ZrOCl_2.8H_2O$) instead of the iron salts with VMO according to the above methods.

3.2.4 As(V) adsorption capacity of modified and unmodified VMOs with different particle sizes

Unmodified VMO of doses 1 – 5 g/L with particle sizes of 0.3 – 0.6 mm, 0.6 – 1.0 mm, 1.0 – 2.0 mm, and the original size of 0.3 – 3 mm were added into 250 mL flasks containing 100 mL As(V) solution of 0.1 mg/L concentration. These flasks were shaken at 120 rpm for 24 h. The supernatant solution was filtered using 0.45 µm filters and filtered samples were analysed for As using an ICP-MS instrument (Agilent Technologies 7900 ICP-MS) (Pic. S3.1, Appendix 1). Similar experiments were also conducted with the eight types of modified VMO of the same particle size of 0.3 – 0.6 mm. In all studies, the initial pH and ionic strength were 7.0 ± 0.2 and $1x10^{-3}$ M $NaNO_3$, respectively.

The results (presented in more detail in Section 3.3.1) demonstrated that VMO of particle size 0.3 – 0.6 mm and Fe^{a}-VMO and Zr^{a}-VMO had the highest As(V) adsorption capacity. Consequently, they were chosen for the subsequent studies and characterisation.

3.2.5 Equilibrium and kinetic adsorption of As(V) on VMO, Fe[a]-VMO and Zr[a]-VMO

All batch experiments were conducted on VMO, Fe[a]-VMO and Zr[a]-VMO (particle size 0.3 – 0.6 mm) at room temperature of 25 ± 1 °C and natural pH of 7.0 ± 0.2 (excluding experiments on pH impact). The ionic strength was kept at $1x10^{-3}$ M $NaNO_3$ for all feed solutions.

The equilibrium adsorption experiments were conducted by adding different adsorbent dosages, i.e. 2.0 – 14 g/L of VMO and 0.1 – 2.0 g/L of modified VMO, into a set of flasks containing 100 mL As(V) solution of 0.5 mg/L. The flasks were agitated on a shaker at 120 rpm for 24 h (Pic. S3.2a, Appendix 1). The supernatant solutions were filtered using 0.45 μm filters and As in filtered samples was analysed.

The amount of As(V) adsorption at equilibrium was calculated using Eq. 3.1 (Nur et al. 2014):

$$q_e = \frac{(C_o - C_e).V}{m} \text{ (mg/g)} \quad [3.1]$$

where C_o is initial concentration of As(V) (mg/L), C_e is equilibrium concentration of As(V) (mg/L), V is volume of solution (L) and m is mass of adsorbent (g)

Adsorption efficiency was calculated using Eq. 3.2 as follows:

$$E(\%) = \frac{(C_0 - C_e)}{C_0} \times 100 \quad [3.2]$$

The adsorption kinetics experiment was conducted by adding predetermined amounts of VMO (2 g/L) and modified VMO (0.1 mg/L) into a set of flasks containing

100 mL solution of 0.5 mg/L As(V). The flasks were then agitated at 120 rpm, and samples were taken at different time intervals, ranging from 5 min to 24 h.

The data of equilibrium and kinetics adsorption was modelled using Langmuir, Freundlich, Temkin models (Table 2.4, Chapter 2) and PFO, PSO, Elovich models (Table 2.5, Chapter 2), respectively.

3.2.6 pH influence on As(V) adsorption

Experiments on pH influence on As(V) adsorption were conducted at a pH range from 3.0 to 10.0. Here, pH of As(V) solution was adjusted using 0.1 M HNO_3 and 0.1 M NaOH solutions after the required amounts of modified VMO (0.3 g/L) and unmodified VMO (3 g/L) were added to a set of glass flasks containing 100 mL of 0.5 mg As(V)/L. The experimental procedure was similar to the previous equilibrium adsorption experiment.

3.2.7 Coexisting anions' influence on As(V) adsorption

A study on the influence of coexisting anions on As(V) adsorption was carried out utilising four typical anions, i.e. phosphate (PO_4^{3-}), sulphate (SO_4^{2-}), silicate (SiO_3^{2-}) and bicarbonate (CO_3^{2-}). In this experiment, Sodium salts of different anions of concentration from 0.1 to 20 mg/L were added separately into 100 mL solutions containing 0.5 mg As(V)/L. Predetermined amounts of 0.1 g modified VMO and 1 g unmodified VMO were added to the above solutions. The experimental procedure was similar to that of the previous equilibrium adsorption experiments.

3.2.8 Column studies

Column adsorption studies were conducted using nine glass columns with a height of 50 cm. They were packed with 40 g of adsorbent (corresponding to 30 cm bed-height). 1.0 mm acrylic beads and cotton balls were used at the top and bottom of the column respectively to prevent the release of adsorbent from the columns (Pic. S3.2b, Appendix 1). A dosing pump (Master flex L/S) was used to continuously pump the As solution through the columns in an up-flow mode at constant flow rates of 0.15 and 0.50 L/h (1.9 and 6.4 m/h). Samples were collected every 2 h on the first day and then once daily and weekly until the adsorbents were saturated with As. The pH of the effluent samples was nearly the same as the influent solution (pH 7.0 ± 0.2).

The samples were filtered using 0.45 μm filters, and filtrates were analysed for As(V) using an ICP-MS instrument (Agilent Technologies 7900 ICP-MS).

The total amount of As(V) adsorption, q_{total} (mg), and column experimental adsorption capacity, q_{exp} (mg/g) were calculated manually from the breakthrough curves using Microsoft Excel spreadsheet according to the following equations (Nguyen et al. 2020, Nur et al. 2014):

$$q_{total} = Q.\int_{t=0}^{t=total}(C_o - C_t)dt \quad [3.3]$$

$$q_{e,exp} = \frac{q_{total}}{m} \quad [3.4]$$

where Q is the volumetric flow rate (L/h), t is flow time (h), C_o is As(V) initial concentration (influent) (mg/L), C_t is As(V) concentration (effluent) at time t (mg/L), m is amount of adsorbent in the column (g).

The nonlinear Thomas model was applied to describe the experimental data (Table 2.6, Chapter 2).

3.2.9 Adsorbent characterisation

Characteristics of unmodified and modified VMOs were determined by: X-ray diffraction (XRD, Bruker D2 Phaser instrument); Scanning electron microscopy (SEM; Quanta-650 instrument); Fourier transform infrared (FTIR, Nicolet iS5 FT-IR Spectrometer); X-ray fluorescence (XRF, Olympus Vanta M series); and Brunauer-Emmett-Teller (BET) nitrogen adsorption.

Zeta potential of the materials was measured to determine their surface charge before and after As(V) adsorption. Here, the zeta potentials of suspensions prepared by adding 0.1 g of fine material (<0.75 μm) in 100 mL Milli-Q water at different pHs were measured using a Zetasizer nano instrument, Nano ZS Zen 3600.

3.3 Results and discussion

3.3.1 Characteristics of adsorbents

Elemental compositions of unmodified and modified VMO as determined by XRF are shown in Table 3.1. The unmodified VMO had high percentages of Si and Mn and a moderate percentage of Fe, but no Zr. The composition was found to be strongly dependent on the coating conditions. The modified materials, Fe^{a}-VMO and Zr^{a}-VMO produced by the first modification process (mixing original VMO with ferric nitrate and sodium hydroxide and heating at high temperature) had the highest percentage of Fe and Zr after modification (21.9% and 9.8%, respectively). Coating metals on VMO increased the percentages of these metals in Fe^{a}-VMO and Zr^{a}-VMO by approximately 6 and 10%,

respectively. Additionally, after As(V) adsorption, the percentages of Fe and Zr did not decrease, indicating a strong coating of these metals. Therefore, there is no risk of heavy metals leaching from the adsorbents and creating secondary pollution in the treated water.

Effluent samples from the columns had no detectable Fe or Zr, which indicates these metals in the modified VMO remained intact and well-conserved. Because original VMO contained many elements, mainly Mn, Fe, Al, these elements could leach out from VMO into the treated water. This was checked by analysing these elements in the leachates. The results showed that the Al concentration in the leachates was below the detection limit, while Fe and Mn concentrations were very low (0.002 and 0.001 mg/L, respectively).

Table 3.1. Metals composition of original and modified VMO determined by XRF

Adsorbent	Si (wt%)	Mn (wt%)	Fe (wt%)	Zr (wt%)	Al (wt%)
Before As adsorption					
VMO	13.0 ± 0.1	25.6 ± 0.2	16.1 ± 0.0	0	2.5 ± 0.1
Fe^{a}-VMO	8.7 ± 0.1	20.9 ± 0.2	21.9 ± 0.2	0	2.0 ± 0.1
Fe^{b}-VMO	15.2 ± 0.1	16.7 ± 0.1	20.0 ± 0.1	0	3.1 ± 0.1
Fe^{c}-VMO	14.4 ± 0.1	19.9 ± 0.1	19.0 ± 0.1	0	2.9 ± 0.1
Fe^{d}-VMO	14.3 ± 0.1	19.7 ± 0.1	19.1 ± 0.1	0	3.0 ± 0.1
Zr^{a}-VMO	7.4 ± 0.1	22.5 ± 0.3	12.2 ± 0.2	9.8 ± 0.1	1.4 ± 0.1
Zr^{b}-VMO	13.0 ± 0.1	21.6 ± 0.1	19.0 ± 0.1	0.1 ± 0.1	2.9 ± 0.1
Zr^{c}-VMO	13.6 ± 0.1	23.4 ± 0.1	18.5 ± 0.1	0.08 ± 0.1	2.8 ± 0.1
Zr^{d}-VMO	13.7 ± 0.1	19.9 ± 0.1	18.9 ± 0.1	0.5 ± 0.1	2.8 ± 0.1
After As adsorption					
VMO	13.1 ± 0.1	26.0 ± 0.2	16.4 ± 0.0	0	2.4 ± 0.1
Fe^{a}-VMO	9.9 ± 0.1	25.0 ± 0.2	23.1 ± 0.1	0	2.2 ± 0.1
Zr^{a}-VMO	7.6 ± 0.1	24.2 ± 0.2	13.6 ± 0.1	10.2 ± 0.1	1.3 ± 0.1

Fig. 3.1a, b, c, d, e, and f show the surface morphologies of original VMO and Fe^{a}-VMO and Zr^{a}-VMO, before and after As adsorption determined by SEM at a high magnification of 3200x, respectively. The relatively irregular and heterogeneous surface morphology of the three materials can be clearly seen in these figures. The images also

indicated that both Fe[a]-VMO and Zr[a]-VMO possessed more porous layers/channels than the original VMO. No visible change in the surface morphologies of the materials was observed after As adsorption in batch and column study (Fig. S3.1, Appendix 1).

Before As(V) adsorption

(a) VMO (b) Fe[a]-VMO (c) Zr[a]-VMO

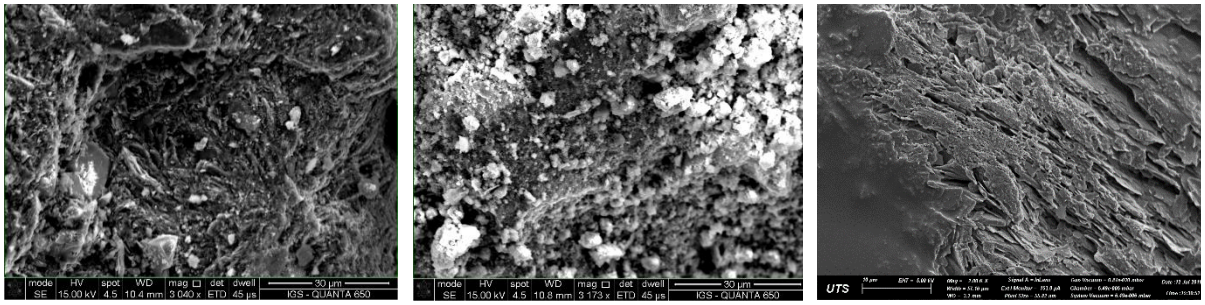

After As(V) adsorption

(d) VMO + As (e) Fe[a]-VMO+As (f) Zr[a]-VMO+As

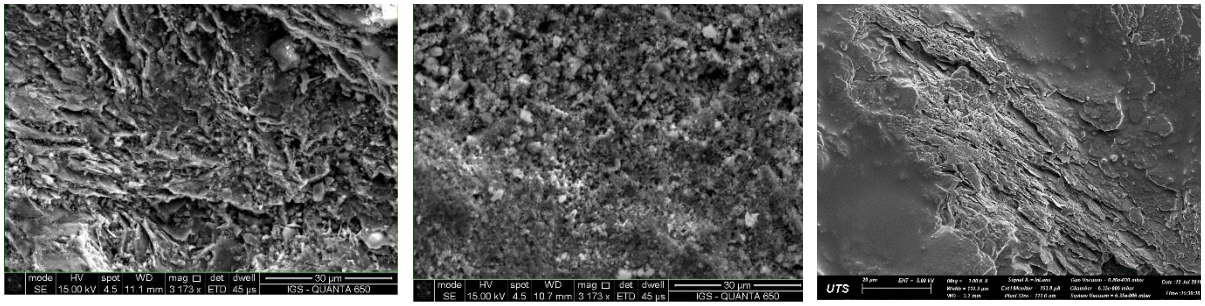

Fig. 3.1. SEM images of VMO before, after coating and adsorption.

A material's adsorption ability strongly depends on its mineral components. According to the XRD diagram (Fig. 3.2), VMO consists of four main minerals, namely quartz, goethite, cryptomelane and muscovite. Quartz and muscovite contributed to the high content of silicon (13%) in VMO; goethite to the high content of Fe (16.1%); and

cryptomelane to the high content of Mn (25.6%) (Table 3.1) Fe modification of VMO slightly changed the XRD pattern. This modification produced new peaks characteristics of hematite, a Fe oxide mineral. It also appears that the goethite peaks in the unmodified VMO were reduced in size. This shows that some of the goethite were transformed into hematite at the high temperatures used in the modification procedure and/or the Fe coatings might have produced the hematite. Zr coating of VMO also produced new XRD peaks, which are characteristics of zirconia minerals such as zirconia/zirconolite. It could also be possible that the Fe and Zr added might have formed some amorphous (non-crystalline) compounds which cannot be identified by XRD. As adsorption did not change the XRD pattern probably either because of the small amounts of As concentration compared to other elements on the adsorbents or the As compounds formed are amorphous that cannot be detected by XRD.

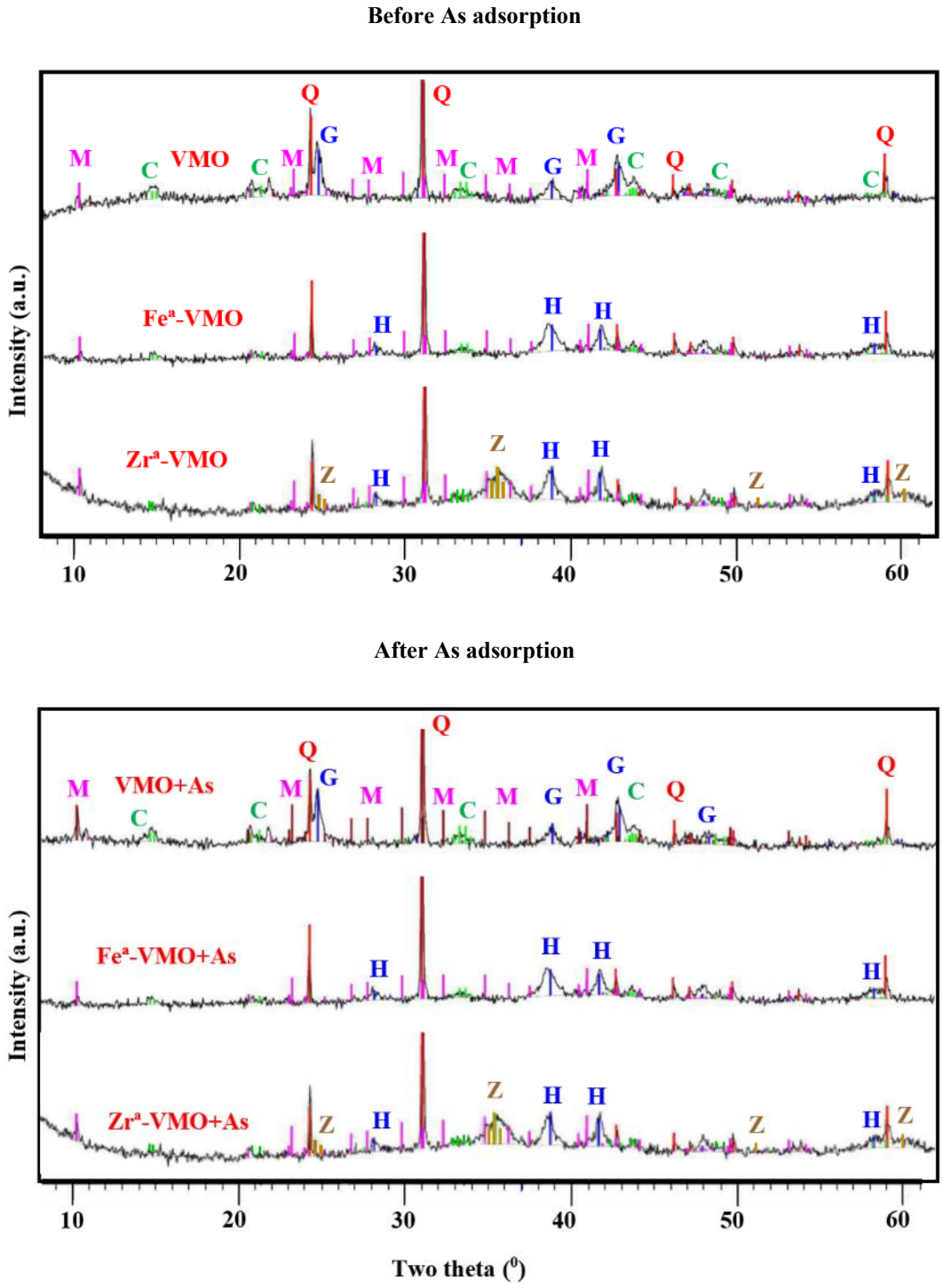

Fig. 3.2. XRD diagram of VMO and modified VMOs before and after As adsorption

BET surface areas of VMO and its modified forms were 27.1 and 37.1 – 37.5 m^2/g, respectively (Table 3.2, Fig. S3.2a, Appendix 1). These values are higher than those of many other natural As adsorbents such as gibbsite, goethite, kaolinite, and iron oxide coated sand (Mohan & Pittman Jr 2007). However, their BET surface area values are lower than those of the popular commercial adsorbents such as activated carbon and activated alumina (Mohan & Pittman Jr 2007). Table 3.2 also shows that the surface area of VMO increased significantly after modification. This may have been triggered by the creation of porous forms of Fe and Zr precipitated particles (Fig. S3.2b, Appendix 1). However, the BET surface area and pore volume of both original and modified VMO decreased after adsorption (Table 3.2). It could be because of the adsorption of As(V)/or formation of As(V) compounds on the surface of the adsorbent and filling-up of some of the pores inside the adsorbent.

Table 3.2. BET surface area and pore volume of adsorbents

Adsorbent	Before As(V) adsorption		After As(V) adsorption	
	BET (m^2/g)	Pore volume (cm^3/g)	BET (m^2/g)	Pore volume (cm^3/g)
VMO	27.1	0.0022	17.3	0.0012
Fe^a-VMO	37.5	0.0017	24.4	0.0004
Zr^a-VMO	37.1	0.0022	26.6	0.0006

FTIR diagrams (Fig. 3.3) depict the presence of some chemical bonds on the adsorbents before and after As(V) adsorption process. Evaluation of the differences in the peak intensity, peak shifting and peak appearance (or disappearance) indicates the types of interaction between surface chemical groups and absorbed As(V).

Generally, the FTIR shapes of the three adsorbents are not too different. After coating, some new peaks appeared that represent new bonds between Fe or Zr with available functional groups. Fig. 3.3a shows that a vibrational spectrum exhibited broad O-H stretching peaks between 3700 and 3300 cm^{-1}, and O-H bending at 1640 cm^{-1} (Myneni et al. 1998; Petit & Puskar 2018; Tomić et al. 2011). The peak of 1384 cm^{-1} could be ascribed to the vibration of C-H (Delva et al. 2013). The bands between 1100 and 900 cm^{-1} are normally assigned to Fe-OH bending, Al-OH bending and Si-O stretching vibration (Tomić et al. 2011; Zhang et al. 2009). The peaks at 794 cm^{-1} and nearby could be attributed to Fe-O (Jia et al. 2007; Tomić et al. 2011). Many peaks were also observed at 525, 524, 523 and 466, 454, 419 cm^{-1}. According to previous reports, these peaks could be assigned to the functional groups of metal such as Mn-O, Mn-O-Mn, Zr-O-Zr, Si-O-Al, and Si-O-Si (Markovski et al. 2014; Tomić et al. 2011).

Fig. 3.3b illustrates that all peaks of the adsorbents reduced evenly after adsorption. Moreover, it shows that no new group appears in the FTIR diagram. It means that As(V) only reacted with the available functional groups of adsorbents.

(a) Before adsorption

(b) After adsorption

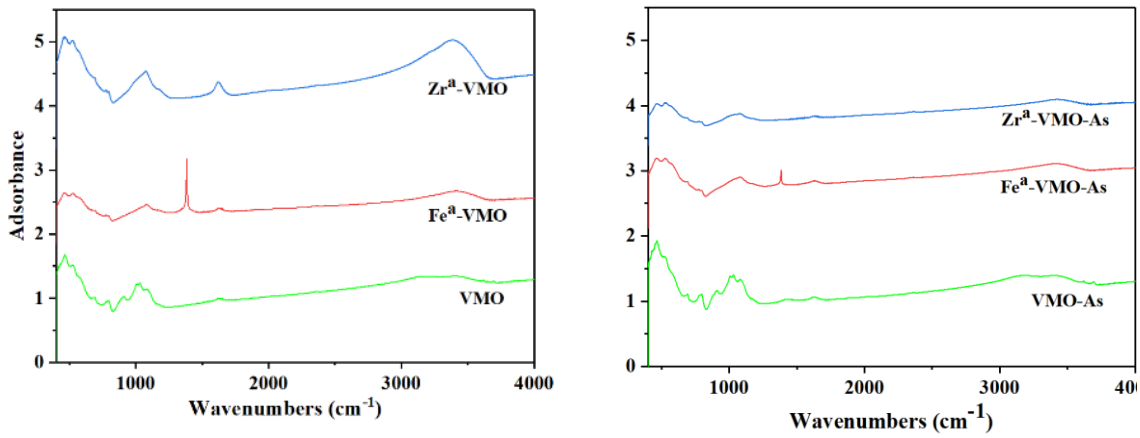

Fig. 3.3. FTIR diagram of original and modified VMO before and after As(V) adsorption

Zeta potential of original and modified VMOs at different pHs is presented in Fig. 3.4. The data shows that zeta potentials of Fe^a-VMO and Zr^a-VMO were more positive than unmodified VMO at all pHs (Fig. 3.4a). This means that the impregnation of Fe and Zr on VMO increased the surface positive charge of VMO. As(V) often exists in anionic forms, depending on pH in water (monovalent $H_2AsO_4^-$, divalent $HAsO_4^{2-}$ and trivalent AsO_4^{3-} within the pH range from approximately 3.0 to 6.0, 7.0 to 11, and 12 to 14, respectively) (Mondal et al. 2007). Therefore, the appearance of a more positive charge on modified VMO is favourable for As(V) removal from water through electrostatic adsorption forces.

The zero point of charges (ZPC, pH at which net surface charge is zero) of VMO, Fe^a-VMO and Zr^a-VMO were at pH 6.3, 7.5 and 7.1, respectively. At pH lower than ZPC, the zeta potentials were more positive and at pH higher than ZPC they were more negative (Loganathan et al. 2014; Oladoja & Helmreich 2014). During As(V) adsorption process, because As(V) exits in negatively charged forms, the original and modified VMO had a better tendency to adsorb As(V) at lower pH through electrostatic forces. In contrast, at higher pH, especially at basic conditions, the surface charges of original and modified VMO change from positive to negative. This leads to a reduction of As(V) adsorption capacity of these materials. In comparison with GAC, the surface charge of VMO and modified VMOs were more positive. At the same pH range (3 – 10), the zeta potential value of GAC varied from -35 to +5 (Kalaruban et al. 2019) whereas this value for VMOs varied from -27 to +38. In addition, the ZPC of GAC (at pH 3.2) was also much lower than that of VMOs (at pH 6.3 ÷ 7.5). The difference in surface charge could affect the adsorption capacity of each adsorbent, which would be discussed in details in the later section (3.3.6).

Fig. 3.4b shows that the negative zeta potentials decreased at all pHs and the ZPC reduced when the negatively charged As(V) adsorbed on all adsorbents. The decrease of zeta potential indicated that As species were adsorbed on the surface of the adsorbent by inner-sphere complexation as well (ligand exchange) (Kalaruban et al. 2016; Loganathan et al. 2014).

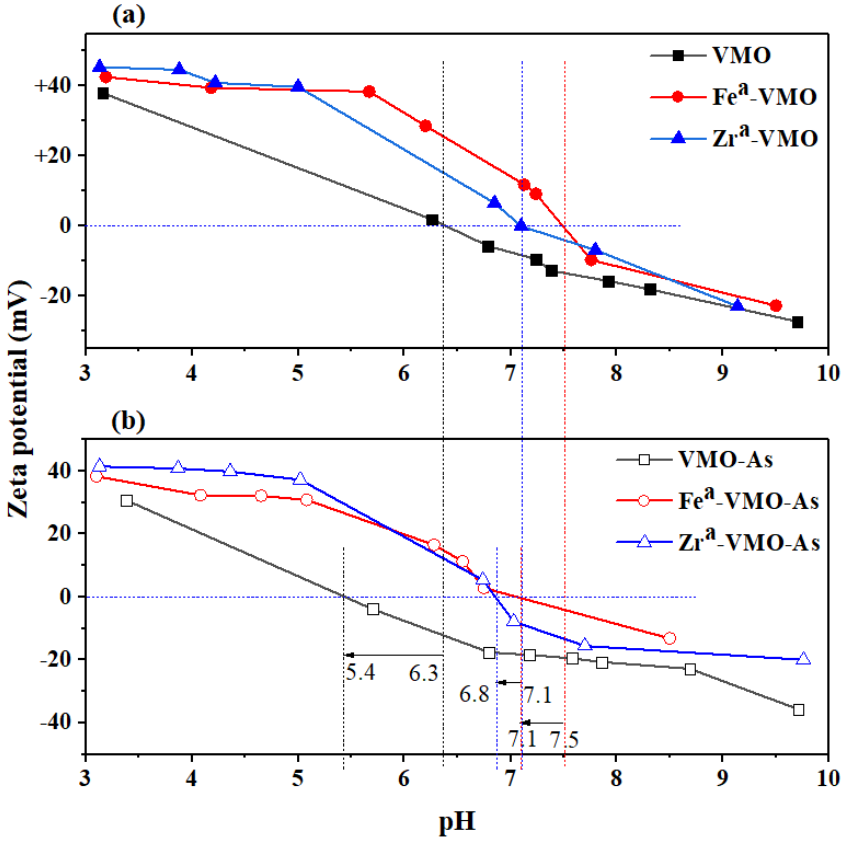

Fig. 3.4. Zeta potential of adsorbents (a) before and (b) after As(V) adsorption

3.3.2 Effect of particle size on As(V) adsorption

As(V) adsorption efficiency (E%) increased with adsorbent doses and reduction in particle size (Fig. 3.5). At the highest dosage of 5 g/L, the E% of particle size 1.0 – 2.0

mm was only 38% while that of smaller sizes of 0.3-0.6 mm and 0.6 – 1.0 mm reached up to 90% and 84%, respectively. With the original commercial size, which is a mix of all sizes (from 0.3 to 3 mm), E% was approximately 52%. The particle size of 0.3 – 0.6 mm was chosen for experimentation in the subsequent studies because of its highest E%.

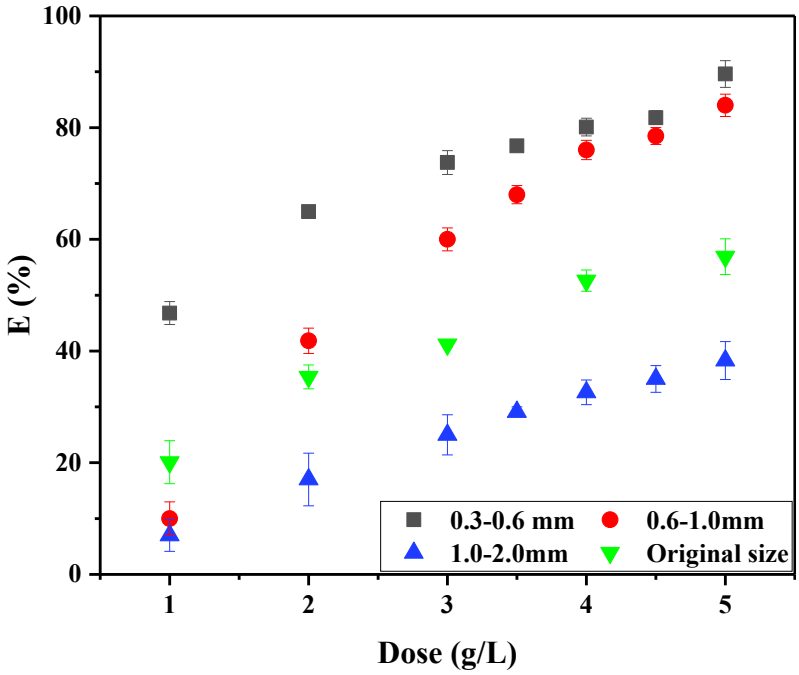

Fig. 3.5. Effect of particle size on As(V) removal efficiency

3.3.3 Effect of modification method on As(V) adsorption

Fig. 3.6 shows that the coating of Fe and Zr on VMO material has improved the material's capacity to remove As(V). However, the level of improvement strongly depended on the modification methods. The Fe^a-VMO and Zr^a-VMO had the highest improvement. At the dose of 1g, the As(V) removal efficiency of modified Fe^a-VMO and Zr^a-VMO was nearly five times higher than that of the unmodified VMO. The other three

modification processes were less effective and only a slight improvement in As(V) removal was observed.

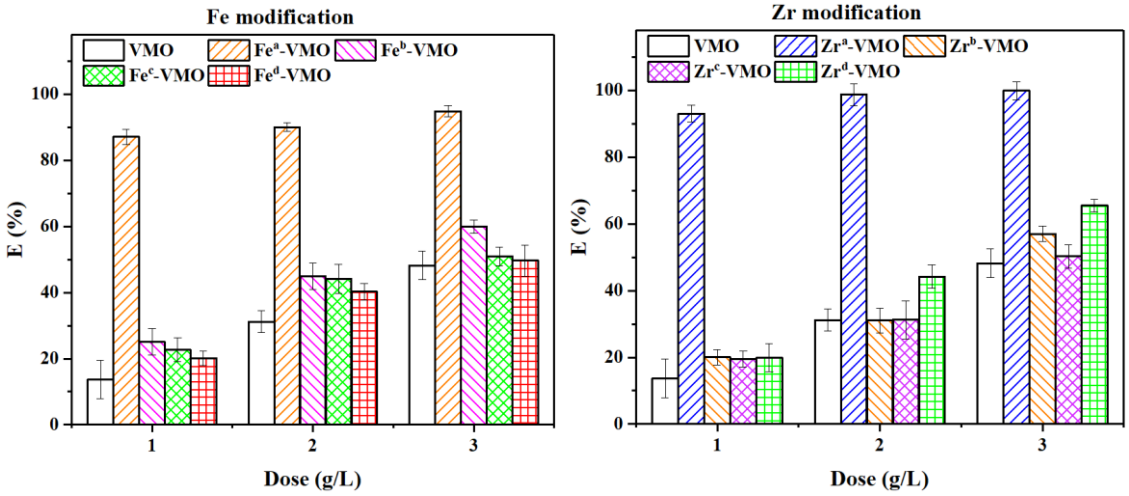

Fig. 3.6. Effect of different methods of VMO modification on As(V) removal efficiency

Temperature played an important role in the effectiveness of the modification processes. The Fe^{a} and Zr^{a} modification method applied to the production of Fe^{a}-VMO and Zr^{a}-VMO involved a light agitation followed by heating at high temperature of 110 ^{o}C and 550 ^{o}C. Here, the modification temperatures were higher than those used in the other three methods (less than 80 ^{o}C). At extremely high temperature, the coating agents might have adhered strongly to the surface of the VMO. Solutions used to wash Fe^{a}-VMO and Zr^{a}-VMO after their preparation were colourless compared to those in other preparations, suggesting strong coatings at high temperature. The Fe and Zr contents of these modifications were also higher than those produced at lower temperatures (Table 3.1). Moreover, a high temperature would also have raised the surface area of the samples

(Thirunavukkarasu et al. 2003). Based on these findings, Fe^a-VMO, Zr^a-VMO and unmodified VMO were used in the subsequent studies.

3.3.4 Batch adsorption studies

3.3.4.1 Equilibrium adsorption isotherms

The equilibrium adsorption experiments for the three adsorbents were conducted at pH 7.0 ± 0.2 with different adsorbent dosages. The Langmuir, Freundlich and Temkin models were employed to describe the data of the adsorption isotherms (Fig. 3.7). Table 3.3 shows that the experimental data fitted well to all three isotherm models with the Freundlich model having the best fit (R^2 = 0.90 – 0.97), followed by the Langmuir (R^2 = 0.87 – 0.95) and Temkin (R^2 = 0.82 – 0.95). Better fit to the Freundlich model is probably because of heterogeneous adsorption sites on VMO and modified VMO such as the different adsorption sites on Mn and Fe minerals (Fig. 3.2) and Zr and Fe coatings. The Langmuir adsorption capacity of VMO increased considerably after modification. Adsorption capacities of Fe^a-VMO and Zr^a-VMO were 2.19 mg As/g and 1.94 mg As/L, respectively. These values are nearly twenty times higher than that of the original VMO (0.11 mg As/g) (Table 3.3). It indicates that the presence of Fe^{3+} and Zr^{4+} on the surface of VMO improved significantly the As(V) adsorption capacity of VMO. The improvement is due to the strong adsorption of the anionic As species on Fe^{3+} and Zr^{4+} hydroxide/oxides on the surface of VMO (Loganathan et al. 2014; Sogaard 2014).

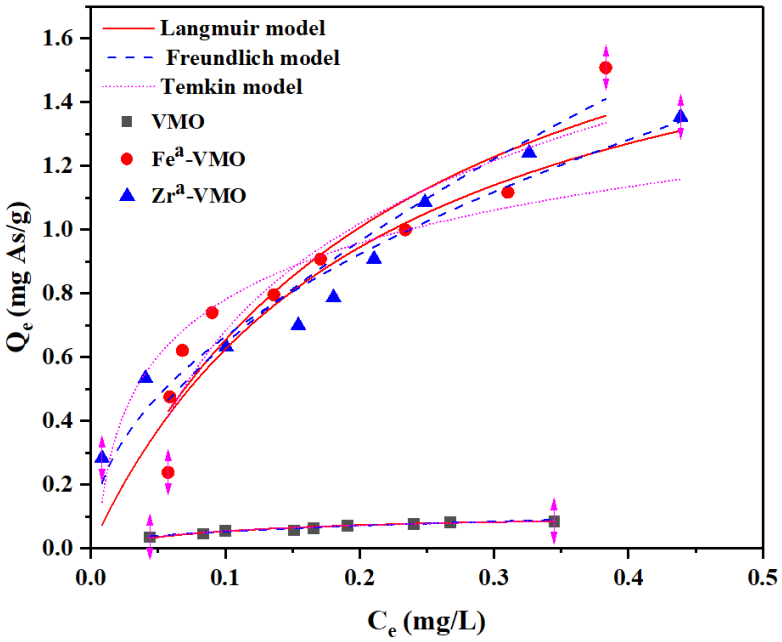

Fig. 3.7. Batch equilibrium adsorption models fit adsorption data for VMO and modified forms of VMO

The R_L value obtained from the Langmuir model fit indicates the nature of adsorption. Adsorption is considered unfavourable if $R_L > 1$, linear if $R_L = 1$, favourable if $0 < R_L < 1$ and irreversible if $R_L = 0$ (Dada et al. 2012). The calculated R_L data of VMO, Fe^a-VMO, Zr^a-VMO were 0.15, 0.24 and 0.23, respectively (Table 3.3). All these values are between 0 and 1 indicating that the adsorption process is favourable for both original and modified VMOs.

In contrast to the Langmuir model, the Freundlich model is used to depict the adsorption characteristics for the heterogeneous surface with multilayer adsorption (Dada et al. 2012). The calculated k_f parameter value from the Freundlich model decreased in the following order: Fe^a-VMO (2.48) > Zr^a-VMO (1.98) > VMO (0.14). This is in the same order of As(V) adsorption capacity calculated using the Langmuir model.

Additionally, all values of 1/n are below 1 indicating that the adsorption of As(V) by these adsorbents is favourable confirming the findings from Langmuir R_L values.

Unlike the Langmuir and Freundlich models, the Temkin model is usually used for heterogeneous surface energy systems (Erhayem et al. 2015; Shahmohammadi-Kalalagh 2011). It contains a factor that explicitly takes into account of adsorbent- adsorbate interactions (Dada et al. 2012). According to the calculated data in Table 3.3, the B values related to heat of sorption are positive indicating that the sorption process is exothermic and the values are higher for modified VMOs (Puttamat & Pavarajarn 2016).

Table 3.3. Parameter values for batch equilibrium adsorption models

Model	Parameter	Adsorbent		
		VMO	Fe[a]-VMO	Zr[a]-VMO
Langmuir	q_m (mg As/g)	0.11	2.19	1.94
	k_L (L/mg)	8.93	4.24	4.75
	R_L	0.15	0.24	0.23
	R^2	0.95	0.89	0.87
Freundlich	k_f (mg/g) $(L/mg)^{1/n}$	0.14	2.48	1.98
	N	2.34	1.70	2.11
	R^2	0.97	0.90	0.95
Temkin	A_T (L/g)	84.27	40.63	211.75
	B (J/mol)	0.025	0.49	0.26
	b_T	99.1	5.1	9.5
	R^2	0.95	0.90	0.82

In comparison with adsorbents that have similar iron oxide modification such as IOCS and IOCS-2, the modifications made in Fe^a-VMO and Zr^a-VMO improved the As(V) adsorption capacity considerably. For example, IOCS and IOCS-2 had As(V) adsorption capacity of 0.018 mg/g and 0.008 mg/g at initial As(V) concentration of 0.325 mg/L and 0.1 mg/L, respectively (Mohan & Pittman Jr 2007, Thirunavukkarasu et al. 2001). Nevertheless, in comparison with other natural manganese ores, As(V) adsorption capacity of unmodified VMO is lower. For instance, manganese oxide (MO1) from France had a capacity of 0.172 mg/g at an initial As(V) concentration (C_o) < 1 mg As(V)/L (Mohan & Pittman Jr 2007, Ouvrard et al. 2002).

3.3.4.2 Adsorption kinetics

The adsorption kinetics of original and modified VMO were conducted at pH 7.0 ± 0.2 with the same initial As(V) concentration of 0.5 mg/L. This kinetics study can help to understand the mechanism of adsorption of As(V) onto VMO and its modified forms (Puttamat & Pavarajarn 2016). The experimental results show that As(V) was adsorbed rapidly within the first 30 min when there were enough adsorption sites for As(V) adsorption (Fig. 3.8). Then, the process slowed down because of the gradual saturation of adsorption sites.

Pseudo-first order (PFO), pseudo-second order (PSO) and Elovich models were applied to investigate the adsorption kinetics of As(V). The values of model parameters and correlation coefficients obtained from the plots are presented in Table 3.4. According to the values of R^2, the PFO and PSO models fitted the data comparatively better than the Elovich model.

Finally, the Elovich model was used to describe the kinetics adsorption data. This model also explained the data well, though the R^2 values were slightly lower than those for PFO and PSO models. The good fit of the model to data is consistent with the chemisorption mechanism (Adeogun & Babu 2015; Firdaous et al. 2017; Önal 2006) for As shown by zeta potential data. The α value was much higher for Fe^a-VMO and Zr^b-VMO than for VMO (Table 3.4) indicating that the initial rate of adsorption was higher for the modified VMOs. This could be due to the increased affinity of Fe and Zr in VMO to As. However, the β value which is a reciprocal of the number of sites available for adsorption (Adeogun & Babu 2015), was higher for VMO, indicating that the number of sites available for adsorption was lower for VMO with higher activation energy for chemisorption on VMO (Firdaous et al. 2017).

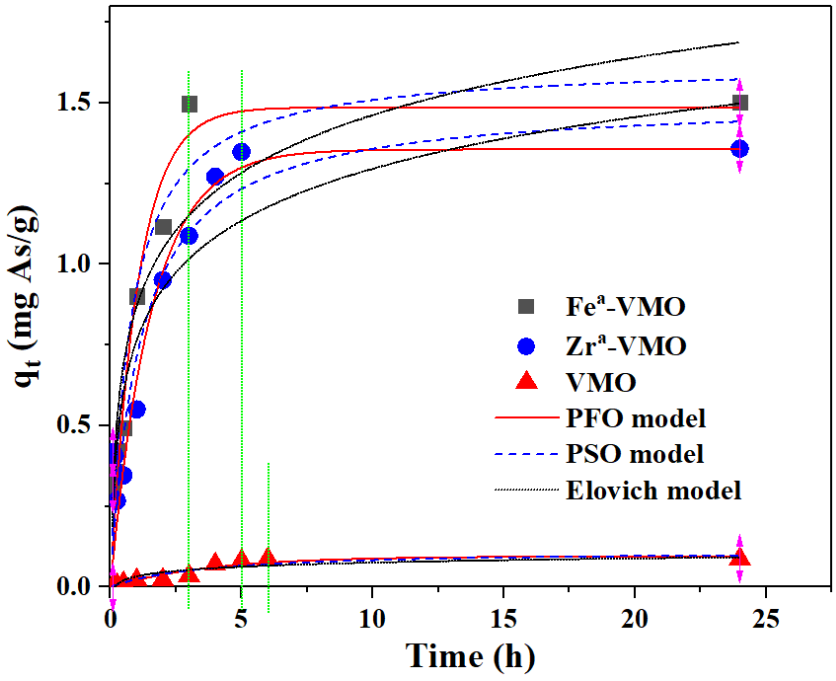

Fig. 3.8. Adsorption kinetics models fit to the data on As(V) adsorption on modified and un-modified VMO

Table 3.4. Parameter values for batch adsorption kinetics

Model	Parameter	Adsorbent		
		VMO	Fe^a-VMO	Zr^a-VMO
	q_{exp} (mg As/g)	0.09	1.50	1.36
PFO	q_e (mg As/g)	0.10	1.49	1.36
	k_1 (1/h)	0.26	0.96	0.63
	R^2	0.92	0.94	0.88
PSO	q_e (mg As/g)	0.11	1.62	1.51
	k_2 (g/mg.h)	2.42	0.82	0.59
	R^2	0.89	0.94	0.88
Elovich	α (mg/g.min)	0.002	0.125	0.105
	β (g/mg)	53.8	3.88	4.32
	R^2	0.82	0.88	0.83

3.3.4.3 Influence of pH on As(V) adsorption

The As(V) adsorption depends on the pH of the solution because pH affects the protonation/deprotonation of the adsorbate, the surface charge of the adsorbents, the degree of ionisation of the surface groups and the nature of the adsorbing ions (Puttamat & Pavarajarn 2016; Worch 2012). Fig. 3.9 illustrates a significant decline in the As(V) adsorption efficiency (E%) when the pH rose from 3 to 10 for all three adsorbents. This phenomenon is due to the decrease in positive zeta potential or increase in negative zeta potential as pH increased from 3 to 10 (Fig. 3.4). The increase in surface negative charge

repels the negatively charged As(V) anions. Also, the negative charge on the As(V) anions increases as pH increases producing unfavourable conditions for adsorption. Another reason for the decreased adsorption at high pH is that at high pH the concentration of OH^- anions increases and it competes with As(V) for adsorption. Others have also reported a reduction in As(V) adsorption when pH increases for other adsorbents (Camacho et al. 2011, Wu et al. 2017).

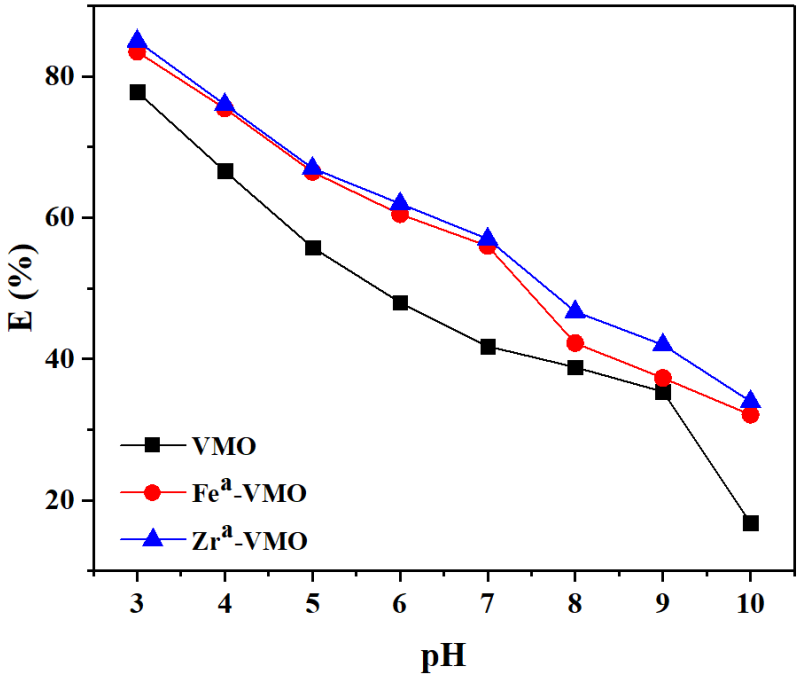

Fig. 3.9. Influence of pH on As(V) removal efficiency of VMO (3.0 g/L), Fe^a-VMO (0.3 g/L) and Zr^a-VMO (0.3 g/L)

3.3.4.4 Effect of co-existing anions on As(V) adsorption

In nature, many ions are present along with As in water and some of them can impact the As adsorption ability of an adsorbent. In this study, the prominent anions

present in water, PO_4^{3-}, SO_4^{2-}, SiO_3^{2-} and CO_3^{2-}, were selected for analysis at different concentrations (0.1, 1, 5, 10, 20 mg/L) to evaluate their effects on As(V) adsorption.

As can be seen from Fig. 3.10, at the lowest concentration of 0.1 mg/L, all anions exerted only minor influence on As(V) adsorption efficiency. When their concentration increased to more than 5 mg/L, the effect of PO_4^{3-} and SiO_3^{2-} was significantly higher than that of CO_3^{2-} and SO_4^{2-}. This observation is consistent with previous studies, which reported silicate and phosphate competing with As for adsorption (Ciardelli et al. 2008). The presence of 20 mg/L of PO_4^{3-} in solution reduced the As removal efficiency of the three adsorbents by about 60 – 70%. The effect of SiO_3^{2-} followed that of PO_4^{3}- with reductions of 47%, 34% and 26% As(V) removal efficiency of VMO, Fe^{a}-VMO and Zr^{a}-VMO, respectively. This is because these oxyanions were strongly adsorbed by $M(OH)_n$, where M is a metal ion such as Fe^{3+}, Mn^{4+}, Zr^{4+}, etc. The oxyanion, CO_3^{2-} and SO_4^{2-}, did not have much effect on As removal. Consequently, the sequence of competitive anions hindering the sorption of As(V) is $PO_4^{3-} > SiO_3^{2-} > CO_3^{2-} > SO_4^{2-}$. Gu et al. (2005) and Ren et al. (2011) also reported that PO_4^{3-} and SiO_3^{2-} reduced As(V) adsorption on Fe modified GAC more than CO_3^{2-} and SO_4^{2-}.

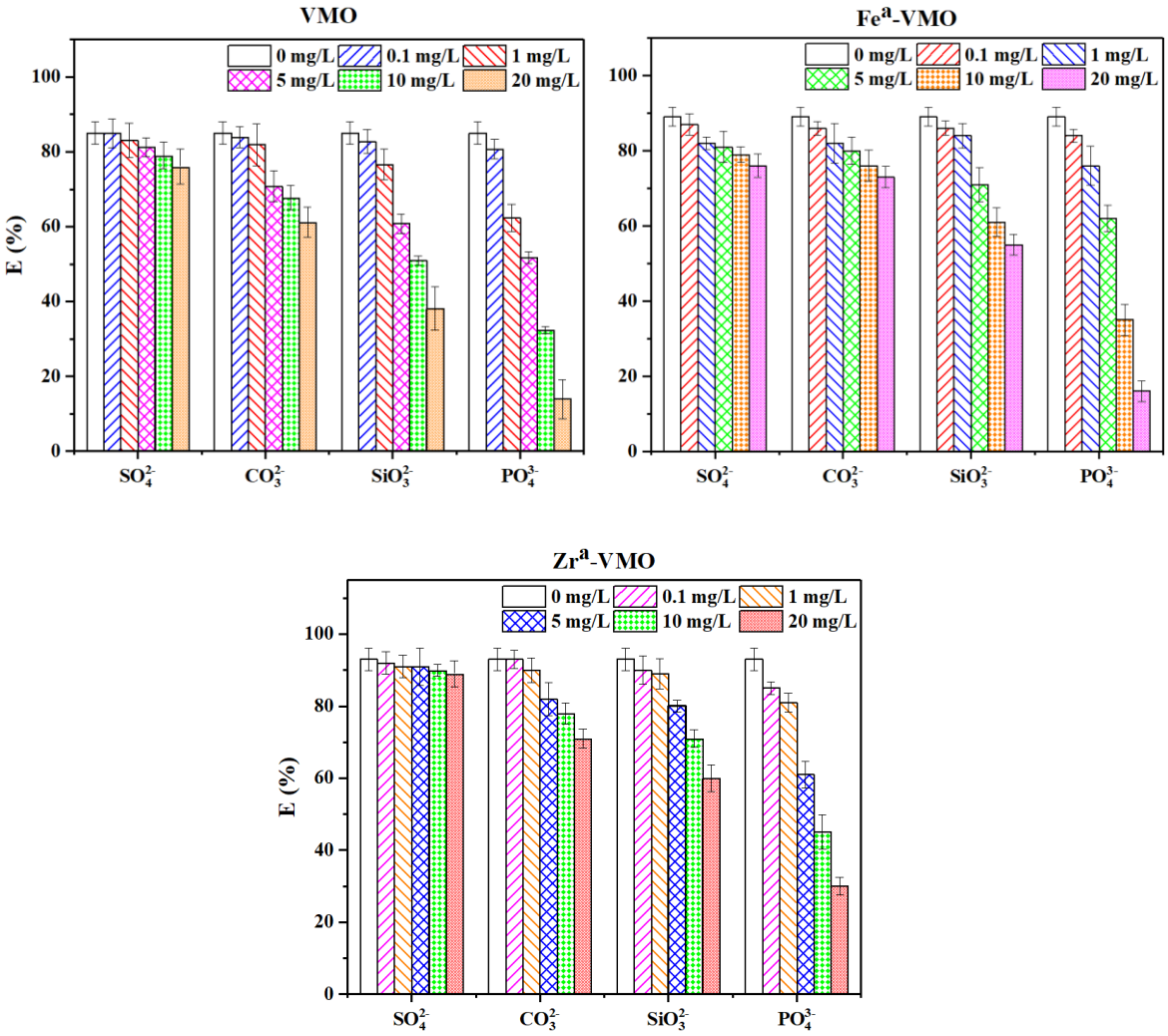

Fig. 3.10. Effects of co-existing anions on As(V) removal at fixed initial As(V) concentration of 0.5 mg/L

3.3.5 Column studies

The column studies were carried out to evaluate the adsorption capacity of the adsorbents in dynamic conditions, and the effects of flow rate, and initial As(V) concentration on As(V) breakthrough. Fig. 3.11 and 3.12 show the breakthrough curves of 9 columns belonging to original and modified VMOs at the flow rates of 0.15 and 0.5 L/h and influent As(V) concentrations of 0.1 and 0.25 mg/L, respectively. The bed

volumes (B.V.) at different times of breakthrough were calculated using the following formula where the flow rates 0.15 and 0.5 L/h correspond to 1.9 and 6.4 m/h, respectively (Kalaruban et al. 2019):

B.V. = flow rate (m/h) x time of breakthrough (h)/bed height (m) [3.5]

At any initial concentration and flow rate, the breakthrough curves of VMO were steeper than those of Fe^a-VMO and Zr^a-VMO (Fig. 3.11 and 3.12). It means that VMO was saturated faster (at lower B.V.) than others did. Furthermore, the breakthrough curves of Zr^a-VMO were steeper than those of Fe^a-VMO. Consistent with the shapes of the breakthrough curves, the adsorption capacities of the three adsorbents followed the order, Fe^a-VMO > Zr^a-VMO > VMO (Table 3.6). This order is the same as that observed in the batch experiments for these three adsorbents.

The effect of the flow rate is depicted in Fig. 3.11. It can be seen that at the higher flow rate (0.5 L/h), the breakthrough curves were steeper, and the plateau of C_t/C_o for all adsorbent columns occurred earlier (at lower B.V.) in comparison with those at the lower flow rate (0.15 L/h). This tendency has also been reported for adsorption of phosphate on ion exchange resin (Nur et al. 2014), As (V) adsorption on Fe grafted GAC (Kalaruban et al. 2019), and magnetite/hematite/organic carbon composite (Li et al. 2018). These trends were explained as due to the larger amounts of As passing through the column per unit time at the higher velocity, resulting in a higher proportion of the available adsorption sites on the adsorbent getting saturated (Nur et al. 2014). The results also showed that at both flow rates, the B.V. required for adsorbent saturation was higher for the adsorbent with greater adsorption capacity (Fe^a-VMO > Zr^a-VMO > VMO). The adsorption

capacities of the modified adsorbents are many times higher than the adsorption capacity of the unmodified adsorbent, as found in our earlier batch study (Table 3.5).

At As(V) initial concentration of 0.1 mg/L and the flow rate of 0.15 L/h, the B.V. of treated water by Zr^a-VMO and Fe^a-VMO, which had As(V) concentration below WHO guidelines (C_{WHO} = 10 µg/L), was 6 and 8 times higher than for VMO, respectively. When the flow rate was increased (0.5 L/h), the B.V. of treated water at C_{WHO} was 12 for Zr^a-VMO and 16 for Fe^a-VMO times, respectively higher than for unmodified VMO (Table 3.5). This means that much larger amounts of As(V) contaminated water can be treated to produce water with safe levels of As(V) by the modified VMOs rather than the unmodified VMO. Such larger amounts of treated water generated by the modified VMOs would lead to a reduction in the cost of the treatment process per unit volume of water produced. This cost reduction is expected to cover the cost of Fe/Zr modification of VMO. The number of B.V. treated is higher at the lower flow rate because the retention time of As(V) in the column is longer, which allowed more effective interaction of As(V) with the adsorbent leading to larger amounts of it being removed (Kalaruban et al. 2019; Li et al. 2018). This is confirmed by the higher As(V) adsorption capacity at the lower flow rate (Table 3.5). These results indicate that a higher volume of treated water can be produced by reducing the flow rate.

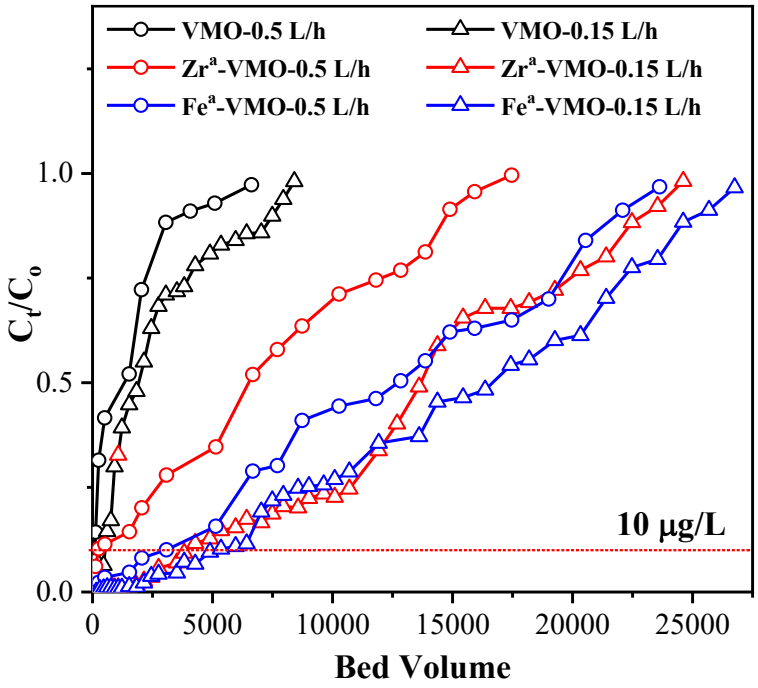

Fig. 3.11. The effect of flow rate on As(V) adsorption breakthrough in VMO, Fe^{a}-VMO, and Zr^{a}-VMO columns at an initial As(V) concentration of 0.1 mg/L. The 10 µg/L horizontal line within the figure indicates the WHO As concentration limit.

Table 3.5. The bed volumes of water treated by original and modified VMO to reduce As(V) concentration to WHO guideline concentration (10 µg/L) and the amount of As(V) adsorbed on adsorbents

Flow rate (L/h)	Adsorbent	Initial As(V) concentration (mg/L)	Bed volume	As(V) adsorption capacity (mg/g)
0.5	VMO	0.1	127	0.013
	Zr^a-VMO	0.1	1541	0.079
	Fe^a-VMO	0.1	2055	0.115
0.15	VMO	0.1	611	0.016
	Zr^a-VMO	0.1	3822	0.217
	Fe^a-VMO	0.1	4892	0.276
0.15	VMO	0.25	153	0.021
	Zr^a-VMO	0.25	2293	0.320
	Fe^a-VMO	0.25	2752	0.388

Fig. 3.12 shows the effect of the initial concentration of As(V) on As(V) removal at the same flow rate (0.15 L/h). The data showed that the columns operated with higher initial concentration (0.25 mg/L) would reach As(V) saturation faster than those at a lower initial concentration (0.10 mg/L). Therefore, these columns treated fewer B.V., and the breakthrough curves reached plateau faster than those at the lower As(V) concentration. This is because larger amounts of As(V) enter the column at higher initial concentrations, and the adsorption sites are used up more quickly than when low As(V) concentration enters the columns. Li et al. (2018) also reported that an increase in the initial As(V) concentration reduced the time taken for the saturation of columns containing

magnetite/hematite/organic carbon composite. However, when the initial concentration rose, although the number of B.V. decreased, the As(V) adsorption capacity also increased (Table 3.5). This can be explained by the fact that at the higher initial concentration, more available adsorption sites were occupied by As(V) rapidly (Han et al. 2009).

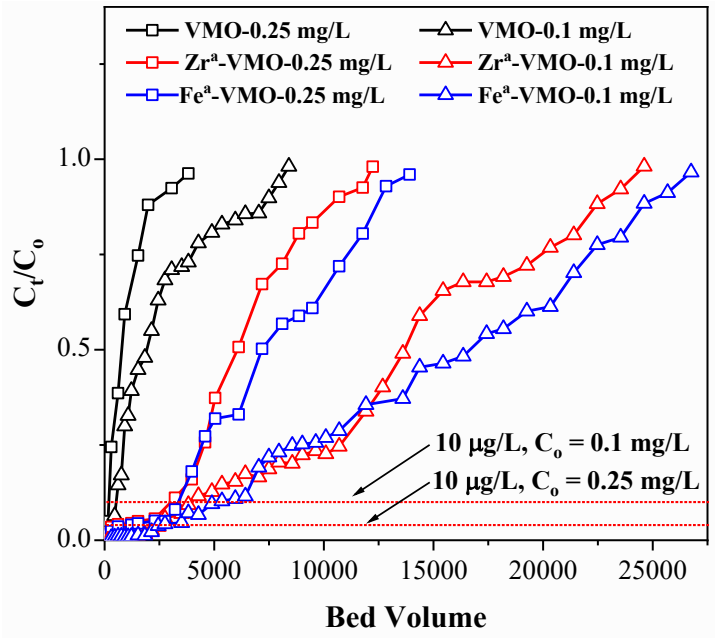

Fig. 3.12. The effect of As(V) initial concentration on As(V) removal by VMO, Fe^a-VMO, and Zr^a-VMO at the flow rate of 0.15 L/h. The 10 µg/L horizontal line within the figure indicates the WHO As concentration limit.

The Thomas model was used to describe the experimental data obtained in the column studies on the effect of flow rate (Fig. 3.13) and initial concentration (Fig. 3.14). Table 3.6 presents the results of the model fits data. At the same C_o, as the flow rate increased, the value of rate constant K_{Th} also increased, but the As(V) adsorption capacity

q_T decreased. Conversely, at the same flow rate, the value of q_{Th} increased, and K_{Th} decreased when C_o increased. Therefore, a higher C_o, along with a slower flow rate, would increase the As(V) adsorption capacity of adsorbent in the column study (Table 3.6) (Han et al. 2009). The reasons for these trends were explained in the previous section. The R^2 values were very high (> 0.92, that is > 92% of the variance in the data is explained by the model. The correlation coefficient r, which is the square root of R^2 is > 0.96 and this is very highly significant (Preece 1982)), indicating that the experimental data fitted very well to the Thomas model. This model can predict the adsorption performance very well under various experimental conditions. According to the prediction of the Thomas model, the maximum As(V) adsorption capacities of VMO, Zr^a-VMO, and Fe^a-VMO were 0.151, 0.925, and 1.145 mg/g, respectively, for C_o = 0.25 mg/L, and Q = 0.15 L/h (Table 3.6).

The adsorption capacities calculated from the breakthrough curves (q_{exp}) were only slightly lower than the respective Thomas adsorption capacities (Table 3.6), suggesting that the breakthrough curves almost reached the plateau point (adsorbent saturation). The Thomas adsorption capacities for the modified adsorbents at the higher concentration and lower flow rate (Zr^a-VMO and Fe^a-VMO with 0.925 and 1.145 mg/g, respectively) are much lower than the Langmuir maximum adsorption capacities (Zr^a-VMO and Fe^a-VMO with 1.94 and 2.19 mg/g, respectively) determined in batch experiments. The column adsorption capacities are lower than the batch adsorption capacities because in the batch experiments, adsorption reached equilibrium, and the Langmuir model predicted the maximum adsorption capacities at a higher solution As(V) concentrations (Kalaruban et al. 2019). These conditions were different in the column experiment, where the adsorption capacities were measured at lower concentrations, and adsorption did not reach equilibrium. However, for the unmodified VMO, the adsorption capacities between the

Thomas and Langmuir models calculated values were not very different, probably because of the very low adsorption capacity of VMO where maximum adsorption occurs at lower As concentrations.

The Thomas adsorption capacities obtained in this study were compared with those reported for other adsorbents in Table 3.7. The data shows that most adsorbents had adsorption capacity lower than VMO and its modified forms, except rice husk. However, the modified VMOs, Fe^a-VMO and Zr^a-VMO, had much higher adsorption capacities than all the other adsorbents.

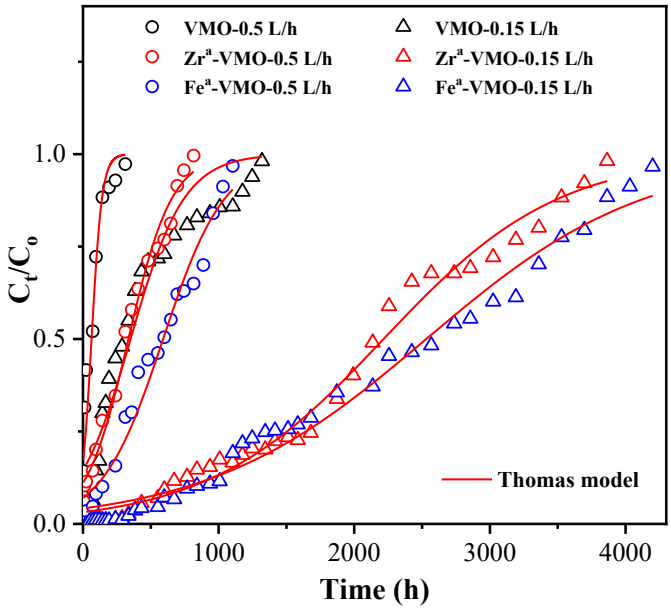

Fig. 3.13. Non-linear Thomas model fits to data on the removal of As(V) by VMO, Fe^a-VMO, and Zr^a-VMO at the two flow rate (C_o = 0.1 mg/L).

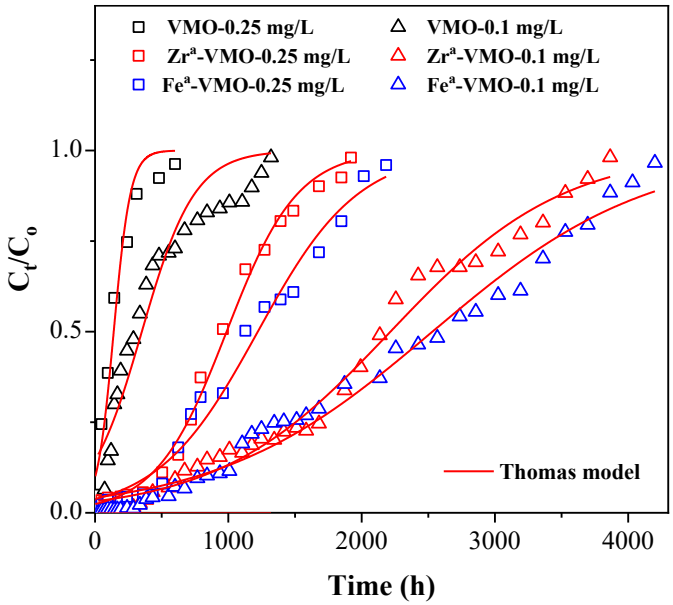

Fig. 3.14. Non-linear Thomas model fits to data on the removal of As(V) by VMO, Fe[a]-VMO, and Zr[a]-VMO at the two initial concentrations (Q = 0.15 L/h)

Table 3.6. Parameter values for the Thomas model fit to breakthrough data of columns loaded with VMO, Fe[a]-VMO, and Zr[a]-VMO.

Column	C_o = 0.1 mg/L Q = 0.15 L/h			C_o = 0.1 mg/L Q = 0.5 L/h			C_o = 0.25 mg/L Q = 0.15 L/h		
Adsorbent	VMO	Zr[a]-VMO	Fe[a]-VMO	VMO	Zr[a]-VMO	Fe[a]-VMO	VMO	Zr[a]-VMO	Fe[a]-VMO
q_{exp} (mg/g)	0.136	0.799	0.901	0.096	0.400	0.700	0.142	0.879	1.074
q_T (mg/g)	0.139	0.831	0.949	0.098	0.422	0.744	0.151	0.925	1.145
K_{Th} (L/h/mg)	0.043	0.015	0.012	0.258	0.062	0.044	0.037	0.015	0.011
R^2	0.92	0.98	0.98	0.94	0.98	0.97	0.96	0.99	0.98

Table 3.7. Comparison of Thomas adsorption capacities obtained in the current study with those reported in other studies

Adsorbent	As (V) concentration (mg/L)	Flow rate (L/h)	Thomas adsorption capacity (mg/g)	Reference
Multi walled carbon nanotubes	0.04	1.20	0.014	Ali (2018)
Rice husk	0.07	0.42	0.416	Asif & Chen (2017)
Natural pozzolan	0.40	0.24	0.003	Kofa et al. (2015)
Thioglycolated sugarcane carbon	1.50	0.18	0.083	Roy et al. (2013)
VMO	0.25	0.15	0.151	This study
Zr^a-VMO	0.25	0.15	0.925	This study
Fe^a-VMO	0.25	0.15	1.145	This study

3.3.6 Cost estimation for treatment

The market price of VMO is A$0.40/kg (including transportation and grinding). The costs of the modified VMOs are calculated using the industrial prices of the chemicals, $Fe(NO_3)_3 \cdot 9H_2O$ (A$0.40/kg), $ZrOCl_2.8H_2O$ (A$1.64/kg), and NaOH (A$0.30/kg) employed in the modification procedure (prices of the chemicals are obtained from https://www.alibaba.com) and the quantities of the chemicals used in the modification. The quantities of the chemicals used are obtained from section 3.2.3. Based on this calculation, the cost of Fe^a-VMO and Zr^a-VMO were estimated to be A$0.80/kg and A$1.67/kg, respectively.

The cost of treating 1 m^3 water containing 0.1 mg As(V)/L to produce safe drinking water (<10 µg As/L) was calculated by multiplying the cost of the adsorbent by the weight of adsorbent in the column (40 g) divided by the volume of water treated (m^3). The volumes of water treated by VMO, Zr^a-VMO, and Fe^a-VMO at the flow rate of 0.15 L/h, initial As(V) concentration of 0.1 mg/L are 0.0144 m^3, 0.0900 m^3, and 0.1152 m^3, respectively (time (h) taken to reach 10 µg As/L in treated water x flow rate (L/h)/1000 L/m^3). Based on this calculation, the costs of treating 1 m^3 water by VMO, Zr^a-VMO, and Fe^a-VMO are estimated to be A$1.111, A$0.742, and A$0.278, respectively.

The lower treatment costs of the modified VMOs compared to the unmodified VMO is due to the larger volumes of water treated, despite their higher costs. The treatment cost of Fe^a-VMO is lower than that of Zr^a-VMO because its production cost is lower, and it treated a higher volume of water. The cost calculated here applies only to a single use of the adsorbents until they get exhausted to produce safe levels of As in the treated water. However, the exhausted adsorbents can be regenerated by desorbing the adsorbed As and repeatedly used. Repeated use of the adsorbents will considerably decrease the cost of the treatment.

Kalaruban et al. (2019) reported that at effluent As(V) concentration below WHO guidelines (0.01 mg/L), As(V) adsorption capacity of the Australian commercial GAC in the column study was 0.118 mg/g, about 7 times higher than that of original VMO (0.016 mg/g) at the same experimental conditions (initial As(V) concentration of 0.1 mg/L and flow velocity of 2.0 m/h). However, after chemical modification, the As(V) adsorption capacities of modified VMOs (0.276 mg/g Fe^a-VMO and 0.217 mg/g Zr^a-VMO) were higher than that of Australian's GAC. In addition, the costs of modified VMOs were much lower (A$0.8/kg Fe^a-VMO and A$1.67/kg Zr^a-VMO compares with A$3.0/kg of GAC).

According to an internal report of the project 'A low energy gravity fed membrane adsorption system for As and bacteria removal from groundwater in developing countries' (Nguyen, 2018), the Langmuir As(V) adsorption capacities of two commercial GAC from Vietnam) were much lower, only 0.04 and 0.07 mg/g. The costs of the two GAC were A$0.8 and A$2.0/kg, respectively. The treatment costs by GAC are higher than original and modified VMOs. It shows that the low-cost absorbents in this study are promising to use.

3.4 Conclusions

As a low-cost commercial adsorbent, VMO was employed to remove As from groundwater in many treatment systems in Vietnam. However, the As(V) removal capacity of pure VMO is not high.

In four different modification methods studied, mixing VMO with ferric nitrate or zirconium nitrate and sodium hydroxide followed by heating at 110 ^{o}C and 550 ^{o}C emerged as the best modification method for improving As(V) removal. The Langmuir adsorption capacities of the modified materials, Fe^{a}-VMO and Zr^{a}-VMO at pH 7.0 were 2.19 and 1.94 mg As/g, respectively, which are approximately 20 times higher than that of the unmodified VMO. Zeta potential data showed that the better As(V) adsorption by the modified adsorbents could be due to inner-sphere complexation of As(V) with Fe and Zr oxide/hydroxides coatings on VMO, as well as outer-sphere complexation of As(V) with the Fe/Mn coatings which provided increased positive charges for electrostatic adsorption of negatively charged As species. Langmuir, Freundlich and Temkin models were applied successfully to describe the equilibrium adsorption of As(V) onto the

original and modified VMO. The adsorption kinetics data also fitted well to the three models, pseudo-first order, pseudo-second order and Elovich models. The As(V) removal efficiency increased by up to 50 – 60% when pH was progressively decreased from 10 to 3. The PO_4^{3-} and SiO_3^{2-} co-ions had a strong competitive effect on As(V) removal efficiency. In contrast, the ions, CO_3^{2-} and SO_4^{2-} had little influence on As removal.

As(V) was effectively removed from water in columns packed with the original VMO or modified VMOs. The As(V) adsorption capacity and the number of B.V. of contaminated water that can be treated to maintain the As(V) concentration below the WHO guideline concentration (C_{WHO} = 10 µg/L) increased in the order, VMO < Zr^a-VMO < Fe^a-VMO. An increase in the initial As(V) concentration increased the adsorption capacity, but an increase in the flow rate of As(V) solution through the column reduced the adsorption capacity of the adsorbent. The results indicated that higher volumes of treated water could be produced by reducing the flow rate. The Thomas model satisfactorily described the column breakthrough curves.

CHAPTER 4

Iron and zirconium modified *luffa* fibre as an effective bioadsorbent to remove arsenate from drinking water

Chapter 4. Iron and zirconium modified *luffa* fibre as an effective bioadsorbent to remove arsenate from drinking water

Summary

Chapter 4 presents the second finding about a bioadsorbent, namely *luffa* fibre (LF), and it modified forms, namely FLF-3 and ZLF-3 in removing As(V) from drinking water. The study was published in the Journal of Chemosphere (Q1 journal, impact factor: 5.78) in 2020, as below.

Nguyen, T.T.Q., Loganathan, P., Nguyen, T.V., Vigneswaran, S. & Ngo, H.H. 2020, 'Iron and zirconium modified *luffa* fibre as an effective bioadsorbent to remove arsenic from drinking water', *Chemosphere*, p. 127370.

This work presents another novel bioadsorbents (LF, FLF-3, ZLF-3) in removing As(V) from water. In this chapter:

- Original LF was grafted with Fe and Zr in three coating cycles in order to produce novel media which had higher adsorption capacities.
- Batch and column studies were conducted to identify the As(V) adsorption capacity and treatment cost.
- Evaluation of the effects of aqueous environmental conditions on the As(V) adsorption (e.g. pH, co-existing anions).
- Testing the adsorbent characteristics to determine the adsorption mechanism.

4.1 Introduction

Arsenic (As) is classified as a Class I human carcinogen because it is very toxic to people's health through the food chain and drinking water (Niazi et al. 2018). High doses of inorganic As cause a number of diseases related to the skin, lungs, and other organs such as vascular disease, renal disease, neurological problems, cardiovascular disease, and chronic lung disease (Berg et al. 2007; Mohan & Pittman Jr 2007). Two of the most toxic species of As in natural aqueous systems are trivalent (arsenite, As(III)) and pentavalent (arsenate, As(V)) ions (Berg 2007). Generally, As(III) exists under mildly reducing conditions in the non-ionised form (H_3AsO_3) at pH < 9 and changes to ionised form ($HAsO_3^{2-}$) at pH > 9. While As(V) predominantly presents in oxidising conditions and exists in the ionised form ($H_2AsO_4^-, HAsO_4^{2-}, AsO_4^{3-}$) in a wide range of pH (pH 2 – 14). As in water is derived from both natural and anthropogenic sources. The major industrial processes that lead to As contamination are smelting of non-ferrous metals, combustion of fossil fuels, and manufacture and use of arsenical pesticides and wood preservatives. In nature, As could be found in minerals (e.g. pyrite) and hydrothermal veins (Sogaard 2014), which on weathering release As to surface and ground waters and sediments. The most common As concentration of highly contaminated groundwater sources is around 0.1 – 0.5 mg/L, which is much higher than the WHO's guideline on drinking water for As (0.01 mg/L) (Nguyen et al. 2020a).

Because As is very dangerous to humans, scientists have implemented various strategies to remove As from drinking water. As well as the As removal efficiency feature of these methods, their cost-effectiveness, sustainability, and environmental-friendliness are prominent concerns. Among the numerous As removal techniques such as coagulation, adsorption, ion exchange, and membrane separation, adsorption is an

efficient, cost-effective, and relatively easy-to-use method with minimum waste generation (Mohan & Pittman Jr 2007). Several natural and synthetic adsorbents have been explored and used widely. Low-cost adsorbents consist of natural materials such as manganese ore, goethite, pisolite, red mud, dry plant materials, etc. (Chiban et al. 2012; Mohan & Pittman Jr 2007). Of these, adsorbents derived from plants have been considered promising media for removing pollutants from water because of their environmental friendliness, low cost, local availability, and sustainability (Abu-El-Halawa et al. 2003, Chiban et al. 2009).

Luffa fibre (LF) is a material derived from the *luffa* plant. The *luffa* plant belongs to the family of *Cucurbitaceae* and is widespread in subtropical and tropical areas, especially in Southeast Asia, South Asia, Africa, and South America (Chen et al. 2014; Wang et al. 2017). The internal structure of old cylindrical *luffa* is a fibre-connecting porous and open-cell foam material with the pattern of branched fibres (Chen et al. 2014). It contains cellulose/hemicellulose, lignin, proteins, amino acids, polypeptides, glycosides, and other inorganic compounds (Chen et al. 2014). *Luffa* is used widely as food (the young and fresh variety), daily household cleaning material, and as a packaging material (the old and dry variety) (Chen et al. 2014; Wang et al. 2017). In the environmental field, it can be used in many applications. For example, natural *luffa* cylindrical fibre has been trialled as an adsorbent to remove methylene blue dye, phenol, and lead from aqueous solutions (Abdelwahab & Amin 2013; Adewuyi & Pereira 2017; Demir et al. 2008). However, it has not been used as an adsorbent for removing As from drinking water.

In this research, LF with and without chemical modification was used to remove As(V) from water. To enhance the adsorption capacity of the original LF, the LF material

was modified by grafting it with iron (Fe) and zirconium (Zr) separately. These metals were selected for grafting for two reasons: firstly, high affinity of their oxides/hydroxides to As adsorption; and secondly, their safety as regards to human health (Nguyen et al. 2020b). The hydroxyl and carboxylic groups on the surface of LF can specifically adsorb Fe and Zr which are known to have high adsorption capacity towards As(V) (Adewuyi & Pereira 2017, Gupta et al. 2013, Kalaruban et al. 2019, Nguyen et al. 2020b). The performance of original and modified LF on As(V) removal from synthetic water was evaluated through batch and column adsorption studies. Whilst the outcomes of the batch studies could use to assess the performance of these adsorbents, the column studies were conducted to assess the application capability of them on a decentralized scale. The effects of pH and coexisting anions on the adsorption process were also evaluated. The novelty of this present study is that it is the first to compare As removal performance of a bioadsorbent originating from a commonly cultivated plant (*luffa*) before and after chemical modification with two metals, Fe and Zr, having very high As adsorption capacities in both batch and column-based experiments. Zeta potential and FTIR measurements are used to explain the Fe and Zr complexation on LF and adsorption of As on the metals-grafted LF. Previously, column-based studies that have direct relevance to practical treatment-plant operations have rarely been reported for As adsorption by bioadsorbents.

4.2 Material and Methods

4.2.1 Feed solution

A synthetic stock solution was prepared by dissolving 4.165 mg sodium arsenate ($Na_2HAsO_4 \cdot 7H_2O$) in 1 L Milli-Q water to obtain a concentration of 1 mg As(V)/L. The

stock solution was diluted to the desired concentration of 0.5 mg/L for batch studies and 0.1 mg/L for fluidised column studies. These concentrations are typical of As contaminated groundwater in many countries. The ionic strength of the solution in batch studies was maintained at 1 mM $NaNO_3$. The solution pH was also adjusted to 7.0 ± 0.2 (except from 3 to 10 in the study on the effect of pH on As adsorption) by adding 0.1 M HNO_3 or 0.1 M NaOH.

4.2.2 *Luffa* material

4.2.2.1 Original material

The raw dry *luffa* appears as a cylindrical sponge column supported by a fibrous network (Fig. S4.1). The *luffa* column has four major areas, these being the inner surface, outer surface, interlayer, and core. They grow in different directions, for instance, the longitude, circumferential, and radial directions. LFs include small empty channels with an internal diameter of 1 – 10 μm. Old *luffa* fruits with dark brown peel were collected from a household in My Duc rural district, Hanoi, Vietnam. It was naturally sun-dried and the *luffa* fibre (in the form of cylinder sponge) was separated. The LF was cut into small pieces manually and crushed to the size of 0.5 – 1 mm using a grinder. It was then washed by deionised distilled water, dried at 70 ^{o}C, and stored in airtight containers.

4.2.2.2 Modified materials

The procedure employed by Gu et al. (2005) was modified and used to prepare iron (Fe)-grafted luffa fibre (FLF) and zirconium (Zr)-grafted luffa fibre (ZLF). The modification method comprised the following three steps.

Step 1: 10 g dried LF of size 0.5 – 1 mm was added into a 150 mL solution of 0.1 M ferrous chloride tetrahydrate ($FeCl_2.4H_2O$). The pH of the suspension reduced to approximately 2.0 probably due to the hydrolysis of Fe 0.1 M NaOH was added to the solution to raise the pH to 4.2 - 4.5, and the mixture was agitated at 120 rpm for 24 h at room temperature (25 ± 1 °C).

Step 2: FLF produced in Step 1 was separated from the above mixture and dried at 70 °C for 24 h. The material was then washed with Milli-Q water till the brown coloured fraction (excess iron) was removed, and the remaining fibre dried again at 70 °C for 24 h to produce FLF-1.

Step 3: To enhance the degree of grafting, the FLF-1 was grafted once and then twice more using the above procedure to produce FLF-2 and FLF-3, respectively. After cooling, all FLFs were stored in airtight containers for testing.

ZLF-1, ZLF-2, and ZLF-3 were also produced using the same methods except by mixing LF with 0.1 M zirconyl chloride octahydrate ($ZrOCl_2.8H_2O$) instead of ferrous chloride tetrahydrate. When the Zr salt was added, the pH reduced to around 2.0 and NaOH was added to raise the pH to 4.2 – 4.5 as in the case of Fe salt addition described above.

4.2.3 Comparison of the As adsorption capacity of different *luffa* modifications

In order to compare the adsorption capability of new adsorbents produced from the two kinds of grafting agents and grafting cycles, three different amounts of modified LFs (0.02, 0.05 and 0.07 g) were mixed with 100 mL As(V) solution of 0.5 mg/L and shaken at 120 rpm for 24 h. The initial pH and ionic strength of the solution were 7.0 ± 0.2 and

1 mM $NaNO_3$, respectively. After shaking the suspensions, the supernatant was filtered using 0.45 μm filters, and the filtrates were analysed for As using an ICP-MS instrument (Agilent Technologies 7900 ICP-MS). The results (presented in Section 4.3.1) demonstrated that FLF-3 and ZLF-3, which were LF grafted three times with Fe and Zr, had the highest As adsorption capacity. Consequently, FLF-3 and ZLF-3 were chosen for the subsequent studies, including their characterisation.

4.2.4 Material characterisation

The morphology and elemental composition of pristine LF, FLF-3, and ZLF-3 were determined using scanning electron microscopy (SEM) and energy-dispersive X-ray spectroscopy (EDS) (Quanta-650 instrument). The main functional groups' presence on the material surface was measured by Fourier transform infrared spectroscopy (FTIR, Nicolet iS5 FT-IR Spectrometer). BET surface area and Zeta potential were determined using N_2 adsorption isotherm at 77 K with a Micromeritics absorptiometer (Accu Pyr II 1340. V1.02) at 77 K and Nano ZS Zen 3600, respectively. The Barrett-Joyner-Halenda (BJH) method served to calculate the total pore volume, pore size distribution and average pore diameter (Kalaruban et al., 2019). The mineralogy was determined using a XRD Empyrean (Netherlands) diffractometer on powder samples of the adsorbents. The X-ray diffractometer was equipped with a Cu target operated at 45 kV and 40 mA with a setting of 5 – 80 ^{o} (2θ), step time 2 ^{o}/min.

The elemental composition of LF and modified LFs were also determined by chemical analysis using strong acid digestion. Here, 0.1 g sample was added into 100 mL mixed solution of 2M HNO_3 and 1M HCl (1:1 volume ratio) and shaken for 4 h at 50 ^{o}C (modification of the method employed by Kalaruban et al. (2016)). The suspensions were

filtered, and the filtrate was analysed for heavy metals using Agilent Technologies 4100 MP-AES instrument.

4.2.5 Batch adsorption studies

The equilibrium adsorption study was conducted by mixing predetermined amounts of adsorbents (1 – 5 g LF and 0.003 – 0.07 g of modified FLF-3 and ZLF-3) with 100 mL of 0.5 mg As(V)/L in 250 mL flasks and shaking them at 120 rpm for 24 h. At the end of this period, the suspensions were filtered, and As in the filtrate was analysed as described earlier. The pH of the solution was kept constant at 7.0 ± 0.2 by checking the pH after 2 – 3 h and adjusting back to the original value. This pH was selected for adsorption studies because most of the As contaminated natural surface and ground waters had approximately neutral pH (Berg 2007; Mohan & Pittman Jr 2007). Initially, the pH increased during adsorption probably due to exchange of As(V) anions with hydroxide groups attached to the Fe and Zr by ligand exchange, leading to increased hydroxide ion concentration in solution (Ren et al. 2011). The Langmuir, Freundlich and Temkin models were then used to model the experimental data (Table 2.4, Chapter 2).

The adsorption kinetics was carried out by mixing 1 g LF or 0.02 g FLF-3 or ZLF-3 with 100 mL of 0.5 mg As(V)/L in 250 mL flasks and shaking the flasks at 120 rpm. The samples were collected at different adsorption periods, from 5 min to 24 h, and As(V) concentration in solution was analysed as described in the equilibrium experiment. The experimental data were then modelled using PFO, PSO, Elovich, and Weber and Morris models (Table 2.5, Chapter 2).

The analysis of the pH influence on As(V) adsorption by LF and modified LFs was carried out by adjusting the pH of feed solution from 3 to 10. The dose of adsorbents was

kept constant at 10 g/L for LF and 0.2 g/L for modified LFs and the initial As concentration was 0.5 mg As(V)/L. The experiments were conducted using a method similar to the one described for the equilibrium adsorption experiment. The final pHs were measured at the end of the adsorption period.

The sodium salts of phosphate (PO_4^{3-}), sulphate (SO_4^{2-}), silicate (SiO_3^{2-}) and carbonate (CO_3^{2-}) at concentrations 0.1 and 10 mg/L were also added separately and together into As(V) solution of 0.5 mg/L. This was done to evaluate the influence of coexisting anions on As(V) adsorption capacity of LF and modified LFs. In this set of experiments, the same predetermined amounts of adsorbents were used (30 g/L of LF and 0.3 g/L of modified LFs). As with the batch experiments, the pH of the solution was kept constant.

4.2.6 Fluidised-bed adsorption studies

Fluidised-bed adsorption experiments were conducted using acrylic glass tubes. The adsorbents were filled in the columns to two bed-heights (H) of 15 cm and 30 cm. Cotton balls were placed at the top and bottom of the column to keep the adsorbents in place without changing the bed heights. In total, there were six columns in this set of experiments, corresponding to 2 columns (at 2 different heights) for each of the 3 adsorbents. Synthetic water containing As(V) of 0.1 mg/L was pumped by a dosing pump (Master-Flux L/S) in the up-flow mode through the columns at a constant flow rate of 47 mL/h (corresponding to 0.6 m/h). The effluent samples were collected at 2 h intervals in the first 24 h, and then once a day until the column was almost saturated with As. The experimental data were modelled using the Thomas model.

4.3. Results and discussion

4.3.1 Comparison of the As(V) adsorption capacity of different modified LFs

The experimental results showed that the As(V) adsorption capacity of the original LF did improve significantly after Fe and Zr modifications (Fig. 4.1). Moreover, the increase in the number of grafting cycles also increased the As(V) adsorption capacity. At a dose of 0.2 g/L, As(V) removal efficiency of ZLF-1 was 30%, then it rose to 45% with ZLF-2 and 78% with ZLF-3. In comparison with the original LF, the As(V) removal efficiency of ZLFs was 15 to 48% higher. The same trend was also observed with FLFs. This improvement can be explained by the increasing amount of Fe and Zr on the surface of *luffa* through the multi-cycle grafting process, as demonstrated by EDS and chemical analysis results (discussed later in the paper). Due to the highest As(V) removal efficiency of FLF-3 and ZLF-3 in comparison with other modification cycles, they were used in the subsequent experiments.

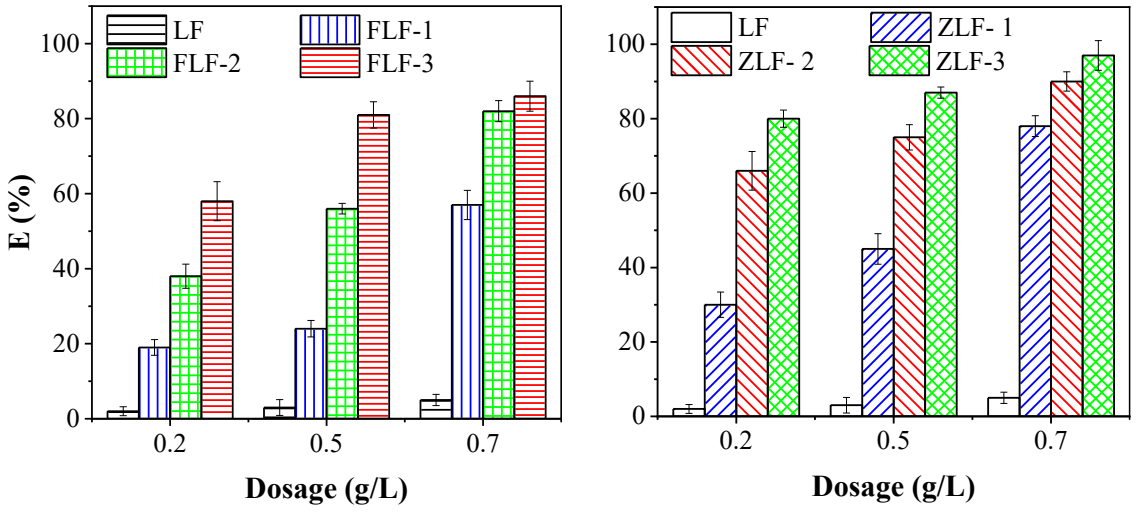

(a) (b)

Fig. 4.1. The As removal efficiency percentage (E%) comparison of the modification methods, (a) Fe grafted-LF and (b) Zr grafted-LF

4.3.2 Characteristics of adsorbents

The SEM images clearly showed the fibre structure of LF (Fig. 4.2). These images also displayed extremely different surfaces before and after the modification of LFs. While original LF possessed a relatively flat, smooth, homogeneous surface (Wang et al. 2017) the modification process caused a reduction in the homogeneity. The modified LFs developed an irregular surface with a rough microstructure formation on the surface as reported for LF after chemical washing by Wang et al. (2017). Chaudhry et al. (2017) reported that when Fe/Zr oxides were coated on sand, the surface became very irregular and porous and ascribed this as due to the formation of amorphous and porous Fe/Zr oxides. Chemical treatment during Fe and Zr grafting (acidity production and subsequent alkali addition to neutralisation of acidity) might have removed the gummy/waxy materials in LF to expose the rough surface as stated by Stella & Vijayalakshmi (2019). The porous structure of the modified LFs is consistent with the increase in the BET surface area and pore volume presented in the section below. No visible change occurred in the surface appearance of the adsorbents after As adsorption. This could be due to the very low concentration of As(V) on the LF surface.

The EDS analysis was carried out to determine the concentrations of the grafting agents in LF. The EDS mapping clearly showed that Fe and Zr are concentrated on LF surface, with the former spread over a larger surface (Fig. 4.2). The concentrations of Fe and Zr in the respective metals grafted LF determined from the spectra are 6.09 and 4.95% (Fig. 4.2). The chemical analysis also revealed the notable increase of Fe and Zr amounts after each grafting cycle. The highest percentages of the grafting agent's metals by the chemical analysis were 5.4% Fe for FLF-3 and 5.3% Zr for ZLF-3, compared to 2.9% Fe and 2.0% Zr for FLF-1 and ZLF-1, respectively. The percentage of Fe and Zr after As

adsorption remained nearly the same, indicating that these metals did not leak into the solution during the adsorption process.

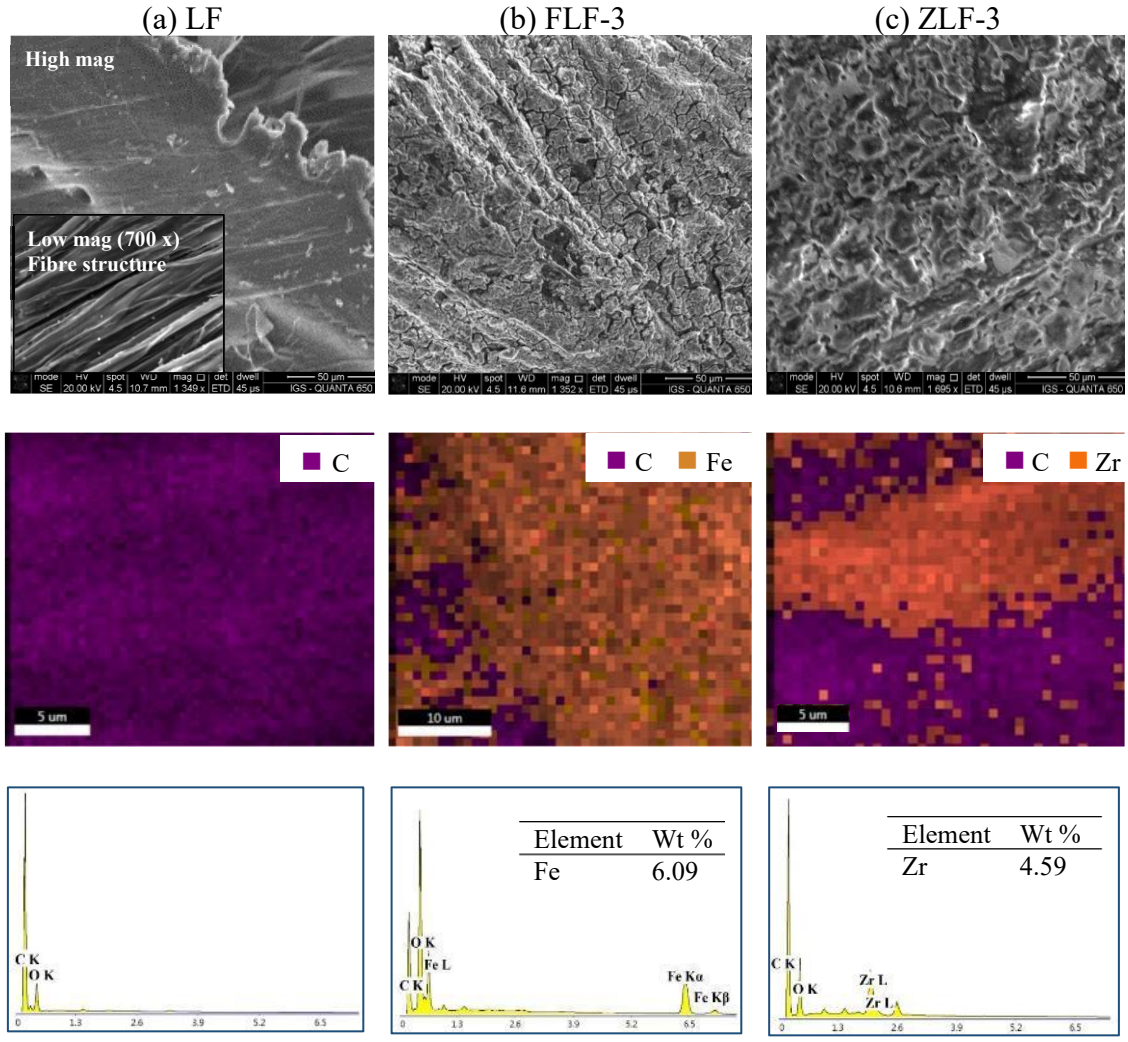

Fig. 4.2. SEM image, EDS mapping and EDS elemental spectrum analysis for (a) LF, (b) FLF-3 and (c) ZLF-3

The BET surface area and pore volume of LF were quite small (0.61 m^2/g and 0.0034 cm^3/g) (Table S4.1, Fig. S4.2a, Appendix 2). These values increased considerably after the grafting process. The BET surface area of FLF-3 and ZLF-3 were 6.7 m^2/g and

10.7 m^2/g, respectively, which are 11 and 18 times the value of the original LF. However, the BET surface areas of the modified LFs are still small in comparison with most other adsorbents (Mohan & Pittman Jr 2007). The BJH total pore volume (cm^3/g) of FLF-3 and ZLF-3 are 0.006 – 0.007 compared to 0.003 – 0.004 of LF (Table S4.1, Appendix 2). Both modified and unmodified LFs had mainly mesopores (> 95% mesopores (2 – 50 nm)) and < 5% micropores (< 2 nm) (Fig. S4.2b, Appendix 2). Adewuyi & Pereira (2017) also reported that the raw *luffa* fibres had mainly mesopores with a range of pores of 10 – 30 nm sizes. The average pore size of LF is 16 – 27 nm, whereas that of FLF-3 and ZLF-3 are 3.3 – 4.9 and 3.5 – 5.0 nm, respectively. The cumulative pore volume increased at a faster rate with decrease in pore size from 4 nm for FLF-3 and ZLF-3, but this was not the case with LF (Fig. S4.2b, Appendix 2).

XRD analysis showed the presence of cellulose in the original and metals grafted LFs (Fig. 4.3a). The peaks at 2θ = 15 – 16, 22.6, and 34.4 are characteristics of commercial cellulose (Stella & Vijayalakshmi 2019). Hemicellulose and lignin in the samples could not be identified in the analysis because they are non-crystalline (amorphous) compounds (Hideno 2016) and XRD can only identify crystalline minerals.

The chemical components of LF are reported to be mainly cellulose (60 – 66%), hemicellulose (17 – 22%), and lignin (11 – 15%), which have hydroxyl and carboxyl chemical groups with a strong affinity to bind with heavy metals (Adewuyi & Pereira 2017, Siqueira et al. 2010). Adewuyi & Pereira (2017) reported that the principal mechanisms of Pb adsorption on *luffa* fibres are ion exchange of the Pb with protons in the carboxylic and hydroxyl functional groups in cellulose and hemicellulose and H-bonding between Pb hydroxide species and these functional groups. Similar mechanisms of adsorption would have occurred for other heavy metals including Fe and Zr in this

study. The FTIR pattern of LF shows peaks at 3690 cm^{-1} and 1640 cm^{-1} corresponding to -O-H stretching and bending, respectively, which are the chemical bands of cellulose (Fig. 4.3b) (Petit & Puskar 2018, Siqueira et al. 2010). The peaks at 1710 cm^{-1} is assigned to -C=O functional group in the components of hemicellulose and lignin (Siqueira et al. 2010). The peak at 1053 cm^{-1} revealed the presence of =C-O group in either phenol or ester groups (Adewuyi & Pereira 2017, Siqueira et al. 2010). The intense peak from 971 to 1127 cm^{-1} for Fe grafted LFs is the bending vibration of hydroxyl groups of Fe (hydr)oxides in LF (Zhang et al. 2009). The peaks at 992 and 1506 cm^{-1} for the ZLF-3 are associated with -Zr-O and -Zr-OH bonds, respectively (Velazquez-Jimenez et al. 2014).

The peaks from 971 to 1127 cm^{-1} of the FLF-3 and 992 cm^{-1} of ZLF-3 adsorbents reduced in size after As(V) adsorption, and no new peak appeared in the FTIR diagram (Fig. 4.3b). This indicates that As(V) reacted only with the available functional groups of the modified adsorbents and not formed any new compounds. Zhang et al. (2009) also reported that these peaks (971 to 1127 cm^{-1}) weakened when As(V) adsorbed on Fe oxide and explained this as being due to As(V) forming a surface complex with Fe in the adsorbent. In the case of ZLF-3, the zirconyl ions on the surface of the Zr grafted LF adsorbent would have chemically adsorbed As(V) (Daus et al. 2004). The FTIR results suggest that chemical adsorption of As(V) on Fe and Zr sites in LF might be the primary mechanism of As(V) adsorption on FLF and ZLF.

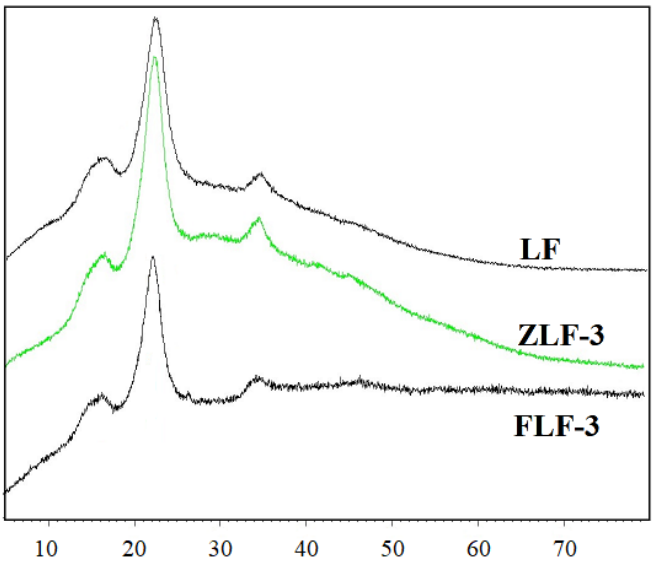

(a)

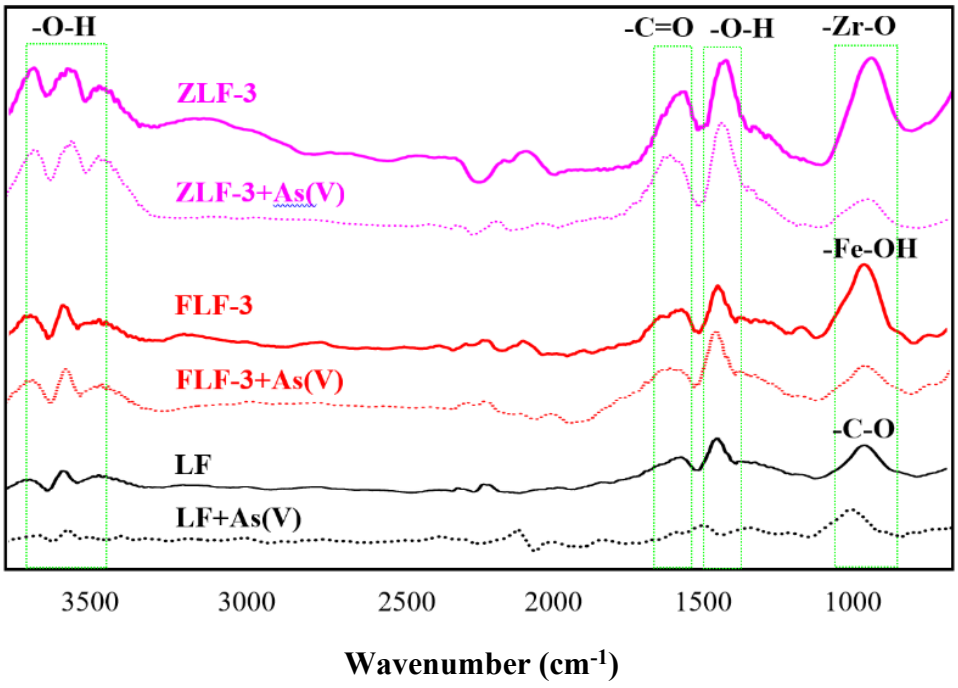

(b)

Fig 4.3. XRD (a) and FTIR (b) graphs of LF, FLF-3 and ZLF-3

Fig. 4.4 shows the zeta potential (ZP) pattern of the three adsorbents before and after As(V) adsorption. The ZP value of FLF-3 and ZLF-3 was much higher than that of LF due to the impregnation of the positively charged Fe and Zr on LF's surface. The zero points of charge (pH at which the net surface charge is zero) of LF, FLF-3, and ZLF-3 were 3.9, 7.4, and 7.6, respectively. The ZP of these adsorbents decreased when pH was increased and also after As(V) adsorption. This is because of the specific adsorption of the increased amounts of OH^- at increased pHs as well as the specific adsorption, i.e., inner-sphere complexation (Loganathan et al. 2014) of the negatively charged As ionic species (Mondal et al. 2007). LF also contains cellulose chains with hydroxyl groups that can bind with As(V) anions by hydrogen bonding and remove it from the solution (Elias et al. 2012; Fang et al. 2014). The positive charges produced as a result of Fe and Zr impregnation would have also adsorbed the negatively charged As(V) by electrostatic forces (physical adsorption or outer-sphere complexation) (Loganathan et al. 2014). The fact that the positive ZP decreased after As(V) adsorption indicates that the adsorption mechanism of modified LFs also included chemical process (inner-sphere complexation). Others have also reported both physical and chemical processes operating for the adsorption of As(V) on Fe (Kalaruban et al. 2019) and Zr (Velazquez-Jimenez et al. 2014)- grafted organic carbon-based adsorbents.

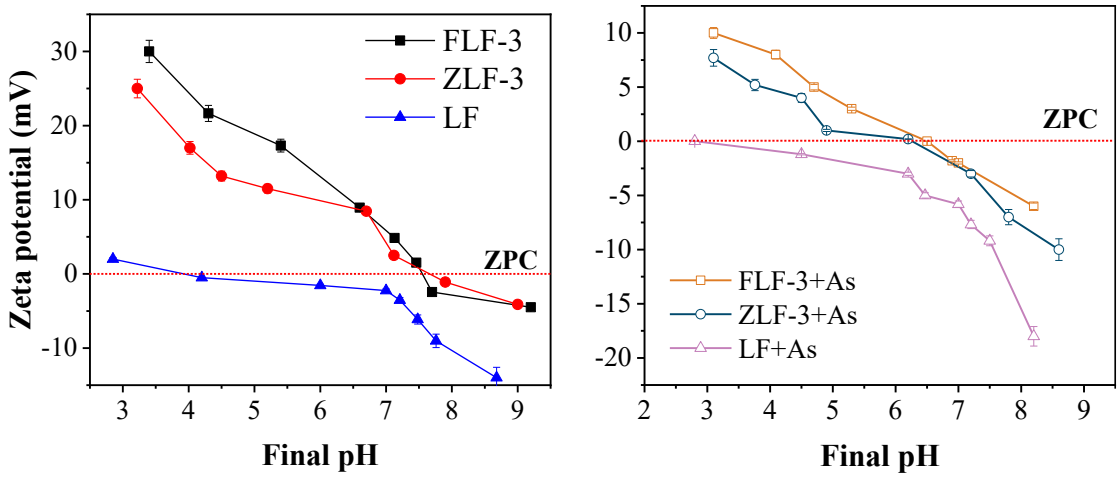

Fig. 4.4. The zeta potential of LF and modified LFs before (a) and after (b) As(V) adsorption

4.3.3 Batch adsorption studies

4.3.3.1 Equilibrium adsorption

Fig. 4.5 illustrates the equilibrium adsorption of As(V) on LF and modified LFs. The data were evaluated using nonlinear forms of the Langmuir, Freundlich, and Temkin models. The adsorption data fitted well to all three adsorption models, with the Temkin model being the best-fitted model for the data of LF. The R^2 values for all model fittings were >0.88, indicating that the fits were very highly significant (probability level = 0.001) (Preece 1982) (Table 4.1). The Langmuir maximum As(V) adsorption capacity (q_m) of LF was 0.035 mg/g, and it increased remarkably after modification. The Langmuir adsorption capacities of FLF-3 and ZLF-3 were 2.55 mg/g and 2.89 mg/g, respectively (Table 4.1). These values are 70 – 80 times higher than that of the original LF. It clearly confirms the beneficial impact of the grafting process. The improvement of As(V)

adsorption capacity is due to the strong adsorption of the anionic As species onto Fe and Zr on the surface of the modified LFs, as explained by the FTIR and zeta potential data earlier. The Langmuir isotherm constant k_L is related to the strength of the interaction between the adsorbent and adsorbate (Kocherbitov & Arnebrant 2010). The k_L value for the three adsorbents is in the order ZFL-3 > FLF-3 > LF, which is the same order of q_m. This shows that grafting of Zr and Fe on LF not only increased the adsorption capacity, but also increased the energy of adsorption.

Furthermore, the favourable nature of As(V) adsorption on LFs was analysed using an essential feature of the Langmuir isotherm model. This is the dimensionless equilibrium parameter R_L as shown in the equation below.

$$R_L = \frac{1}{1+(1+K_L.C_0)} \quad [4.1]$$

The R_L values for all the adsorbents in this study are $0 < R_L < 1$ (LF 0.23, FLF-3 0.172, ZLF-3 0.051), indicating that the adsorption process is favourable (Demir et al. 2008).

Although the Freundlich constant k_f does not give the maximum As(V) adsorption capacity like the q_m parameter of the Langmuir model, it is related to the adsorption capacity (Dada et al. 2012). The model results showed that the k_f values ((mg/g) $(L/mg)^{1/n}$) of FLF-3 and ZLF-3 are 3.020 and 3.851, respectively, which are 65 – 80 times higher than that of the unmodified LF (0.047) (Table 4.1). This is consistent with the q_m value differences between the adsorbents. The values of the Freundlich exponent n term for all the adsorbents were between 1 and 10 (LF 1.89, FLF-3 2.45, ZLF-3 3.32). Thus, the values for 1/n were between 0 and 1, indicating again a favourable sorption process,

which is consistent with the conclusion made from the Langmuir model (Nguyen et al. 2020b).

The Temkin model is usually used for heterogeneous surface energy systems and chosen to evaluate the adsorption potentials of the adsorbent for adsorbates (Nguyen et al. 2020b). The Temkin isotherm equilibrium binding constant A_T (L/g) (464, 83 and 50 for ZLF-3, FLF-3 and LF, respectively) corresponding to maximum binding energy (Nayl et al. 2020), correlates well with the Langmuir constant k_L relating to the energy of adsorption (ZLF-3 > FLF-3 > LF) (Table 4.1). Temkin isotherm constant b_T is inversely related to the heat of adsorption B calculated from the equation $B = RT/b_T$ (unit of B, J/mol; R gas constant, 8.314 J/mol.K; T, absolute temperature K) (Dada, 2012). The positive values obtained for b_T suggest that the adsorption process is endothermic (Adeogun & Babu 2015). Others have also reported endothermic reaction for the adsorption of As(V) on Fe-Zr binary oxide coated sand (Chaudhry et al. 2017) and on natural laterite containing Fe oxides (Nguyen et al. 2020a) based on thermodynamic adsorption studies. The B value for LF of 0.009 J/mol is much lower than that for FLF-3 (0.586 J/mol) and ZLF-3 (0.543 J/mol), indicating that the thermal energy created in the adsorption reaction of LF is lower than that of the others.

The Langmuir adsorption capacity of LF is generally lower than those of other natural plants (Table 4.2). However, the adsorption capacity of LF improved remarkably after modification. The adsorption capacities of FLF-3 and ZLF-3 are comparable or much higher than those of many other chemically modified bioadsorbents (Table 4.2). Some As adsorption studies (Chiban et al. 2009; Daus et al. 2004; Zhang et al. 2013) were conducted at an exceptionally high solution As concentrations up to 100 – 200 mg/L, which are rarely found in contaminated groundwaters and therefore they are not included

in Table 4.2. As(V) is mostly adsorbed by inner-sphere complexation onto the Fe and Zr hydroxy-oxides grafted on LF as shown by the zeta potential and FTIR data, and therefore, the As(V) adsorption capacity is not influenced by the surface area of the adsorbent matrix. In fact, there are many studies that have shown that adsorbents having very low surface area can have high adsorption capacities because of certain constituents in the adsorbents having very high affinity towards As. For example, a study on As(V) adsorption by a Fe oxide grafted on biomass which had a very low surface area of 2 m^2/g resulted in a Langmuir maximum adsorption capacity of 1.54 mg/g (Pokhrel & Viraraghavan 2008b). On the other hand, adsorbents having very high surface area do not necessarily have high adsorption capacity. This was demonstrated in a study of As(V) adsorption on granular activated carbon (GAC) and Fe grafted GAC, where GAC having a surface area of 1124 m^2/g had a low adsorption capacity of 1.01 mg/g, whereas Fe-GAC with a surface area of 876 m^2/g had an adsorption capacity of 1.43 mg/g (40% increase over GAC) (Kalaruban et al. 2019).

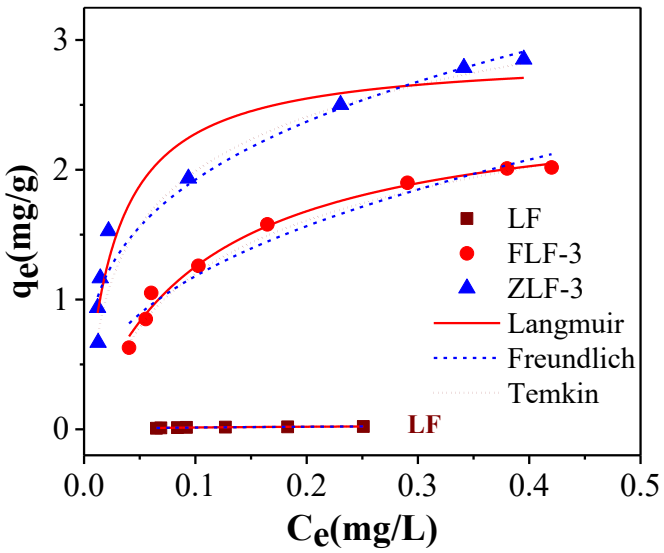

Fig. 4.5. Batch adsorption isotherms by LF and modified LFs

Table 4.1. Parameter values for batch equilibrium models of As adsorption

Model	Parameter	Unit	LF	FLF-3	ZLF-3
Langmuir	q_m	mg/g	0.035	2.553	2.894
	k_L	L/mg	6.680	9.629	36.91
	R_L		0.230	0.172	0.051
	R^2		0.919	0.989	0.945
Freundlich	k_f	L/g	0.047	3.020	3.851
	n		1.886	2.451	3.317
	R^2		0.889	0.958	0.951
Temkin	A_T	L/g	49.50	82.75	463.5
	B	J/mol	0.009	0.586	0.543
	b_T		275.3	4.228	4.563
	R^2		0.991	0.986	0.984

Table 4.2. Comparison of As(V) adsorption capacities of some bioadsorbents

Adsorbent	Solution pH	C_o (mg/L)*	Q (mg/g)**	Reference
LF	7	0.5	0.035	This study
FLF-3	7	0.5	2.55	This study
ZLF-3	7	0.5	2.89	This study
Iron hydroxide modified activated carbon	7	0.025 – 1.5	0.37 – 1.25	Vitela-Rodriguez & Rangel-Mendez (2013)
Granular activated carbon	6	0.1	1.01	Kalaruban et al. (2019)
Iron coated granular activated carbon	6	0.1	1.43	Kalaruban et al. (2019)
Coal-based activated carbon	6	0.5	1.76	Li et al. (2014)
Manganese oxide-modified pine biochar	7	1 – 20	0.59, 0.91	Wang et al. (2015)
Iron oxide coated *A. niger* biomass	6	0.1	0.526	Pokhrel & Viraraghavan (2008b)
Fish scale	6.8	0.333	0.0266	Rahaman et al. (2008)
Rice polish	4	0.1 – 1	0.147	Ranjan et al. (2009)
Anaerobic biomass	5	0.5-4	0.164	Chowdhury & Mulligan (2011)

*Initial As concentration, **Langmuir maximum adsorption capacity

4.3.3.2 Adsorption kinetics

The experimental data for the adsorption kinetics on LF, FLF-3, and ZLF-3 were fitted to non-linear PFO, PSO, Elovich models, and the linear Weber and Morris model (Fig. 4.6). The results show that As adsorption on ZLF-3 reached the fastest saturation within 60 min (Table 4.3). LF and FLF-3 needed more time to reach the saturated point, 4 h and 6 h, respectively. The adsorption rate on all adsorbents during the initial period increased rapidly because a large number of adsorption sites were available for As(V) adsorption. As time progressed, it slowed down because of the gradual saturation of the adsorption sites before finally reaching an equilibrium state with no change in adsorption capacity. Between the PFO and PSO models, the latter fitted the data better for FLF-3 and ZFL-3, as revealed by the higher R^2 values (0.985, 0.986 for PSO; 0.894, 0.953 for PFO). In addition, the experimental maximum adsorption capacity (q_{exp}) was closer to the predicted adsorption capacity of the PSO model (q_e) than those for the PFO model for these modified LFs. This suggests that the main As(V) adsorption mechanism was chemical adsorption for the modified LFs (Kalaruban et al. 2019), as also found from the zeta potential data. The PSO adsorption rate constant (k_2, g/mg.h) of ZLF-3 (5.1) is higher than that of FLF-3 (0.8) (Table 4.3), indicating that it had a higher rate of adsorption than FLF-3. For the unmodified LF, the R^2 of the model fits the data, and the q_{exp}/q_e difference between the two models was nearly the same. Therefore, the results could not suggest whether PSO or PFO is a better predictive model for LF adsorption and whether the adsorption process is chemical or not.

The Elovich model fitted well to the adsorption data of all three adsorbents (Fig. 4.6a). The α values of FLF-3 and ZLF-3 were much higher than that of LF, indicating that the initial rate of adsorption was increased significantly after modification. This

phenomenon can be explained by the higher affinity of Fe and Zr modified LFs to As(V). The value of β (g/mg), the desorption constant, which is inversely related to the affinity of adsorbate to adsorbent (Wang et al. 2015; Zhang et al. 2013) is much lower for FLF-3 (4) and ZLF-3 (6) than for LF (233) (Table 4.3), indicating that the modified LFs have stronger affinity to As(V) than LF.

Because LF consists of pores and channels, the Weber and Morris model was chosen to investigate the rate of As diffusion into this material through these pores/channels (Fig. 4.6b). The As(V) adsorption capacity of LF was too small, and therefore the change in adsorption rate could not be determined. For this reason, the Weber and Morris model fit to LF adsorption data was described by a single straight line. However, the As(V) adsorption process for FLF-3 and ZLF-3 appears to take place in two phases. The two phases were described by the two straight lines that fit the data in Fig. 4.6b. The data fit the two straight lines for both the modified adsorbents are very highly significant with R^2 values > 0.960. The k_p values of the first set of straight lines (k_{p1}) were higher than the respective k_p values (k_{p2}) of the second set of straight lines, indicating that the intra-particle diffusion rates of As(V) into these adsorbents at short-term adsorption are faster than those at the long-term process. The faster rate is due to intra-particle diffusion of As into the larger sized pores of the absorbents (mostly > 4 nm, Fig. S4.2, Appendices), and the slower rate is due to intra-particle diffusion of As into the smaller sized pores (mostly < 4 nm, Fig. S4.2, Appendices). Kalaruban et al. (2019) also reported a good fit of data to the Weber and Morris model for the kinetics of adsorption of As on Fe-coated granular activated carbon (GAC) with two distinct straight lines. They considered that the two straight lines fit, indicating As diffusing initially (short-term

process) through the mesopores in GAC and later (long-term process) through the micro-pores in GAC.

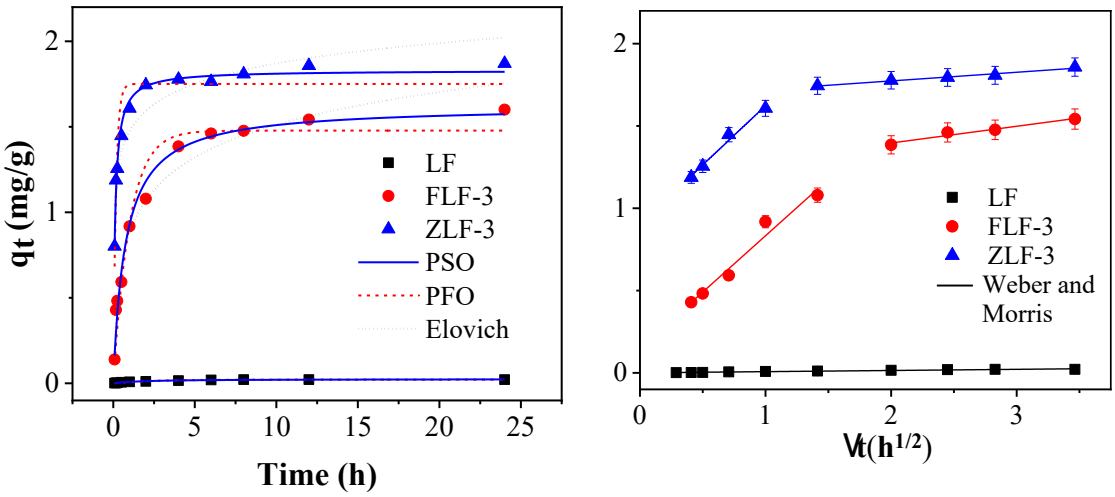

(a) (b)

Fig. 4.6. Batch kinetics adsorption by LF and modified LFs, (a) PFO, PSO and Elovich models and (b) Webber and Morris model

Table 4.3. Parameter values for batch kinetics models of As adsorption

Model equation	Parameter	Unit	LF	FLF-3	ZLF-3
	q_{exp}	mg/g	0.022	1.600	1.870
PFO	q_e	mg/g	0.022	1.478	1.751
$\frac{dq_t}{dt} = k_1(q_e - q_t)$	k_1	1/h	0.425	1.000	5.933
	R^2		0.981	0.953	0.894
PSO	q_e	mg/L	0.025	1.623	1.830
$\frac{dq_t}{dt} = k_2(q_e - q_t)^2$	k_2	g/(mg.h)	21.77	0.827	5.097
	R^2		0.985	0.986	0.986
Elovich	α	mg/(g.min)	0.001	0.112	15.00
$\frac{dq_t}{dt} = \alpha e^{-\beta q_t}$	β	g/mg	232.9	3.632	5.808
	R^2		0.956	0.977	0.882
Weber and Morris	Short-term adsorption				
$q_t = k_p\sqrt{t} + B$	k_{p1}	mg/(g.h$^{1/2}$)	0.007	0.685	0.719
	B	mg/g	6x10^{-4}	0.149	0.904
	R^2		0.960	0.968	0.985
	Long-term adsorption				
	k_{p2}	mg/(g.h$^{1/2}$)	-	0.101	0.053
	B	mg/g	-	1.193	1.668
	R^2		-	0.961	0.976

4.3.3.3 Influence of pH on As(V) adsorption

pH is one of the most important parameters of the adsorption process. It impacts the surface charge of the adsorbents, the extent of ionisation of the surface groups, the nature of the adsorbing ions, and finally influences the adsorption mechanisms (Firdaous et al. 2017). Fig. 4.7 shows the influence of pH on As(V) adsorption by LF, FLF-3, and ZLF-3. The As(V) adsorption efficiency of the three adsorbents declined when the pH rose from 3 to 10 (from 53 – 68%). This fall in adsorption capacity is due to the increase in the surface negative charges on the adsorbents as pH increases (as shown in the zeta potential diagram, Fig. 4.4), which is not favourable for the adsorption of the negatively charged As species. Additionally, the number of negative charges on the As species would have also increased with pH to aggravate this situation. Another reason is that the increasing concentration of hydroxyl ions at high pHs might have competed with As species for specific adsorption on the adsorbents.

The decline in As(V) adsorption capacity with rise in pH has also been reported by others. For example, for a granulated activated carbon (GAC) and iron grafted GAC, it was reported that the adsorption capacity continued to decrease with increase in pH from 6 to 8 (Kalaruban et al. 2019). For an iron-zirconium binary oxide adsorbent, it was shown that As(V) adsorption efficiency continuously declined with increase in pH from 5 to 11 (Ren et al. 2011). Similarly, the adsorption of As(V) on iron and zirconium grafted manganese oxide ore decreased from pH 3 to 10 (Nguyen et al. 2020b). Also, for three types of iron oxide minerals and zero-valent Fe, As(V) adsorption decreased from pH 6 to 12 (Mamindy-Pajany et al. 2011).

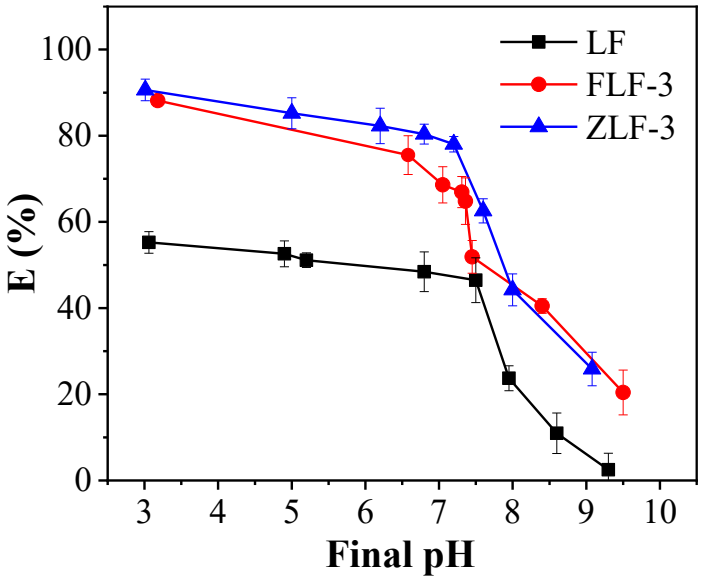

Fig. 4.7. Influence of pH on As(V) removal efficiency of LF (10 g/L), FLF-3 (0.2 g/L) and ZLF-3 (0.2 g/L)

4.3.3.4 Effect of co-existing anions on As(V) adsorption

In nature, many ions present in water, but some of them are able to interfere with the uptake of As through competitive adsorption. Four typical anions PO_4^{3-}, SO_4^{2-}, SiO_3^{2-} and CO_3^{2-}, which commonly co-exist with As in water, were selected to evaluate the influence of co-existing anions on As(V) adsorption.

The results showed that the performance of the three adsorbents was affected depending on the presence of co-existing anions and their concentrations (Fig. 4.8). At the lower concentration (0.1 mg/L), the effect of SO_4^{2-} and CO_3^{2-} ions on As(V) removal efficiency was almost invisible, while the influence of PO_4^{3-} and SiO_3^{2-} ions was remarkable (As removal reduced by 20 – 30%, in the case of FLF-3). At the higher concentration (10 mg/L) of each ion, PO_4^{3-} and SiO_3^{2-} ions impacted greatly on the As(V)

removal efficiency (As removal reduced by 50 – 70%), especially PO_4^{3-} because of their chemical similarities (Ren et al. 2011).

In general, the order of competition for adsorption is: $PO_4^{3-} > SiO_3^{2-} > CO_3^{2-} > SO_4^{2-}$. The same order of competition was also reported by Nguyen et al. (2020a) for As(V) adsorption by a natural laterite containing Fe oxides. The reason for PO_4^{3-} and SiO_3^{2-} having higher competition than CO_3^{2-} and SO_4^{2-} is that they are adsorbed mostly by inner sphere complexation onto the Fe and Zr in the adsorbent compared to the latter two ions which are adsorbed mostly by outer sphere complexation (Tuutijärvi et al. 2012). Inner sphere complexation leads to strong chemical adsorption usually involving ligand exchange mechanism (adsorbent surface OH groups exchanging with anions such as As(V)) (Loganathan et al. 2014; Ren et al. 2011). Tuutijärvi et al. (2012) reported that SO_4^{2-} and NO_3^- had negligible effect on As(V) adsorption by maghemite but PO_4^{3-} and SiO_3^{2-} had strong adverse effect. Gu et al. (2011) also reported that SO_4^{2-} did not affect As(V) adsorption by Fe grafted GAC, whereas PO_4^{3-} and SiO_3^{2-} did. Ren et al. (2011) observed that the adsorption of As(V) by Fe/Zr binary oxide was not affected by SO_4^{2-}, slightly by CO_3^{2-}, and severely by PO_4^{3-} and SiO_3^{2-}. Of the last two anions, the former was considered to compete more intensively with As(V) because they have similar molecular structure and located in the same group in periodic table (Ren et al. 2011; Zhang et al. 2009). Another similarity is that both are oxyanions and have similar types of ionic species at neutral pH ($H_2PO_4^-, HPO_4^{2-}, H_2AsO_4^-, HAsO_4^{2-}$) (Tuutijärvi et al. 2012).

The competitive ability of the co-existing anions was enhanced when all of them were present in the same solution. The presence of multiple anions in solution competed for a greater number of adsorption sites of As, thus leading to the significant decline in

As(V) removal efficiency. This decreased from 40% to 90% as the mixed anions concentration increased from 0.1 mg/L to 10 mg/L.

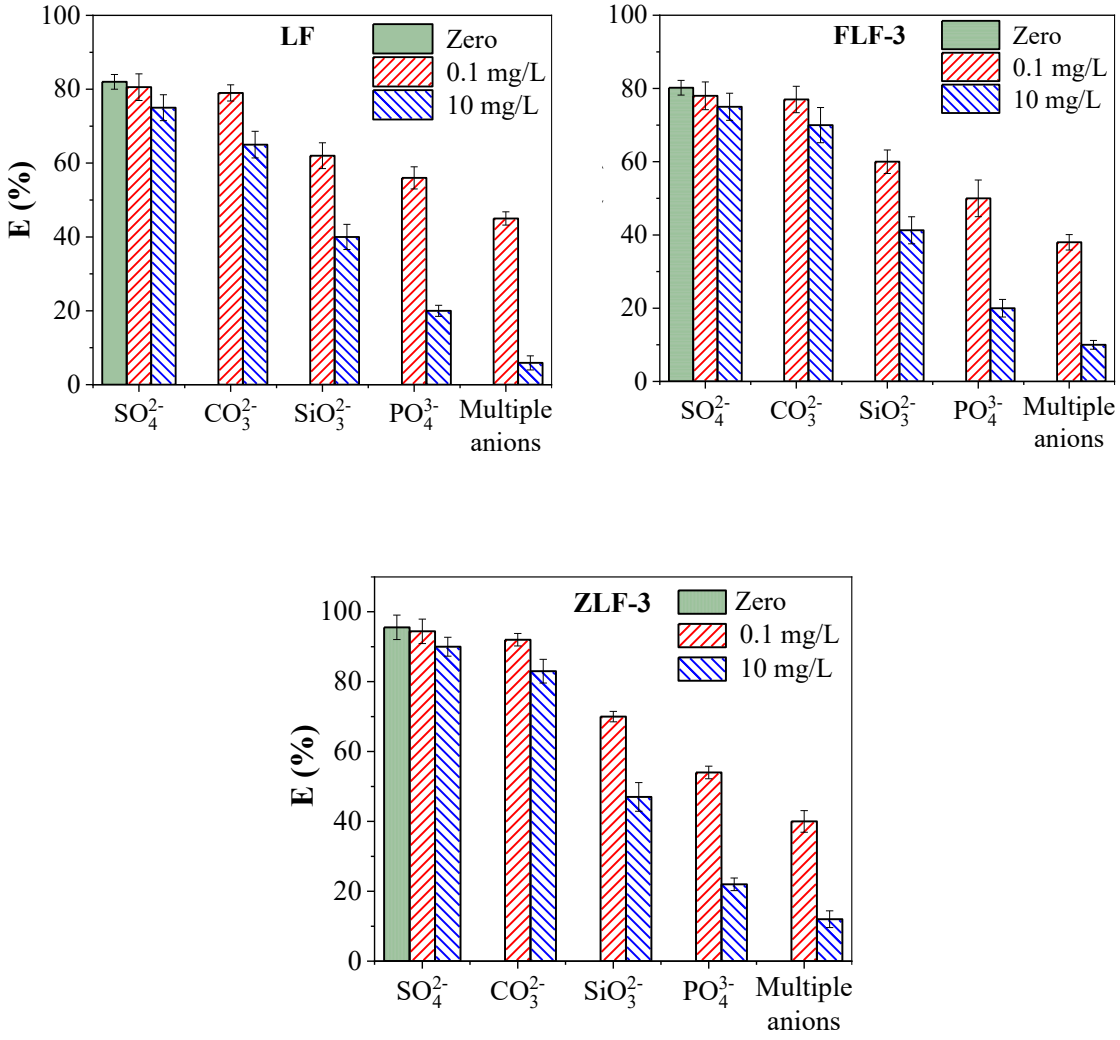

Fig. 4.8. Effect of single and multiple anions on As(V) removal capability of (a) LF, (b) FLF-3, and (c) ZLF-3

4.3.4 Fluidised-bed studies

Fig. 4.9 depicts the As breakthrough curves of six columns. At the same initial As(V) concentration (C_o = 0.1 mg/L) and filtration velocity (Q = 0.047 L/h), the breakthrough curves of LF were always steeper than those of FLF-3 and ZLF-3. It means that LF saturated faster than the others did. At the same bed height, the plateau of C_t/C_o of these columns occurred at different periods and bed volumes (B.V.). For example, with the 15 cm columns, the life cycle of LF was the shortest, and the plateau of C_t/C_o occurred around 120 h (B.V. 479, C_t/C_o = 0.99). Meanwhile, FLF-3 and ZLF-3 operated for much longer, and the ratio C_t/C_o = 0.98 occurred approximately at 1824 h, B.V. 7281, and 2832 h, B.V. 11304, respectively. In the case of 30 cm columns, a similar trend was also observed. For LF, C_t/C_o of 0.80 was reached at B.V. = 239 (120 h), while for FLF-3 and ZLF-3, this C_t/C_o was reached at B.V. of 3640 (1824 h) and B.V. of 5652 (2832 h), respectively.

For each adsorbent, the higher column height became saturated after a longer time than the shorter one. This is because the column packed with an adsorbent to a greater height had a larger number of adsorption sites for As(V) adsorption. The longer operational time of the column with greater height enables it to treat larger volumes of water to maintain As concentration below the WHO recommended level of 10 µg/L. For instance, the 30 cm column with ZLF-3 adsorbent treated 33 L of water to the WHO level compared to 6.8 L water the 15 cm column treated. The corresponding volumes of water treated by LF columns were 0.2 and 0.1 L, respectively.

The total amount of As(V) adsorption, q_{total} (mg), and column adsorption capacity, $q_{e,exp}$ (mg/g) in the fluidised-bed studies were calculated using the following equations (Kalaruban et al. 2016):

$$q_{total} = Q.\int_{t=0}^{t=total}(C_o - C_t)dt \quad [4.2]$$

$$q_{e,exp} = \frac{q_{total}}{m} \quad [4.3]$$

where: Q is the filtration velocity, (L/h); C_o is the initial As(V) concentration (mg/L); and C_t is the As(V) concentration at time t (h), (mg/L).

The calculations showed that ZLF-3 had the highest As(V) adsorption capacities at both the column heights (2.630 and 1.950 mg/g with H 15 and 30 cm columns, respectively), followed by FLF-3 (1.237 and 1.031 mg/g) and LF (0.054 and 0.053 mg/g) (Table 4.4).

The linear Thomas model (Table 2.6 Chapter 2) fitted well to the experimental data with values of $R^2 > 0.87$ (Fig. 4.9).

The modelling results showed that the maximum As adsorption capacity of ZLF-3 was the highest (2.7 and 2.2 mg/g for 15 cm and 30 cm height columns, respectively) while that of LF was the lowest (0.06 mg/g for both column heights) (Table 4.4). The corresponding values of FLF-3 were 1.26 mg/g and 1.10 mg/g, respectively.

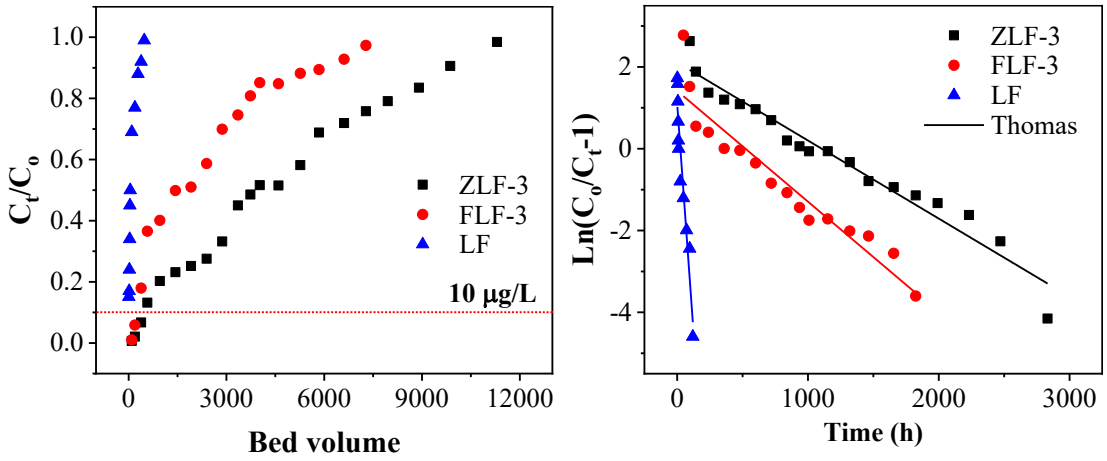

(a)

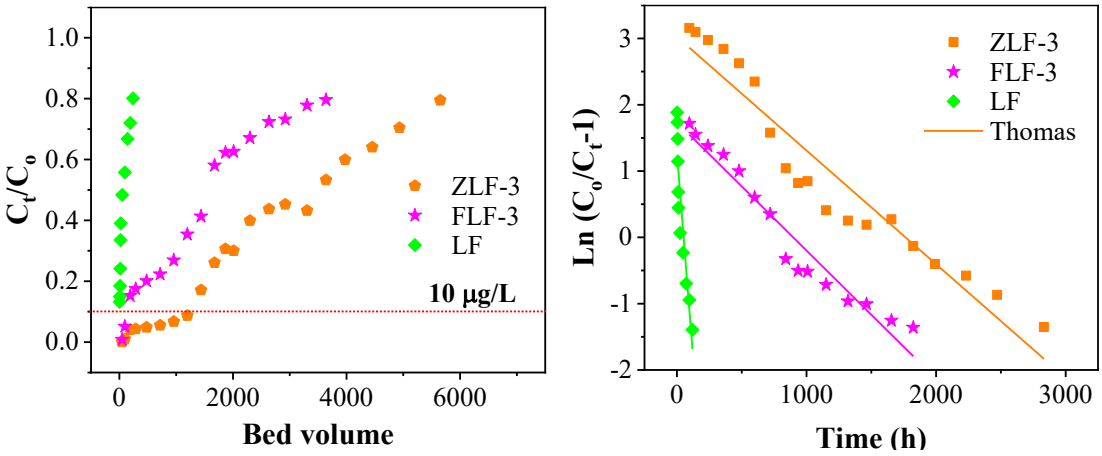

(b)

Fig. 4.9. The experimental breakthrough curves and Thomas model fit to data for As(V) removal at V = 0.047 L/h, C_o = 0.1 mg/L and H = 15 cm (a) or H = 30 cm (b)

Table 4.4. Column experimental parameters for As adsorption

Parameter	Unit	H = 15 cm, m = 1.95 g			H = 30 cm, m = 3.9 g		
		LF	FLF-3	ZLF-3	LF	FLF-3	ZLF-3
q_{total}	mg	0.106	2.412	5.133	0.213	4.019	7.600
$q_{e,exp}$	mg/g	0.054	1.237	2.630	0.053	1.031	1.950
Thomas model							
q_e	mg/g	0.060	1.263	2.677	0.059	1.102	2.145
K_{Th}	L/(h.mg)	0.446	0.027	0.019	0.264	0.019	0.017
R^2		0.921	0.902	0.952	0.873	0.946	0.924

4.3.5 Cost estimation for treatment

Currently, *luffa* fibre has not been used for water treatment purposes. Its cost was estimated based on the raw material price, collection, transportation, and processing, about A$0.2/kg. The costs of the modified LFs are calculated using the industrial prices of the chemicals, $FeCl_2.4H_2O$ (A$1.37/kg), $ZrOCl_2.8H_2O$ (A$1.64/kg), and NaOH (A$0.30/kg) employed in the modification procedure (prices of the chemicals are obtained from https://www.alibaba.com) and the quantities of the chemicals used in the modification (section 4.2.2.2). Based on this calculation, the cost of FLF-3 and ZLF-3 was estimated to be A$1.02/kg and A$1.81/kg, respectively.

The cost of treating 1 m^3 water containing 0.1 mg As(V)/L to produce safe drinking water (<10 µg As/L) was calculated by multiplying the cost of the adsorbent by the weight of adsorbent in the column (3.9 g) divided by the volume of water treated (m^3).

The volumes of water treated by LF, FLF-3 and ZLF-3 at the flow rate of 0.047 L/h are 0.2 L, 15 L, and 33 L, respectively (time (h) taken to reach 10 µg As/L in treated water x flow rate (L/h)/1000 L/m^3). Based on this calculation, the costs of treating 1 m^3 water by LF, FLF-3, and ZLF-3 are estimated to be A$3.9, A$0.26, and A$0.21, respectively. The cost calculated in this section applies only to a single use of the adsorbents until reaching the safe limitation of As in the treated water. However, the adsorbents can be used until absolutely exhausted. They could be continuously utilised by connecting in a series with a new column. This method would reduce the water treatment cost by using these adsorbents. In addition, desorption/regeneration of the exhausted adsorbents is also an option to reduce the cost of water treatment by using the absorbents repeatedly. However, the applicability of this method depends on many factors, such as adsorbent cost, market value of adsorbate, which would be discussed in detail in Chapter 5.

In comparison between three adsorbents, the water treatment costs of the original LF is higher than that of modified LFs due to the smaller volume of water treated, despite its lowest cost. A similar reason is also applied to explain the difference in the water treatment cost between ZLF-3 and FLF-3. Comparing with other adsorbents, the cost of treated water by modified LFs is lower than that of Zr^a-VMO (A$0.742/$m^3$) and Fe^a-VMO (A$0.287/m^3) in the previous study (Nguyen et al. 2020b). The Langmuir adsorption capacity of modified LFs is also much higher than that of Vietnamese high quality GAC while their cost is comparable (0.07 mg/g and A$2.0/kg of high quality GAC compares with 2.55 mg/g and A$1.02/kg of FLF-3 and 2.89 mg/g and A$1.81/kg of ZLF-3) (Section 3.3.6, Chapter 3).

4.3.6. Adsorption mechanism

Zeta potential data showed that when LF was modified with the positively charged Fe and Zr, the negative charges on LF significantly decreased at all pHs and reversed to positive values at pHs 4.0 to 7.5. FTIR data provided evidence that Fe and Zr were complexed with the hydroxyl and carboxylic groups mostly present in the cellulose component of LF. XRD data proved that cellulose was present in LF. The grafting of Fe and Zr produced significant amounts of these metals on the grafted product as shown in EDS mapping.

The positive charges generated on LF by Fe and Zr would have helped the adsorption of some As(V) by coulombic (electrostatic) forces leading to outer-sphere complexation. However, the major mechanism of As(V) adsorption is through inner-sphere complexation caused by ligand exchange of surface hydroxyl groups attached to Fe and Zr with As(V) species ($H_2AsO_4^-, HAsO_4^{2-}$) (Kalaruban et al. 2019; Mohan & Pittman Jr 2007; Nguyen et al. 2020b, Ren et al. 2011, Tuna et al. 2013). The evidence for this process is provided by the zeta potential data. The zeta potential of FLF and ZLF decreased and even became negative at pHs above 6.5 due to the negatively charged As(V) ions complexing with the Fe and Zr oxides/hydroxides. Because As(V) was adsorbed mainly by inner-sphere complexation the non-specifically adsorbing anions such as SO_4^{2-} and CO_3^{2-} were not able to compete well with As(V) for adsorption sites. The scheme of As(V) adsorption mechanism is illustrated in Eq. 4.4 – 4.7 below. Eq. 4.4 and 4.5 are for $H_2AsO_4^-$, the dominant anionic species at pH 2 – 7, and Eq. 4.6 and 4.7 are for $HAsO_4^{2-}$, the dominant species at pH 7 – 12 (Ren et al. 2011). The complexation could have occurred by As(V) species acting as electron donors and the metal hydroxide groups acting as electron acceptors (Tuna et al. 2013). SEM images showed that Fe and

Zr modifications exposed the pores and channels of the fibrous LF in the acidic conditions prevalent during the modification process, which removed the gummy/waxy substances on the LF surface. The adsorption of As(V) on FLF and ZLF is not only on the planer surface of the adsorbent but also inside these pores/channels by As(V) diffusion as demonstrated by Weber and Morris kinetic data analysis.

$$LF] - Fe - OH + H_2AsO_4^- \rightarrow LF] - Fe - H_2AsO_4^- + OH^- \quad [4.4]$$

$$LF] - Fe - OH + HAsO_4^{2-} \rightarrow LF] - Fe - HAs_4^{2-} + OH^- \quad [4.5]$$

$$LF] - Zr - OH + H_2AsO_4^- \rightarrow LF] - Zr - H_2AsO_4^- + OH^- \quad [4.6]$$

$$LF] - Zr - OH + HAsO_4^{2-} \rightarrow LF] - Zr - HAs_4^{2-} + OH^- \quad [4.7]$$

4.4. Conclusions

This study has demonstrated that porous fibres of the *luffa* plant (LF), which is found in most parts of the world, can be easily grafted with Fe and Zr, and the As(V) adsorption capacity can be increased by 70-80 times when compared to the unmodified raw LF. Grafting with Fe and Zr increased the zeta potential and zero point of charge (ZPC) of LF (from pH 3.9 to 7.4 for Fe-grafting and to 7.6 for Zr grafting), due to chemical bonding of the metals, possibly with the hydroxyl and carboxylic groups in LF as indicated in the FTIR pattern of peaks. Zeta potential and ZPC decreased after As adsorption owing to inner-sphere complexation mechanism of adsorption. The adsorption capacities of the grafted materials (2.55 – 2.89 mg/g) are higher than many of the other bioadsorbents. The Fe- and Zr-grafted LF are very promising cost-effective, and environmentally friendly bioadsorbents for the removal of As(V) from contaminated drinking water.

CHAPTER 5

Solid waste management

Chapter 5. Solid waste management

Summary

Chapter 5 presents the third key findings about management/safe disposal of the exhausted adsorbents, including waste from original and modified manganese oxide ore and *luffa* fibre. The first part of this study (section 5.1) on managing the exhausted original and modified manganese oxide ore was published in the Journal of Environmental Chemical Engineering (Q1 journal, impact factor: 4.02).

Nguyen, T.T.Q., Loganathan, P., Nguyen, T.V. & Vigneswaran, S. 2020, 'Removing arsenate from water using modified manganese oxide ore: column adsorption and waste management', *Journal of Environmental Chemical Engineering*, p. 104491.

After use as adsorbents in the previous chapters, VMO, LF, and their modified forms need to be managed properly to prevent the return of As(V) to the environment. The encapsulation method through solidification/stabilisation was applied to the used VMO and modified VMOs. Testing of the quality of concrete and the leaching test was conducted to identify the application and safety degree of concrete (Fig. S5.1, Appendix 3).

The exhausted original and modified LFs were managed by the phytoremediation method using *Pityrogramma calomelanos*. The study presents the level of As(V) transformation from the soil to different sections in the plants as well as the As(V) residue remaining in the soil after phytoremediation.

5.1 Original and modified manganese oxide ore

5.1.1 Introduction

After the adsorption treatment process, the exhausted adsorbent media must be well managed to prevent As being released into the environment. Four options could be chosen to treat the exhausted adsorbent waste, which includes: (1) desorption/regeneration (D/R), (2) concentration and containment, (3) dilution and dispersion, and (4) encapsulation of the material (Leist et al. 2000; Mohan & Pittman Jr 2007; Nguyen et al. 2014). These options have been applied selectively depending on such issues as economic efficiency, safety, concentration, and purity of the substance. Practically, the D/R process is usually applied to valuable adsorbents and adsorbates. Because there is a limited demand for As in the market and it is unsafe to store the As after recovery, the D/R method used for valuable elements is not attractive for As (Mohan & Pittman Jr 2007). Furthermore, the D/R approach has problems regarding: firstly, the safe disposal of the highly concentrated As in the desorbed solution; secondly, inability to completely desorb all the adsorbed As from the adsorbent; and thirdly, the decline in As adsorption capacity of the adsorbent after each adsorption cycle. The second method of concentration and containment is relatively costly and not affordable for local people, where most of the As-related problems exist. The third method of dilution and dispersion, although it reduces the immediate environmental problem of As, can cause environmental problems in the future at the site where it is repeatedly disposed of. Moreover, humans exposed to low concentrations of As over the long-term will pose serious health problems (Leist et al. 2000).

Unlike other methods, the encapsulation option through solidification/stabilisation (S/S) is more attractive and considered to be an effective technique to treat As-containing

solid waste (Jing et al. 2005). The United States Environmental Protection Agency (USEPA) also recognized S/S processes as the Best Demonstrated Available Technology (BDAT) for the land disposal of hazardous elements (Yoon et al. 2010). The advantage of this method is that the toxic substance (As) is immobilised and incorporated into solid materials such as cement, slag, or polymer so that the As-encapsulated materials become a reduced or non-hazardous solid waste (Leist et al. 2000; Mohan & Pittman Jr 2007). Moreover, the S/S method can be cost-effective if the incorporation and stabilisation are done using a material that is manufactured locally for another purpose without affecting its quality. The product of the S/S process can be safely disposed of in a secure landfill or used as a construction material that has limited contact with humans.

The popular agents of the As(V) S/S process that have been evaluated successfully are cement and mixtures of cement, such as Portland cement, mixtures of Portland cement with Fe (II, III), lime, fly ash, or silicate (Leist et al. 2000, Mohan & Pittman Jr 2007; Sullivan et al. 2010). The advantages of these agents are that they are low-cost, easy to incorporate with wet/solid waste, and have high alkalinity, which could restrict the solubility of hazardous metals (Singh & Pant 2006). However, the As, which is incorporated and stabilised into these materials, should not leak out into the environment in the future. Some studies find that As concentration in leachates from the encapsulated materials determined according to the Toxicity Characteristic Leaching Procedure (TCLP) of USEPA was below the acceptable limit of 5 mg/L (below this concentration, As is unlikely to cause toxicity) (Jing et al. 2005; Lincoln et al. 2007). However, detailed studies about the characteristics of encapsulated material regarding the physico-chemical characteristics with reference to the reaction of As within the encapsulated material and the potential As release in the long-term are limited. Moreover, evaluating the quality of

the S/S product using measurements such as compressive strength, rapid chloride penetrability test (RCPT), and volume of permeable voids (VPV), which are important features to decide whether the construction material can be used widely or not, has been rarely performed.

The aims of this research were to evaluate the feasibility of disposing of the exhausted adsorbent waste by encapsulating it into concrete made from cement and test whether As(V) leaching from the material is within the safety level. The physico-chemical characteristics of the encapsulated product and the possible reactions of As(V) within the product are also investigated in this study to determine the product's stability.

5.1.2 Material and methods

5.1.2.1 Material

The used exhausted adsorbents from the column experiments were rinsed quickly with tap water to remove the adsorbent residues stuck to the column surface. They were then dried at a temperature of 50 ^{o}C for 8 h. The As ions in the adsorbents would not have leached out of the adsorbents during the rinsing with water because they were strongly adsorbed through electrostatic adsorption forces and chemical bonds. The exhausted VMO, Fe^{a}-VMO and Zr^{a}-VMO adsorbents were mixed at a ratio of 1:1:1 and encapsulated with concrete.

5.1.2.2 Solidification/stabilisation

Five levels of the exhausted adsorbents were used in the concrete mix. The compositions of the 5 mixtures are shown in Table 5.1. The concrete mix samples are

named C0, C5, C10, C15, C20, corresponding to the replacement levels of sand by the exhausted adsorbent mixture (0%, 5%, 10%, 15%, and 20%). The materials for the concrete mix, such as river sand, aggregates (gravels of 10 - 20 mm size), and Portland cement, were supplied by a local construction material store. The concrete samples were prepared utilising a 100 mm x 200 mm cylindrical mould (Pic. S5.1, Appendix 3). One day after casting, the concrete samples were unmoulded and soaked in a curing chamber containing a lime solution for 27 days, as described by Baweja et al. (2003). The weight of each fresh concrete sample was kept constant at 2365 kg per m^3. The initial As(V) loading was estimated based on the results of the column study and the proportions of the constituents in the concrete (Table 5.1). It is approximately 8.97, 17.95, 26.92, and 35.89 mg As(V) per 1 kg of fresh concrete corresponding to C5, C10, C15, and C20.

The characteristics of the final products were determined, and they consisted of compressive strength, RCPT, and VPV (Pic. S5.2, Appendix 3). Compressive strength was measured using UTC-4727G-2000 kN Capacity general-purpose compression testing frame - standard method ASTM C39/C39M-20 (El-Zohairy et al. 2020). In this method, a load of 0.25 ± 0.05 MPa/s was applied at a rate of movement, corresponding to a stress rate on the cylindrical sample, until the load indicator presents a steady decrease of the load, and the concrete sample displays a definite fracture pattern. The RCPT was measured using Proove's It - Germany Instrument in accordance with standard method ASTM C1202-19 (Xuan et al. 2019). In this method, a 50 mm-thick slice of the concrete sample was introduced to a potential of 60 V with two ends of the slice immersed in sodium chloride solution and sodium hydroxide solution, respectively. After 6h, the total charge that passed through the sample was measured to obtain the sample's resistance to chloride ion penetration. The VPV of the product was measured according to the standard

method ASTM C642-13 (Kumendong et al. 2019). The VPV percentage of each concrete sample was calculated based on the decrease in mass of a 50 mm-thick slice sample after drying in an oven at 110 ºC for 24 h, followed by immersing in water for 48 h and boiling for 5 h.

Table 5.1. Concrete mixture compositions

Name	Exhausted adsorbent waste (kg/m^3)	Sand (kg/m^3)	Aggregate gravels (kg/m^3)		Cement (kg/m^3)	Water (L/m^3)
			10 mm	20 mm		
C0	0	745	460	655	325	180
C5	37	708	460	655	325	180
C10	75	671	460	655	325	180
C15	112	633	460	655	325	180
C20	149	596	460	655	325	180

5.1.2.3 Leaching test

The leaching test on all concrete samples was conducted to determine whether leaching of As into the natural environment would comply with the stipulated USEPA regulation. Method 1313 of the Leaching Environmental Assessment Framework (LEAF), which was conducted in a batch extraction procedure, assessed the leaching potential (Kosson et al. 2014). This is a short-term procedure (24, 48 or 72 h, depending on the sample's particle size) performed at a wide range of pH (from 2 to 13).

The waste incorporated concrete sample (28 days-old) was crushed into a size of approximately 5 mm using a jaw crusher. The crushed concrete was then washed by deionized (DI) water to remove the dust and dried at 50 ºC for 8 h. 80 g of each dried

crushed concrete sample was mixed with 800 mL of DI water (solid/solution ratio of 1:10) whose pH was adjusted to 2, 4, 5.5, 7, 8, 9, 10.5, 12 and 13 using 2N HNO_3 and 1N KOH. The mixture was placed inside a 1L vessel and shaken at 28 ± 2 rpm for 72 h in an orbital shaker. The suspensions were filtered through 0.45 μm filters, and As in the filtrates was analysed using an Agilent Technologies 7900 ICP-MS instrument. The pH of the filtrate was also measured.

5.1.2.4 Characteristics of material

The characteristics of the exhausted adsorbent encapsulated concrete samples were evaluated using Scanning electron microscopy/energy-dispersive X-ray spectroscopy (SEM/EDS, Quanta-650 instrument), and X-ray diffraction (XRD, Empyrean-PANalytical instrument, Netherlands). These have been described in detail elsewhere (Nguyen et al. 2020b).

5.1.3 Results and discussion

5.1.3.1 Characteristic of concrete

a. SEM, EDS, and XRD

The SEM images revealed that generally, the surface of the concrete mix samples was rough and heterogeneous, and there was no visible change in the surface morphology of the samples before and after incorporating the contaminated unmodified VMO and modified VMOs (Fig. 5.1a, b). The absence of any change in morphology could be because the VMO derived from the mine contains many minerals/compounds whose morphologies are similar to the sand and aggregate gravels of the concrete mixture.

The EDS results showed that As element was not detected on the surface of all concrete samples (Fig. 5.1c). Only the elements included in the compositions of Portland cement, sand, and aggregate gravels were identified, which included Si, Ca, and Al (Aïtcin 2016; Kaur et al. 2019). The spectra of C5, C10, C15, and C20 were similar to that of C0, with no change in peak intensities, and no peak disappeared, or a new peak appeared after adding the adsorbent wastes into the concrete mixture.

Similarly, the XRD analysis of the various mixtures of concrete showed only peaks for the major minerals of concrete (Fig. 5.1d). The peaks at $2\theta = 21^{o}$, 26.5^{o}, 50^{o}, and 60^{o} are characteristics of quartz. The peak at $2\theta = 21^{o}$ can additionally be due to the presence of gismondine (Karanac et al. 2018). The peaks around $2\theta = 28^{o} – 29^{o}$ are due to calcite and feldspars (Karanac et al. 2018). No As(V) minerals were identified in the XRD result, and this is consistent with the EDS finding, which did not show any As elemental peak. This may be because the amount of As(V) in the adsorbent waste (< 0.05%) and the percentage of waste in the concrete mixture (< 7%) were very small in comparison to a large amount of concrete mixture. However, Singh & Pant (2006) detected a peak for calcium arsenite in XRD for a concrete mixture of As waste (As adsorbed to activated alumina). This was probably due to the much higher proportion of As in the mixture (approximately 75% waste in the mixture and 12.5% As in adsorbent) than what was used in the current study.

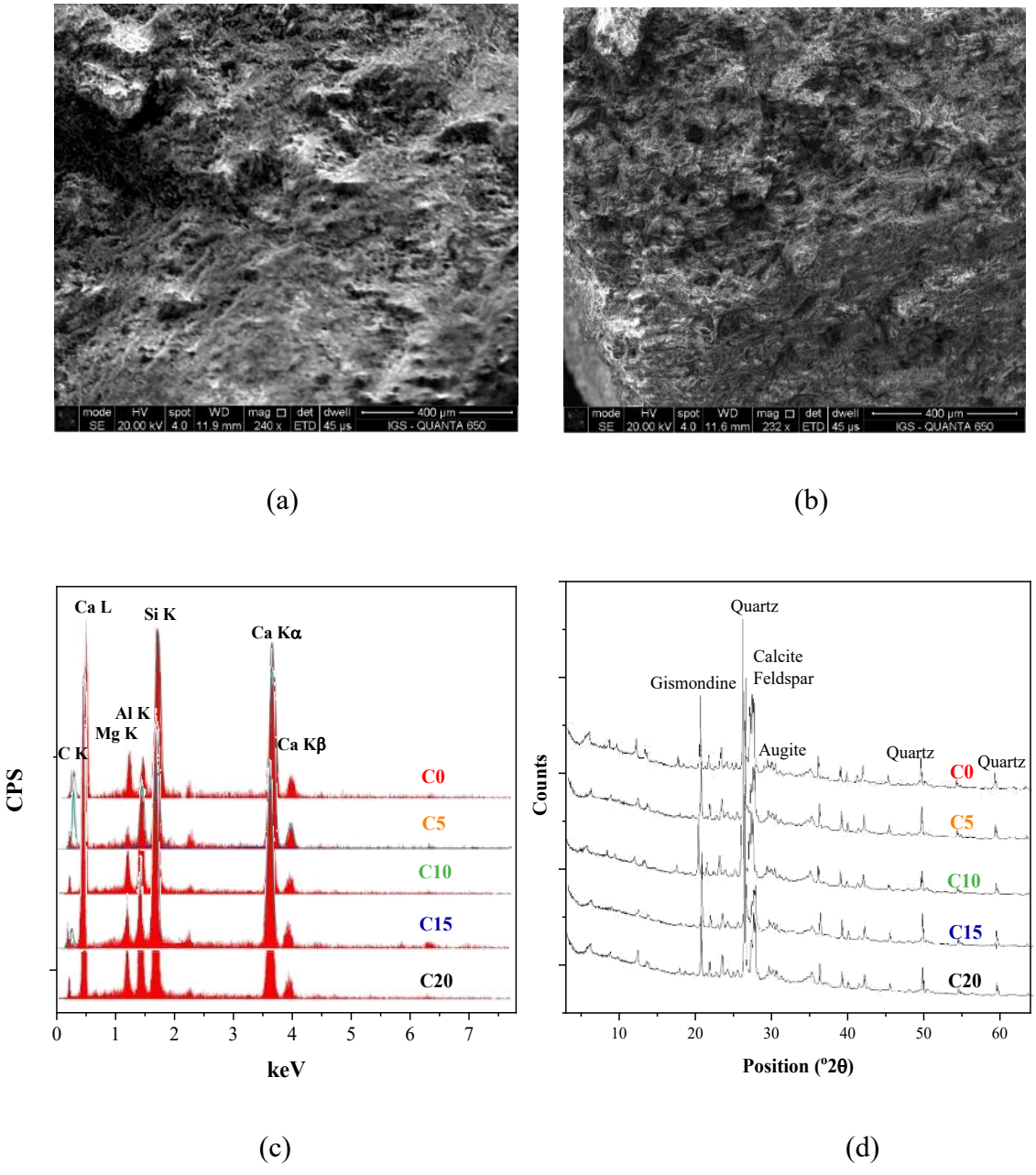

Fig. 5.1. SEM of the concrete mixture with (a) 0% and (b) 20% of adsorbent waste, (c) EDS spectrum, and (d) XRD patterns of five concrete mixture samples

b. Compressive strength, RCPT, and VPV

The compressive strength, RCPT, and VPV measurement results are presented in Table 5.2. The compressive strength results showed that after replacing sand by up to

20% exhausted unmodified and modified VMOs, the compressive strength declined only by a maximum of 4 MPa from the original value of 35 MPa. According to the Concrete Structures Standard of Australia AS 3600:2018, the concrete product with a minimum compressive strength of 20 - 32 MPa can be used to build footpaths and residential driveways (20 MPa), commercial and industrial floors not subject to vehicular traffic (25 MPa), and pavements or floors subject to pneumatic-tired traffic (32 MPa) (Khalajestani et al. 2018). Based on these standards, the concrete mixture produced by mixing exhausted adsorbent in this study can be used in many construction projects, such as the driveways, pavements, where humans will not have direct contact. The reason for the adsorbent waste addition not seriously affecting the compressive strength is that the original VMO adsorbent is also a crystalline inorganic material having similar mineral composition as sand and gravel in the concrete mixture, as well as due to the small amounts of waste added.

The ASTM C1202-19 determines the electrical conductance of concrete to provide a rapid indication of its resistance to the penetration of chloride ions via the rapid chloride penetrability test (RCPT) (Kaur et al. 2019). As the electrical charge passed through the concrete increases, the strength, performance, and the appearance of certain concrete structure will reduce, hence can lead to the corrosion of embedded steel bars within concrete (Sekar & Kandasamy 2019). Using this method, the charge passed through the five concrete mixes was measured to be 1175 – 1281 coulombs, which indicated that the chloride ion penetrability is low and the increase was only <1% with the adsorbent waste replacement of sand in all mixes (Table 5.2) (Kaur et al. 2019). The low charge transport through the concrete mixes suggests that the concrete mixes have greater compressive strength, denser materials with less porous microstructure, hence enhancing the chloride-

ion transport resistance (Kaur et al. 2019). In contrast, Kaur et al. (2019) found that when incinerated biomedical waste ash replaced sand in concrete at various proportions (5 – 20%), the charge increased from 1200 to 7825 coulombs. They stated that >10% replacement producing RCPT values of 6890 – 7825 coulombs was not acceptable as it can cause problems involving ions permeability.

According to standard ASTM C642-13, the VPV gives an indication of the amount of moisture and air, which can penetrate into the concrete. The VPV values of the 5 concrete mixes are in the 12.2 - 14.7% range (Table 5.2), which are similar to that of lightweight concrete having many applications (Sekar & Kandasamy 2019). As in the case of RCPT, VPV value also changed very little with an increase in percentage replacement of sand by the adsorbent waste in the concrete mix.

Table 5.2. The characteristics of the concrete mixes

Features	Unit	C0	C5	C10	C15	C20
Compressive strength	MPa	35.4	33.2	31.7	32.5	31.2
RCPT (charge passed)	coulombs	1270	1175	1225	1275	1281
VPV	%	12.2	13.5	14.4	12.6	14.7

5.1.3.2 Leaching test

VMO and modified VMOs have proved to be low-cost, safe, and environmentally friendly adsorbents (Nguyen et al. 2020b). The coating agents used to modify VMO to increase its As(V) adsorption capacity, such as Fe and Zr, are also safe with regard to human health (Nguyen et al. 2020c). The commercial components (sand, cement, aggregates) used to make the concrete mixes have been employed widely and found to be

very safe. Therefore, in investigating the potential toxicity of elements that might leach from the concrete mixes, only As was tested in the leachate.

The results of the leaching test are presented in Table 5.3. They indicate there is virtually no As leaching from the solidified/stabilised samples. Only in 3 samples (at pH 13 of C15, at pH 4 and 13 of C20) was As detected, but its concentration is extremely low (0.0005, 0.0001, and 0.0014 mg/L, respectively). It is insignificant in comparison with the recommended limit stipulated in the TCLP of USEPA (up to 5 mg/L for As) (Jing et al. 2005).

The pH of all leachates in the leaching test, which had an initial pH from 2 – 13, increased to 10 – 13 after the leaching test process. The highly alkaline conditions of the cement, due to the presence of calcium (Ca) hydroxide, would have increased the leachate pH, and this could restrict the solubility of hazardous metals (Singh & Pant 2006). Both the high alkalinity and presence of a high concentration of Ca in cement would have resulted in the formation of Ca-As precipitates, and this may be the main mechanism that reduced or prevented the leachability of As (Jing et al. 2005; Sullivan et al. 2010).

Therefore, based on the results of compressive strength, RCPT, VPV, and As leachability tests, it can be concluded that the solidification/stabilisation product in this study is safe to dispose of or use as a structural construction material.

Table 5.3. As concentration in the leachates (mg/L)

Initial pH / Sample	2	4	5.5	7	8	9	10.5	12	13
C0	0	0	0	0	0	0	0	0	0
C5	0	0	0	0	0	0	0	0	0
C10	0	0	0	0	0	0	0	0	0
C15	0	0	0	0	0	0	0	0	0.0005
C20	0	0.0001	0	0	0	0	0	0	0.0014

5.2 Original and modified *luffa* fibre

5.2.1 Introduction

Phytoremediation is a promising soil pollution treatment method. This method has been trialled for As remediation from contaminated soil. Although phytoremediation takes a long time to attain results, it is still attractive due to its cost-effectiveness, in-situ application, environmental friendliness, and less damage being done to the world's biodiversity (Vithanage et al. 2012). In order to limit the negative effects of operating for a long time, native plant species are usually chosen for phytoremediation to reduce conflict with local ecosystems (Moreno-Jiménez et al. 2010). In the phytoremediation process, As transfers from bulk soil to the root surface and from the root to the shoot system via different mechanisms. It moves from the soil to the root through three separate mechanisms: (1) passive uptake through the apoplast, (2) direct transcellular transport from the environment to the plant vascular system, and (3) active uptake through the symplast. In plants, As is then moved from the root to the shoot through the translocation mechanism (Dabrowska et al. 2012).

There are many studies reported in the literature on As removal from As-contaminated soil by the phytoremediation method. Nahar et al. (2017) used transgenic and wild tobacco plants to reduce As(V) in soil. They transformed the *AtACR2 gene (arsenic reductase 2)* of *Arabidopsis thaliana* into the genome of tobacco *(Nicotiana tabacum, var Sumsun)*. As a result, the transgenic tobacco could accumulate 2,400 mg As/kg dry root weight, whereas the un-transgenic plant contained 2,100 mg As/kg dry root weight within 35 days. Titah et al. (2018) employed 8 week-old *Lludwigia octovalvis* plants to remove As(V) in soil. *Ludwigia octovalvis* was evaluated as a high biomass plant, which was suitable for the phytoremediation of As-polluted sites. It could remove 70% of As concentration from contaminated soil at 39 mg As(V)/kg soil after 42 days. The *Raphanus sativus* (radish plant) was also used to treat As(V) in As-contaminated soil. Smith et al. (2008) reported that radish plants could be able to reduce As concentration in the mine waste. The As concentrations were 120, 100 and 80 mg/kg in dry leaf, stem and root, respectively, after 35 days.

Amongst the various plants used in the phytoremediation method, plants that belong to the fern species have the most promising As removal capacity. Recently, Yang et al. (2020) reported that the As accumulation capacity of *Pteris vittata* and *Pteris multifida* was up to 22,630 mg/kg dry biomass and more than 1,000 mg/kg fronds (Du et al. 2005; Ma et al. 2001). In long-duration studies, Raj & Singh (2015) and Niazi et al. (2012) demonstrated that some fern plants such as *Pteris vittata, Pityrogramma calomelanos var. austroamericana, Adiantum capillus veneris* and *Christella dentata* performed well in removing As from contaminated soil.

In this study, the exhausted *luffa* fibre (LF) and their modified forms (FLF-3, and ZLF-3), which were collected after water treatment by the column filters, were managed

by the phytoremediation method. This strategy was selected since *luffa* fibre is a soil-friendly product that can be a good bio-material and is biodegradable. Similar to other plant fibres, *luffa* fibre can benefit the soil by improving water retention, supporting seedlings and aeration to the plant's roots, providing bedding for worms and creating potting mix. Here, the performance of phytoremediation in transferring As(V) from waste *luffa* fibre to plants was evaluated in terms of As(V) concentration that remained in the soil.

5.2.2 Material and methods

5.2.2.1 Material

The exhausted LF, FLF-3 and ZLF-3 adsorbents from the column experiments were dried at a temperature of 50 ^{o}C for 4 h. The exhausted LF, FLF-3 and ZLF-3 adsorbents were then mixed at a ratio of 1:1:1 before being added into the garden soil. This mixture was given the term waste LFs.

5.2.2.2 Phytoremediation

Pityrogramma calomelanos, a species of fern, was chosen in this phytoremediation study. The fern seedlings with strong roots and garden soil were purchased from a local landscaping shop in Sydney, New South Wales, Australia. The contaminated potting mix was created by adding waste LFs into garden soil at a ratio of 1g waste LFs : 30 g garden soil. This ratio was selected based on the recent results documented by Titah et al. (2018). The potting mix was manually mixed until it was visually homogenous.

Three seedlings were planted in three pots, namely LF1, LF2, and LF3. All pots contained the same amount of contaminated potting mix, i.e. 400 g. The amount of initial

As(V) in the potting mix calculated from data of column experiment and above mixing conditions was 38.56 mg As(V)/kg of potting mix. Two similar seedlings were also planted in the same garden soil. They were named LF01 and LF02 and used as control samples. All five *Pityrogramma calomelanos* pots were located next to the glass window in a laboratory. They were watered using tap water in a normal gardening process. Plants were grown naturally without adding any fertilisers or nutrients. The temperature in the laboratory was kept at 23 ± 2 ^{o}C. Fig. 5.1 illustrates the preparation process for the potting mix.

After six months, the plants were harvested. They were washed thoroughly with tap water to wash out the soil on the root and further rinsed with distilled water. The plants were then sectioned into root, stem, and leaf. Each part of the plants was dried at 70 ^{o}C for 6 h and ground using an electric grinder to produce dried powder samples.

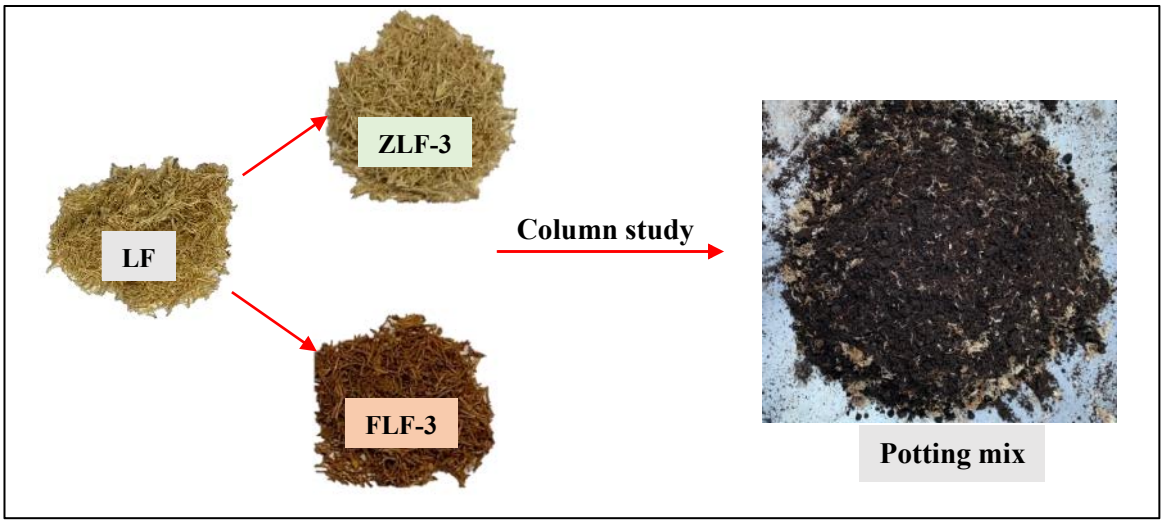

Pic. 5.1. The preparation of gardening soil mixture in the phytoremediation process

5.2.2.3 As determination test

In this study, a nitric acid digestion method introduced in the study by Smith et al. (2008) was applied to extract As(V) from the plant samples. Firstly, 500 mg of dried sample was digested by adding10 mL of concentrated HNO_3 (70%) onto a hot plate at 120 °C for 6 h. When the volume of samples reduced to 1 mL, 3 mL of 30% hydrogen peroxide was added. It was kept heated until the volume of samples was again evaporated down to 1 mL. Then, double-distilled water was added in to make final digested samples at a volume of 20 mL (Pic. S5.3, Appendix 3). The final digested samples were then filtered by a 0.45 µm filter and the filtrate was analysed for As using Agilent Technologies 7900 ICP-MS instrument.

5.2.3 Results and discussion

By observing the plants' growth, it can be seen that five plants, including three As-contained plants (LF1, LF2, LF3) and two blank plants (LF01, LF02), grew normally. There were no visual signs of As toxicity on LF1, LF2 and LF3. Although the budding of LF01 and LF02 was observed to be a little bit slower (15 days) than others (10 days) at the beginning, it is difficult to see any difference between the two groups of plants. It can therefore be stated that at the experimental conditions, there was no impact of As(V) on the growth of the plants. In their study, Raj & Singh (2015) studied the As treatment capability of four types of plants *(Pteris vittata, Adiantum capillus veneris, Christella dentata* and *Phragmites karka)* in three years. They also revealed that these plants grew well regardless of the difference in As concentrations in soil. However, some studies reported that the As concentration in soil could affect the growth of plants. In their study,

Ma et al. (2001) trialled the treatment of chromated copper arsenate (CCA) contaminated soil at a site in central Florida, United States, by *Pteris vittata*. They reported that the fern biomass production increased by 40% when the As(V) concentration in the contaminated soil was added at 100 mg/kg more in comparison with the control. Conversely, Smith et al. (2008) stated that in the study of liquid cultivation of radishes, the total yield of shoots and roots of *Raphanus sativus* declined to half when the As(V) concentration of growth solution rose from 0 to 30 mg/L. Moreover, when As concentration increased to 60 mg/L, the leaf tips became discoloured and necrotised. These changes were assumed to be signs of As toxicity.

After six months, all plants were harvested and prepared for the As determination test. In previous long-term studies, six months is considered to be enough time for As to be transferred from soil into fern species (Raj & Singh 2015). Fig. 5.2 illustrates the diffusion of As(V) from waste LFs into different parts of plants. It shows that most of the As(V) was transferred into the shoot (69 – 77%). Only 23 – 31% of As(V) was accumulated into the roots of the plants. The same tendency was also reported in previous studies. The As(V) amount identified at 61 – 64% in fronds and 36 – 39% in roots of *Pteris vittata, Adiantum capillus veneris, Christella dentata* and *Phragmites karka* plants in a three-year study (Raj & Singh 2015). After 35 days, the accumulation of As in radish was 73% in leaf and stem, and 37% in root (Smith et al. 2008). It confirms that most of the As in contaminated soil were transferred from soil to root and finally to the stem and leaf of plants.

The results show that the weight of a dry plant varied from 4.9 – 5.1 g, much lower than that of exhausted LFs. The concentrations of As extraction from each section of dried plants are presented in Table 5.4. The total As concentration in a dry plant was 2276 –

2298 mg As/kg dry plant, corresponding to the amount of 11.38 – 11.49 mg per plant. The analysis result for the blank plants, LF01 and LF02 shows that no As was found in all parts of the plant samples. In comparison with other fern species, particularly *Pteris vittata,* which is reported as As hyper-accumulating species (more than 3,500 mg/kg dry weight of fronds), the plants' accumulation of As in this study was lower (Niazi et al. 2012). However, the As(V) accumulation of plants in this study is similar to that of the transgenic and wild tobacco plants (2,400 and 2,100 mg/kg dry plant, respectively) (Nahar et al. 2017) and more than that of *Nephrolepis exaltata*, which can remove As(V) 29 times less than *Pteris vittata* (Silva Gonzaga et al. 2006).

Compared to the initial amount of As(V) in soil, 73.6% – 74.3% of As(V) in the LF1, LF2, and LF3 samples were transferred from soil to the plants. Based on this calculation, the As(V) concentrations remaining in the potting mixes – LF1, LF2, and LF3 – were 9.92, 10.13 and 10.20 mg As/kg, respectively. Unlike the regulations, these values were well below the recommended permissible soil As concentration as specified by the USEPA of 24 mg/kg (Abbas et al. 2018) and the ecological investigation level (EIL) limit of As in soil in Australia of 20 mg/kg (Niazi et al. 2012). Therefore, the As contaminated soil after phytoremediation can be safely reused or disposed of in the environment.

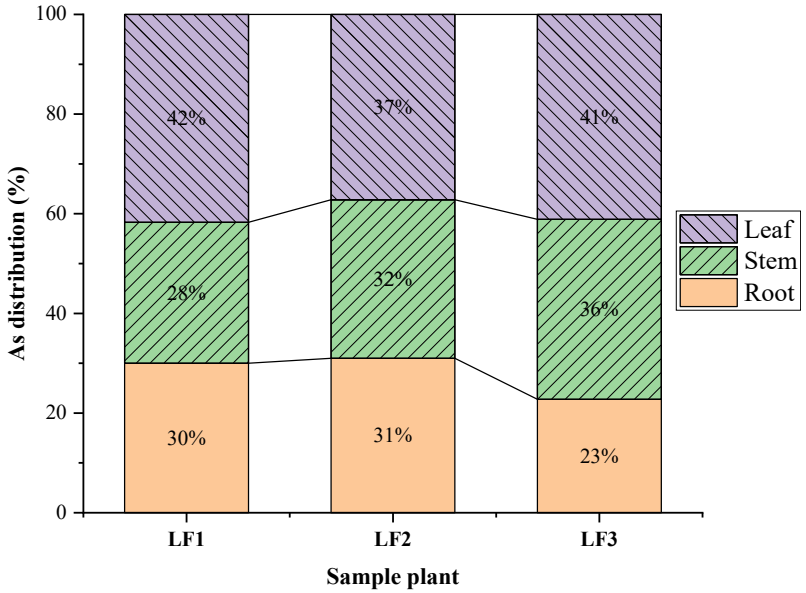

Fig. 5.2. The diffusion of As(V) from waste LFs into different parts of *Pityrogramma calomelanos* plants

Table 5.4. As concentration in the plant after six months of phytoremediation process

Sample	Concentration of As per plant section (mg/g dry weight)			mg As/dry plant
	Leaf	Stem	Root	
LF01	0.00	0.00	0.00	0.00
LF02	0.00	0.00	0.00	0.00
LF1	2.94	1.99	2.11	11.49
LF2	2.50	2.14	2.08	11.41
LF3	2.81	2.47	1.56	11.38

5.2.4 Conclusion

The waste of VMO and its modified forms, after adsorbing As(V) from treatment process could be managed successfully by the solidification/stabilisation method. The As exhausted media could be encapsulated together with cement, sand and gravel into the concrete. This solidified concrete had satisfactory compressive strength, RCPT, and VPV, which demonstrated good stability of the material. Therefore, it can be used as a building material in construction works. The amount of As(V) leaching from these materials into the environment was found to be negligible.

Most As(V) from exhausted bioadsorbent *luffa* fibre could be transferred to the fern plant through the phytoremediation method. After six months, *Pityrogramma calomelanos* could remove a large amount (73.6 – 74.3%) of As(V) from contaminated soil at 38.56 mg As(V)/kg. The dried plant was less than 40% of the initial amount of waste LFs. The As concentration in soil after phytoremediation proved to be much lower than the As permissible level of USEPA and the EIL level of Australia.

CHAPTER 6

Removing arsenate from water using batch and continuous-flow electrocoagulation with diverse power sources

Chapter 6. Removing arsenate from water using batch and continuous-flow electrocoagulation with diverse power sources

Summary

This chapter presents the fourth finding about a novel electrocoagulation process in As(V) removal from water. The paper based on this finding was submitted to the *Journal of Environmental Chemical Engineering* for possible publication. The details are given below.

Nguyen, T.T.Q., Loganathan, P., Dinh, B.K., Nguyen, T.V., Vigneswaran, S., Ngo H.H., Removing arsenate from water using batch and continuous-flow electrocoagulation with diverse power sources

The attraction of this work is the use of alternative power sources such as DC electricity, rechargeable battery, and solar energy. It is found to be an effective, simple, and low-cost method to treat As in the rural and isolated areas where electricity is limited. A series of experiments was carried out to identify the optimal conditions. The water treatment cost of this EC system was calculated and it shows very competitively.

[Production Note: Citation updates – This article has been accepted and published in *Journal of Water Process Engineering* in June 2021]

View/Download: UTS OPUS or Publisher's site

6.1 Introduction

Arsenic (As) is one of the world's most hazardous contaminants. It is estimated that more than 200 million people in 100 countries have been affected by drinking As polluted water (Singh & Stern 2017). A potential human carcinogen, As causes many other diseases related to skin, lungs, etc. (Sogaard 2014). It is distributed in the environment through natural and anthogenesis processes (Mohanty 2017). The two most toxic forms of As are arsenite (As(III)) and arsenate (As(V)), and their concentrations are controlled mainly by redox conditions and solubility. Whilst As(III) occurs at low redox potential, and its solubility is 10 g/100 mL of water, As(V) appears at a higher redox state and its solubility is up to 66 g/100 mL of water (Sogaard 2014). Although many technologies have been developed and applied to remove As from drinking water (Alka et al. 2020), As treatment is still a great challenge for the water industry, especially at a small and affordable scale applicable to rural and isolated areas. Among these methods, electrocoagulation (EC) is a promising method, which could eliminate the disadvantages of other traditional water treatment techniques (Kalaruban et al. 2017). For example, adsorption has the problem of adsorbent regeneration, interference from co-existing anions, and toxic exhausted adsorbent waste production, while chemical precipitation requires a large amount of chemical coagulants and sludge disposal problem. Some advantages of EC are its simple equipment requirements, easy operation, no use of chemicals, oxidisation of As(III) to As(V) during the process, and less sludge production (Kobya et al. 2016; Kumar et al. 2004). However, removing As through this method strongly depends on the operational conditions (type of electrodes, voltage, current, inter-electrode distance, operation time, solution pH and initial As concentration) and an

electrical source that can be expensive or unavailable in many rural or isolated regions (Mollah et al. 2001).

Many kinds of metal can be used as electrodes, such as iron (Fe), aluminium (Al), stainless steel, copper (Cu), titanium (Ti), and zinc (Zn) (Nidheesh & Singh 2017). Among these, Fe electrodes are the most widely used (Nidheesh & Singh 2017). Ucar et al. (2013) reported that when Fe electrodes in monopolar parallel electrode connection mode were employed, EC could remove up to 95% As(V) from 0.5 mg/L synthetic water at an electrical input of 4.5 mA/cm^2 in a batch experimental process. The hybrid electrodes with the combination of Fe, Al, or Cu were also tested for removing As (Song et al. 2017). The removal efficiency of the EC technique on treating As(V) with the above electrodes was reported to be 75 to 99% (Nidheesh & Singh 2017). The application of stainless steel electrodes also produced high As removals (Balasubramanian et al. 2009; Lakshmanan et al. 2010, Vasudevan et al. 2010). Though Fe electrodes are the most popular electrodes used in the EC process, they can create a problem in the form of water with a yellow colouration, principally due to the production of fine particles of rust. To overcome this challenge, stainless steel anodes have been used (Dura & Breslin 2019).

In order to reduce the electricity cost of the EC method, a few studies used solar power in EC to remove different contaminants in water. An EC system utilising solar power and batteries (60 W capacity) was shown to remove 92% of chemical oxygen demand and 49% of total dissolved solids by aluminium electrodes at a distance apart of 1 cm in 20 min (Nawarkar & Salkar 2019). In another study, an EC system using a 30.2 V solar-photovoltaic module (containing 12 polycrystalline silicon cells) was able to remove 99.9% of lead (Pb) from a solution containing 10 mg Pb/L in 10 min (Hussin et al. 2017). Studies on the application of solar energy in the EC system for removing As

from water are limited. Recently, Oh et al. (2019) used an EC system with large solar panels (380 to 750 W) to remove As from groundwater in Vietnam. Although this system obtained a high As removal efficiency (96.6% from a solution containing 0.376 mg/L in 10 min), this system was in fact large, and therefore the initial cost to install it was probably high. Moreover, it can only be installed, operated, and maintained by qualified technicians, and not by local residents. Instead of this type of large centralised solar energy system, a simple and smaller sized EC unit using smaller solar panels applicable to individual households, as and when clean water is required, is more suitable and affordable for rural areas.

In the present study, a new EC process using stainless steel electrodes was utilised to remove As(V) from synthetic water. The objectives of the study were to: firstly, determine the removal efficiency of As(V) from synthetic solution using an EC system with stainless steel electrodes in both batch and continuous flow mode experiments; secondly, determine the influence of many operating conditions of the EC system on As(V) removal, including voltage/current intensity, inter-electrode distance, operation time and solution pH; thirdly, compare different power supply sources (DC, rechargeable battery, and solar power) on As(V) removal and their cost of operation. The information obtained from the EC system in a continuous mode operation is useful in designing decentralised scale water treatment systems.

6.2 Material and Methods

6.2.1 Feed solution

A stock solution was prepared by dissolving 4.165 mg sodium arsenate ($Na_2HAsO_4.7H_2O$) in 1 L Milli-Q water to obtain a concentration of 1 mg As(V)/L. The stock solution was diluted with distilled water to the desired As(V) concentrations of 0.1, 0.25, and 0.5 mg/L for batch studies and 0.1 mg/L for continuous flow mode studies. The ionic strength of the solution was maintained at $1x10^{-3}$ M NaCl. The initial solution pH was adjusted to 6.0 – 8.0 (the pH range found to occur in groundwater) to study the effect of pH on As(V) removal, and in the other experiments, the pH was kept constant at 7.0 ± 0.2 by adding 0.1 M HNO_3 or 0.1 M NaOH.

6.2.2 EC system

A couple of commercial stainless-steel plates, grade 316 and size of 11 cm × 6 cm × 0.09 cm, were used as an anode and cathode. The electrodes were hung inside a transparent polypropylene tank (size of 10.2 × 10.2 × 20 cm) by a glass stick in a monopolar parallel connection mode so that the submerged part of the electrodes in the solution was 8 cm × 6 cm × 0.09 cm. The solution volume was 1L. To retain a uniform concentration, the solution was mixed by using a magnetic stirrer rotated at 120 rpm at the bottom of the tank. Batch and continuous-mode experiments with DC electricity and rechargeable battery were conducted using this set-up at room temperature of 25 ± 1 °C.

The voltages and generated electrical current supplied by this DC system could be varied through its converter. The performance of the EC system on As(V) removal was investigated at different conditions: electric potential difference 3.0 – 10 V, operation

time 5 – 120 min, initial As(V) concentration 0.1 – 0.5 mg/L, the distance between electrodes of 0.5 – 4.0 cm, and solution pH of 6 – 8. In each experiment, samples were periodically collected, filtered through 0.45 μm filters, and the filtrates were analysed for As using an ICP-MS instrument (Agilent Technologies 7900). The experimental scenario, which produced an As(V) concentration smaller than the WHO's permissible limit for As in drinking water at the lowest energy consumption, was considered to be the optimal treatment condition. The sacrifice rate of the anode was also determined in some experiments by measuring the electrode's weight before and after the experiment. The initial and final pH of the solution in all experiments were measured using a pH meter (model HQ40D) to investigate whether the pH of the solution changed and, if so, to what extent.

In order to evaluate the feasibility of using renewable energies, two other experiments were carried out at the optimal condition of the EC system determined in the initial experiments, using a 9 V rechargeable battery and a 12 V solar panel separately instead of the DC source of electricity. The 9 V rechargeable battery was simply connected to electrodes by using clips (Pic. 6.1b). The small 12 V solar panel (Powertech) was designed with 36 multi-crystalline silicon solar cells and a maximum power of 5 watts. The size of the solar panel was 25.1 × 20.5 × 1.8 cm with a weight of 0.7 kg (Pic. 6.1c). It was fitted with a blocking diode making it suitable for direct connection to the EC system by means of clips without using any intermediate equipment. The experiments with the solar panel were conducted outdoors and in the winter season from 10.00 am to 14.00 pm (July and August 2020, Australia). The voltage and current density of the solar panel were measured using a Multimeter Voltage Sensor (model QM1529). It

demonstrated that solar energy during this period was enough for the EC system's operation.

The operation of the solar panel, in general, depends on the weather conditions. On days when the sunlight is insufficient, it is recommended that a simple and low-cost rechargeable battery be employed for storing solar energy captured during bright sunny periods and then supply this stored power for the EC system on days with insufficient sunlight.

To evaluate the sacrifice (dissolution) rate of the anode, in addition to the calculation using Faraday's Law, a chemical analysis was conducted to measure the Fe concentration in the EC reactor. 1 mL of solution in the EC reactor at different operation times and currents was sampled and mixed with 5 mL each of 2M HNO_3 and 1M HCl. The mixture was then shaken at 50 rpm at room temperature for 1 hour, filtered and analysed for Fe using an ICP-MS instrument (Agilent Technologies 7900). This is a modification of the method utilised by Kalaruban et al. (2016).

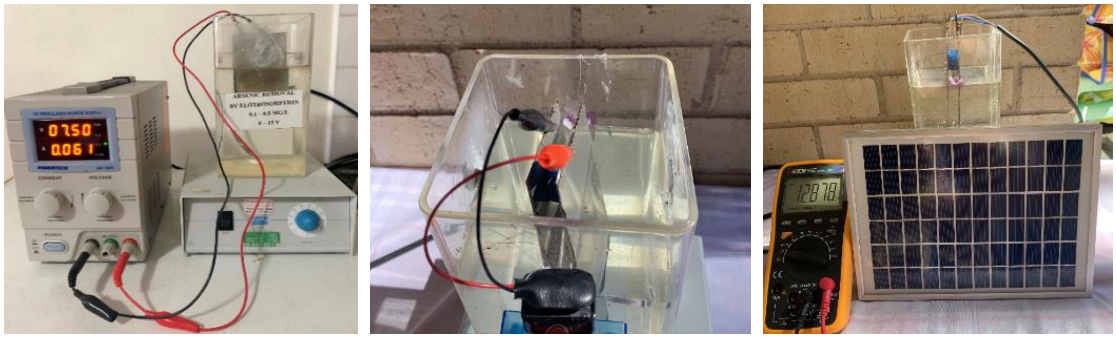

(a) (b) (c)

Pic. 6.1. Installation of EC system with (a) DC power supply, (b) 9 V rechargeable battery and (c) 12 V solar panel

In the continuous flow mode study, both the DC power supply system and the small 12 V solar panel were utilised separately with a small EC reactor (containing 1L of As-contaminated water) to investigate the As(V) removal efficiency. The system was operated at different hydraulic retention times (HRT) of 5, 10, and 20 min [HRT (min) = reactor volume (L)/flow velocity (L/h) × 60 (min)], corresponding to flow velocities of 12 L/h, 6 L/h, and 3 L/h. A schematic diagram of the continuous flow reactor is presented in Fig. 6.1. The synthetic feed solution containing 0.1 mg As(V)/L was pumped continuously by a dosing pump (Masterflex L/S) into the 1 L reactor at the optimal operating condition determined in the batch study (U = 7.5 V, I = 0.030 A, pH = 7.0 ± 0.2, electrodes distance 1 cm). The treated solution then automatically flows into the 2 L clarifier (Pic. S6.2, Appendix 4). The effluent samples in the clarifier were collected after 1, 2, and 4 h, then they were filtered and analysed for As, Fe and Chromium (Cr) using an ICP-MS instrument (Agilent Technologies 7900).

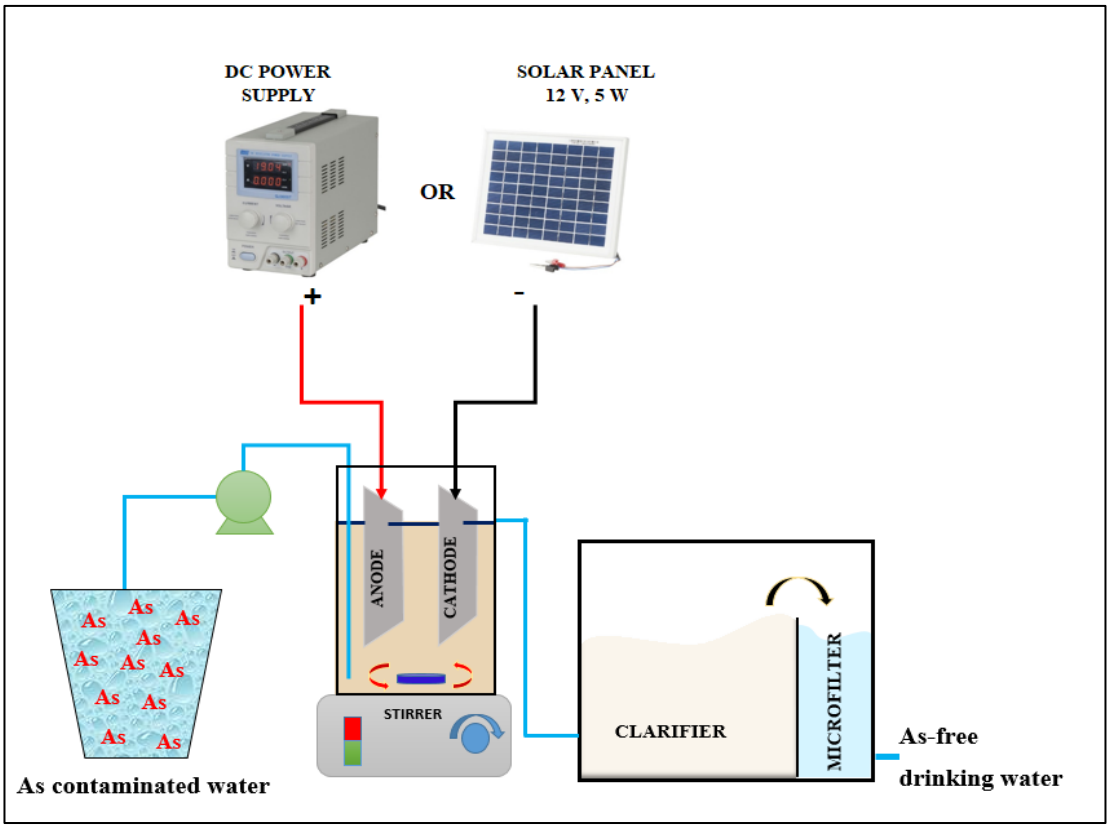

Fig. 6.1. The schematic diagram of the EC continuous flow reactor

6.3 Results and discussion

6.3.1 Batch study

6.3.1.1 Effect of initial concentration and operation time

Effect of initial As(V) concentration (C_o) was investigated at three concentrations, 0.1, 0.25 and 0.5 mg/L. In this experiment, the distance between electrodes, initial pH, and electrical potential difference (U) were 1 cm, 7.0, and 3 V, respectively. Under these conditions, the current produced was very small, only 0.007 A. Samples from the reactor container were collected at 5, 10, 15, 30, 45, 60, 90, and 120 min, and analysed for As, pH, and Fe. Fig. 6.2 depicts the effect of C_o on the residual As(V) concentration in water samples as a function of operation time (t_{EC} (min)). As can be seen from this figure, the

WHO permissible limit for As in drinking water (C_{WHO} = 10 µg/L, Nguyen, Loganathan, Nguyen & Vigneswaran (2020)) was attained after 60 min with C_o of 0.1 mg/L and 90 min with C_o of 0.25 mg/L. At C_o of 0.5 mg/L, the C_{WHO} could not be obtained within the 120 min tested in the experiment. Since As(V) concentration of around 0.1 mg/L is the typical level reported for As-contaminated groundwater in many countries (Nguyen, Loganathan, Nguyen, Vigneswaran, et al. 2020), it was chosen for use in the subsequent studies.

Fig. 6.2 also shows that the As(V) removal rate was sharp during the first hour and then decreased slowly with time for all As(V) concentrations as reported by others (Balasubramanian et al. 2009; Kumar et al. 2004a). This decline in the rate of As(V) removal is due to the decrease in solution concentration of As(V), which was in equilibrium with the As(V) adsorbed on the hydrous iron oxide/hydroxide precipitates formed from Fe dissolution derived from the anode during the EC process. When the As(V) concentration drops, so does the maximum loading of As(V) per mg of Fe precipitates in equilibrium (Amrose et al. 2013). These precipitates were formed by the reaction of Fe with the OH^- ions generated in the cathode at the neutral pH of the solution (Balasubramanian et al. 2009; Kobya, Demirbas & Ulu 2016). It is also possible that at longer EC times, the As(V) concentrations became very small to produce additional Fe/As co-precipitation, mainly because the soluble products of Fe/As precipitates would not have reached at these low As(V) concentrations.

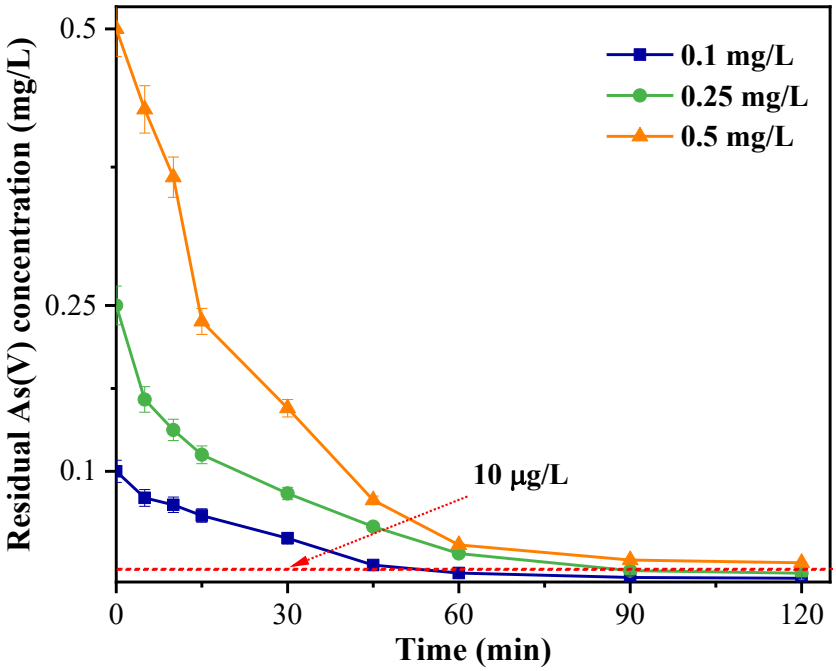

Fig. 6.2. The effect of As(V) initial concentration at 3V, pH = 7.0, and electrodes distance = 1 cm. The 10 µg/L horizontal line within the figure represents As concentration limit in the WHO drinking water guideline

6.3.1.2 Effect of electric current and anode dissolution

The effect of electrical current was studied by keeping the distance between electrodes, $C_{o,}$ and pH constant at 1 cm, 0.1 mg/L, and 7.0, respectively. The voltage of power supply source (U) was adjusted to 3 V, 5 V, 7.5 V, and 10 V, and the corresponding values of the electrical current (I) were measured as 0.007 A, 0.018 A, 0.030 A, and 0.061 A, respectively. The experiment remained running for up to 120 min. Results showed that C_{WHO} could be reached in 15 min at 0.018 A (U = 5 V), which is much faster than that at 0.007 A (U = 3 V) (Fig. 6.3a). At the higher currents of 0.030 A (U = 7.5 V) and 0.061 A (U = 10 V), C_{WHO} was reached extremely quickly (within 5 min). Consistent with these data, the increase in the electrical current led to rising As(V) removal efficiency. For

example, at t_{EC} of 5 min the removal efficiency (E%) increased from 24% to 58.5%, 92%, and 96%, corresponding to the rise of the current values from 0.007 A to 0.018 A, 0.030 A, and 0.061 A, respectively. The possible reason for this is that at a higher electrical current, a larger amount of hydrous iron oxides/hydroxides was generated (Amrose et al. 2013; Balasubramanian et al. 2009; Kobya, Demirbas & Ulu 2016). This led to the removal of a larger percentage of As(V) due to As(V) replacing the increasing number of hydroxyl groups in the iron precipitates (Kobya, Demirbas & Ulu 2016). It is also possible that at high concentrations of Fe, As is removed by co-precipitation with Fe (Nur et al. 2019). Other studies also reported that As removal efficiency was proportional to the current density (Amrose et al. 2013; Kobya, Demirbas & Ulu 2016; Vasudevan, Lakshmi & Sozhan 2010).

Fig. 6.3a also shows that the As(V) removal efficiency significantly increased when t_{EC} increased from 5 min to 120 min. For example, at the current value of 0.018 A (U = 5 V), As(V) removal efficiency at 5 min was only 58.8%. However, it increased to 79.7% after 10 min and reached almost 99% at 30 min. The increase of t_{EC} elevated the amount of dissolved Fe as observed for the effect of an increase in current. The higher amounts of dissolved Fe would have produced abundant Fe hydrous oxides/hydroxides, leading to a greater amount of As(V) being removed by adsorption. Greater amounts of As(V) are also removed by co-precipitation with Fe at high concentrations of Fe (Nur et al. 2019).

In order to evaluate the sacrifice (dissolution) rate of the anode, the mass of Fe generated at the anode m_{Fe} (mg), and the electrode consumption concentration $C_{electrode}$ (mg/L) for the As removal from water were calculated using chemical analysis and Faraday's Law. The Faraday's Law equations are presented below (Kobya, Demirbas & Ulu 2016):

$$m_{Fe} = \frac{I \times t_{EC} \times M_{Fe}}{z \times F} \quad [6.1]$$

$$C_{electrode} = \frac{I \times t_{EC} \times M_{Fe}}{z \times F \times v} \quad [6.2]$$

where I is the current value (A), M_{Fe} is the molecular weight of iron (55,850 mg/mol), z is the number of electrons involved in the oxidation/reduction reaction (z_{Fe} = 2), F is the Faraday's constant (1F = 1608.06 A.min/mol), t_{EC} is EC operation time (min), v is the solution volume (v = 1 L).

Fig. 6.3b depicts that the calculated amounts of Fe ions generated as well as the weight of the anode lost increased with I and t_{EC} (Pic. S6.1, Appendix 4). For example, the increase of I from 0.007 A to 0.061 A led to a rapid increase in the sacrifice rate of the anode, from 5.2 mg/L to 127.1 mg/L after 120 min reaction. The Fe concentrations calculated from this equation at the end of the experiment (t_{EC} = 120 min), at I = 0.007, 0.018, 0.030 and 0.061 A were 14.6, 37.5, 62.5 and 127.1 mg/L, respectively. However, the corresponding concentrations of Fe measured by chemical analysis were much smaller, i.e. 7.9, 10.8, 22.6 and 35.2 mg/L, respectively (Fig. 6.3c). A possible reason for the difference in the chemical analysis and calculated values is that Faraday's law is valid only when all the electrons in the system participate solely in the metal-dissolution reaction at the anode, which seldom happens. Another reason for the lower measured value is that the anode used does not consist of pure Fe; it is stainless steel, which contains other metals such as Cr in addition to Fe. This is not taken into consideration in Faraday's equation.

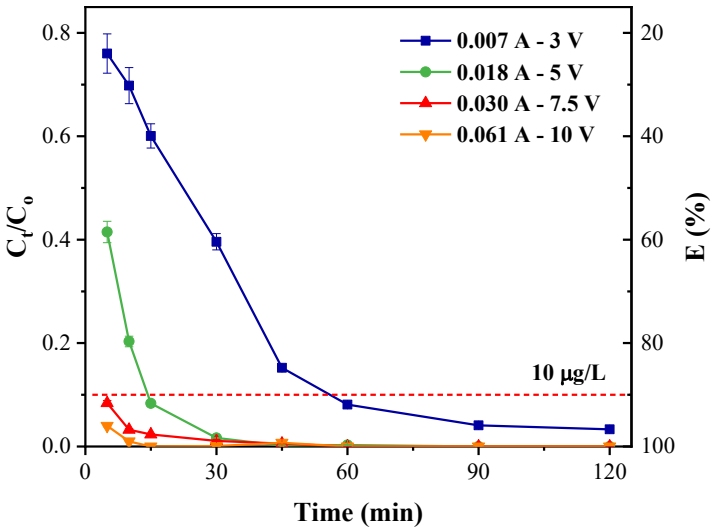

(a)

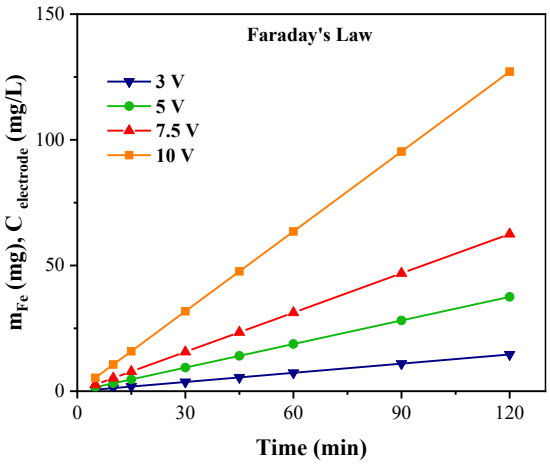

(b)

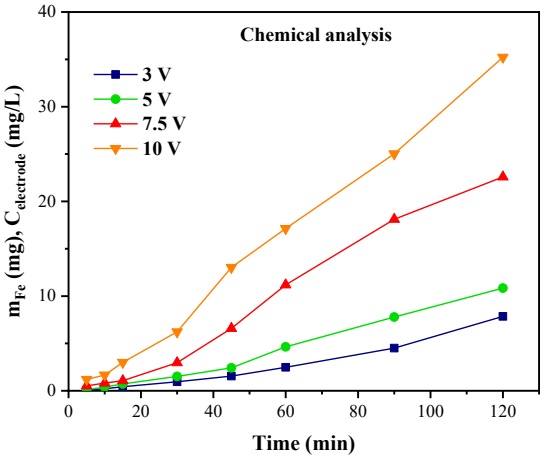

(c)

Fig. 6.3. The effect of electric current on As(V) removal (a) and the sacrifice rate of anode in the EC process as (b) calculated using Faraday's Law and (c) measured using chemical analysis, at C_o = 0.1 mg/L, electrodes distance apart = 1 cm, $pH_{initial}$ = 7.0. The 10 µg/L horizontal line within Fig. 6.3a indicates As concentration limit in the WHO drinking water guideline.

The initial solution pH of 7.0 increased slightly up to a maximum of 8.0 during the EC process. The precipitation of Fe dissolved from the anode would have reduced pH, but the amounts of OH^- generated at the cathode and OH^- ions released during As adsorption on the hydrous Fe oxide/hydroxides would have been more than the H^+ released during Fe precipitation. These reactions are possible reasons for the slight increase in solution pH.

According to the above results, t_{EC} = 5 min and the potential of 7.5 V were identified as optimal conditions for As(V) removal. In these conditions, C_{WHO} can be reached quickly (only 5 min compared to 15 and 60 min at the potentials of 3 V and 5 V, respectively) while ensuring minimum energy usage (less energy than that at the potential value of 10 V). This condition was chosen for analysis in the subsequent studies.

6.3.1.3 Effect of distance between electrodes

This study was carried out at C_o of 0.1 mg/L, pH of 7.0, t_{EC} of 5 min, U of 7.5 V, and varying electrodes distance apart of 0.5, 1.0, 2.0, 3.0, and 4.0 cm. As can be seen from Fig. 6.4, As(V) removal efficiency and current values increased when the distance between electrodes was reduced. At electrodes distance apart of 0.5 cm, the current intensity and As(V) removal efficiency reached 0.087 A and 99.5%, respectively. These values fell to 0.030 A and 92%, respectively, at an electrodes distance apart of 1 cm. When the electrodes distance apart increased to 2, 3, and 4 cm, the EC system increasingly proved to be inefficient for removing As(V), reaching values of less than 20%. This decline in removal efficiency can be explained as being caused by the increase in the space between the electrodes, which in turn decreased the current generated (down to 0.003 A). The end result was less Fe dissolution from the anode for its interaction with

As(V) ions (Kalaruban et al. 2017). Similar outcomes were reported for the removal of other contaminants from water via the EC process, such as removing water hardness using Fe-rod electrodes (Malakootian, Mansoorian & Moosazadeh 2010), mercury using Al and Fe electrodes (Nanseu-Njiki et al. 2009), and indium ions using Fe electrodes (Chou & Huang 2009).

Although the inter-electrode distance of 0.5 cm produced the best As(V) removal efficiency, the cost of electrical power (voltage x current) consumed is high due to the high current generated. Therefore, the next shortest inter-electrode distance of 1 cm was selected as the optimal distance and applied in subsequent studies. Moreover, this distance is more practical to maintain in the EC installation set-up.

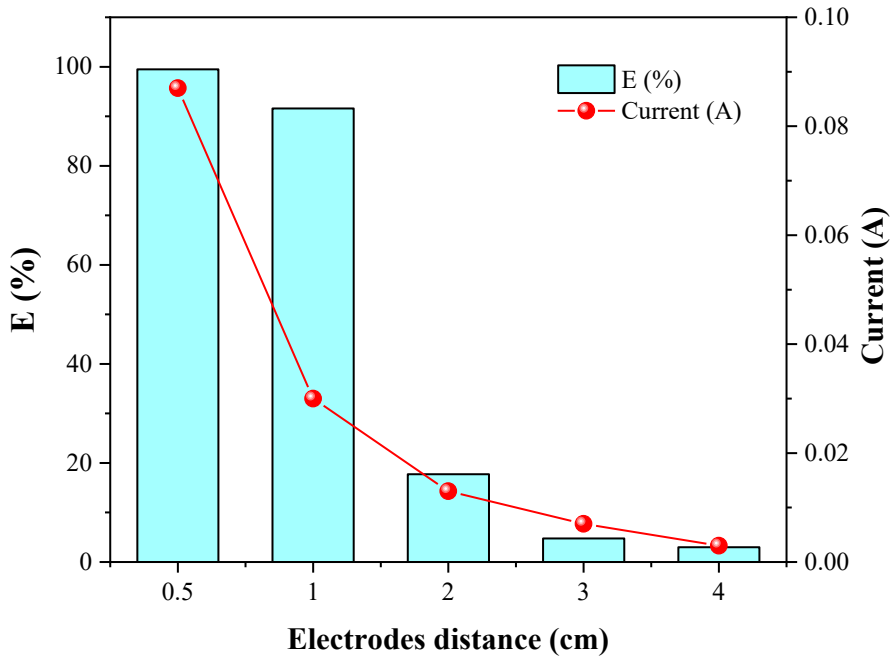

Fig. 6.4. The effect of distance between electrodes on As(V) removal efficiency and current generated, C_o = 0.1 mg/L, pH = 7, potential value = 7.5 V.

6.3.1.4 Effect of solution pH

The solution pH is one of the important factors influencing contaminants removal in the water treatment process. Investigation of the effect of solution pH was conducted at pH varying from 6 to 8 because it is a common pH range in most As-contaminated groundwater (Kumar et al. 2004a). Fig. 6.5 shows that As(V) removal efficiency slightly increased when pH was increased from 6 to 7 and then decreased as the pH is further increased to 8. A slight increase in the final solution pH was also observed, the reasons for which were presented in Section 6.3.1.2. The decrease in As(V) removal at lower pH is possibly due to the dissolution of iron hydroxide precipitates that were responsible for adsorbing the added As(V) (Balasubramanian et al. 2009). The reduction in As removal at the higher pH of 8 could be due to reduced adsorption of the more negatively charged As species on the negatively charged iron hydroxide precipitates (Nguyen, Loganathan, Nguyen, Vigneswaran, et al. 2020). It is well known that the negative charges on the surface of Fe oxide/hydroxide (Kalaruban et al. 2019) and on the As species increase ($H_2AsO_4^-$ to $HAsO_4^{2-}$) with pH (Thakur & Mondal 2017).

Based on the results of all the batch studies conducted, it can be concluded that the highest As(V) removal at C_o 0.1 mg/L could be achieved at pH of 7, t_{EC} of 5 min, electric potential of 7.5 V (corresponding to the current value of 0.030 A), and electrodes distance apart of 1 cm. These conditions were therefore considered as the optimal conditions for the EC process and employed in the subsequent studies on the use of alternative power sources and continuous flow mode process.

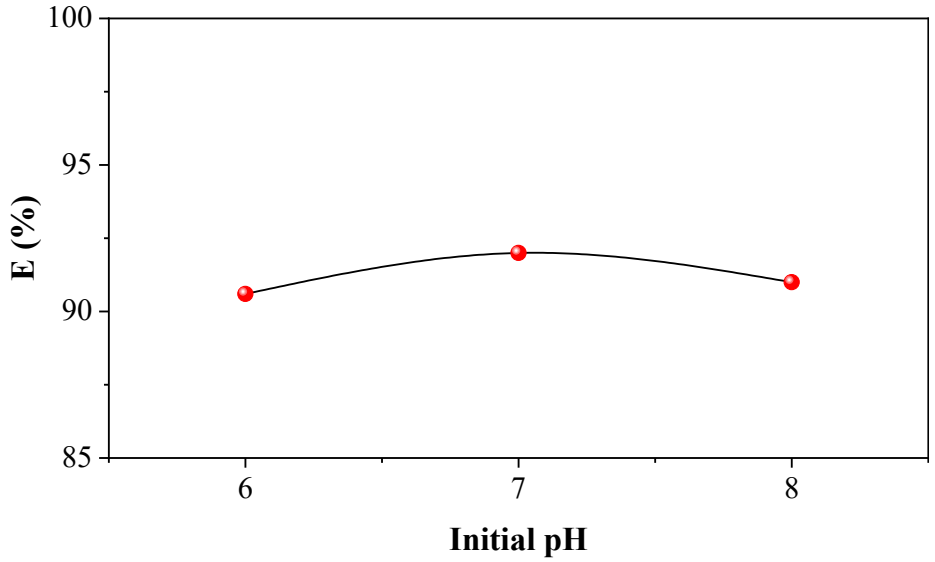

Fig. 6.5. The effect of initial solution pH on As(V) removal efficiency, C_o = 0.1 mg/L, electrodes distance apart = 1 cm, electric potential = 7.5V, t_{EC} = 5 min.

6.3.1.5. Use of alternative power supply sources

Batch experiments with alternative power supply sources were conducted using either a small 12 V solar panel or 9 V rechargeable battery. These experiments can provide vital information on whether renewable energy can replace the DC power supply used to treat As(V) in the EC system. Fig. 6.6 shows that the As(V) removal efficiency of both renewable energy sources was approximately the same as that of the DC power supply (93% for rechargeable battery and 98% for solar panel compared with 96% for the DC electrical source). This result indicates that renewable energy sources such as a rechargeable battery or a small-scale solar energy system can remove As(V) effectively in miniature portable EC systems that are suitable and affordable for rural households.

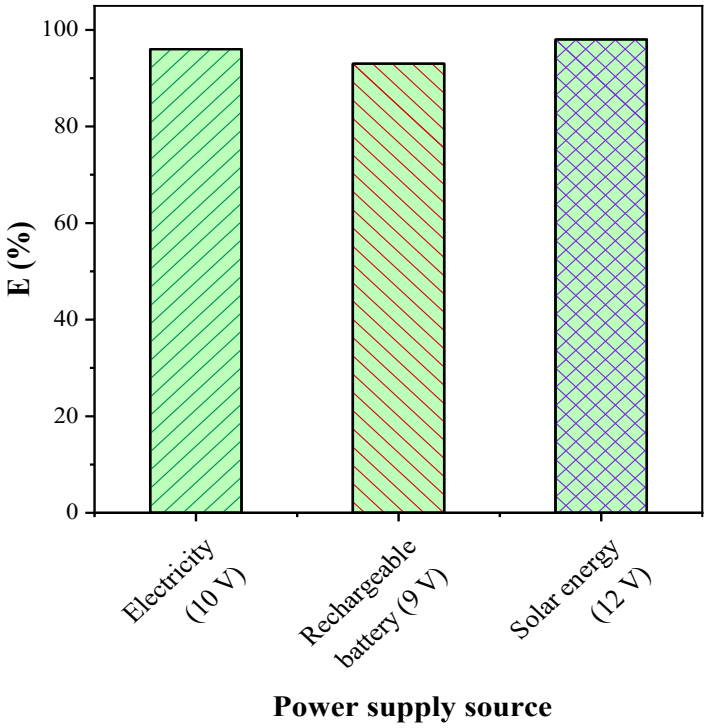

Fig. 6.6. The As(V) removal efficiency of EC system using different energy sources in batch study, C_o = 0.1 mg/L, pH = 7, t_{EC} = 5 min and electrodes distance apart = 1 cm

6.3.2. Mechanisms of As(V) removal in the EC process

The main chemical reactions in the EC process and the reactions involving As(V) removal from the solution are presented in Fig. 6.7 (Gilhotra et al. 2018). The two prime mechanisms of As(V) removal in the EC process are co-precipitation of As(V) with the various Fe ion species generated in the EC process and adsorption of As(V) on the hydroxide precipitates of Fe^{2+} and Fe^{3+}. These are depicted in the last four equations in the solution compartment of Fig. 6.7 (Kobya et al. 2020).

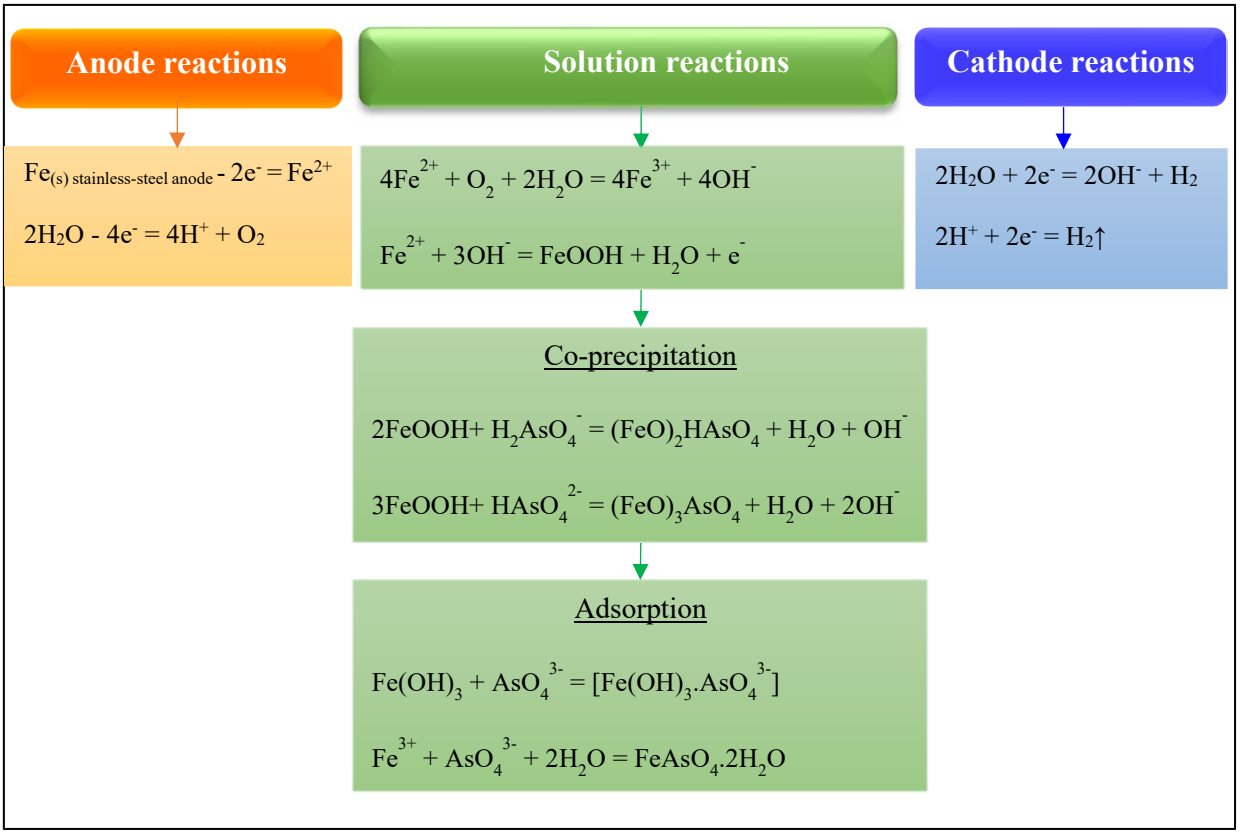

Fig. 6.7. Mechanism of As(V) removal from water using EC process with stainless-steel electrode

6.3.3. Continuous flow mode study

This study was conducted in two EC systems. The first EC system was operated with the 7.5 V DC electrical source, and the second one was with the small 12 V solar panel. Solution with 0.1 mg As(V)/L was continuously supplied to the EC reaction chamber at three different flow rates (12, 6, 3 L/h, corresponding to HRT of 5, 10 and 20 min). Fig. 6.8 shows that the As(V) removal efficiency of both systems was maintained at more than 91% during 4 h operation at all 3 flow rates. The residual As(V) concentration in the effluent was always lower than that of the WHO drinking water guidelines. The solar energy system's As(V) treatment efficiency (> 96%) was higher

than that of the electrical system (> 91%) at all flow rates due to the higher voltage of the solar panel. Results also show that the Fe concentration was below the WHO guideline value and Vietnam's water quality standard of 0.3 mg/L for drinking water (Le Luu 2019; Mohora et al. 2018). The effluent concentration of Cr, one of two main elements in the stainless steel was not detected by the ICP-MS instrument (< 0.01 µg/L).

Fig. 6.8 also shows that a decrease of flow rate (an increase of HRT) increases the efficiency of As(V) removal. This is because at higher HRT, As(V) had longer time to interact with Fe hydroxides leading to greater adsorption and co-precipitation.

The results show that the solar-EC system with a flow rate of 12 L/h could be chosen for application in decentralised water treatment systems in rural and isolated areas. Though lower flow rates can remove higher percentages of As(V), the volume of water treated would be lower. However, for contaminated water containing very high As concentrations, lower flow rates (higher HRTs) may be necessary. At the flow rate of 12 L/h, an EC reactor of a small volume of 1 L could provide 12 L clean water per hour. This flow rate is nearly the same as that of many commercial household filters currently being used. On a normal day, the system can produce 48 L of As(V)-free water during an 4-hour operation, which is enough to meet the drinking water demand of the average family.

Although the solar energy system has many advantages such as simplicity, cost-effectiveness, and non-electrical appliance requirements operating the solar panel depends on the weather conditions. The recommended solution for this issue, as stated in section 2.2, is using an appropriate rechargeable battery for storing solar energy during favourable weather conditions and using it when solar energy is limited.

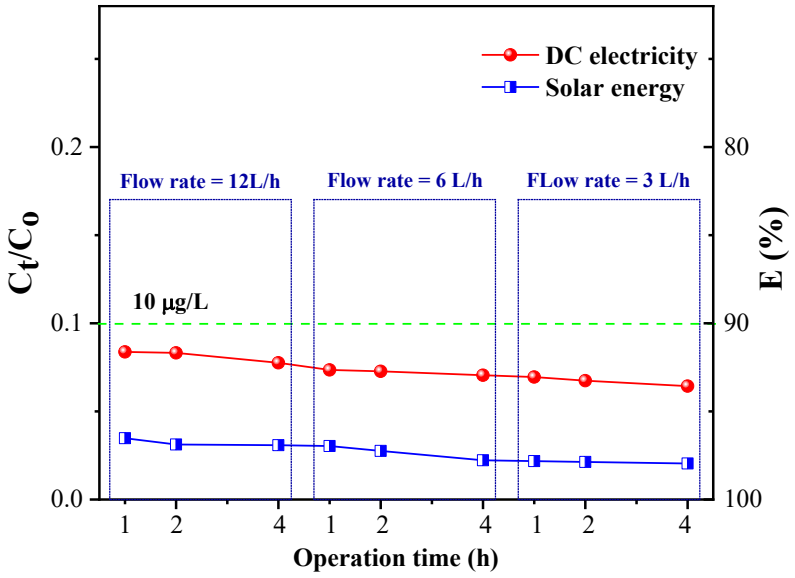

Fig. 6.8. The As(V) removal efficiency of EC system using DC electricity and solar energy at various flow rates, feed solution concentration C_o = 0.1 mg/L, pH = 7, electrodes distance apart = 1 cm. C_t (mg/L) is As concentration in the treated solution at time t (h). The 10 µg/L horizontal line within the figure represents As concentration limit in the WHO drinking water guideline.

6.3.4. EC operation cost

Operating cost is one of the most important factors in water treatment technologies because it decides the applicability of the treatment method in real-life situations, which primarily depends on users' budgets. The operating cost of the EC system in continuous flow mode was calculated for DC and solar power sources according to Eq. 6.3 and presented in Table 6.1. Here the price of Australian electricity was assumed to be A$0.30/kWh (Energy Australia, 2020):

$$\text{Treatment cost/m}^3\text{ water} = \text{Electricity cost/m}^3 + \text{Electrode cost/m}^3 + \text{Reactor cost/m}^3 \quad [6.3]$$

The lifespan of the anode for the small-scale reactor was determined by measuring the amount of Fe in solution. For a given reactor of 1L operated at the optimal conditions (initial As(V) concentration 0.1 mg/L, pH 7.0, electrode distance 1 cm, U= 7.5 V for DC power or 12 V for solar energy), the sacrifice rate of anode $C_{electrode}$ was measured to be 0.516 mg/L for the DC electrical EC system and 0.664 mg/L for the solar energy EC system. In one day, the EC system could treat 48 L water for 4 hours (1 m^3 in 20.83 days; see Section 3.3 for calculation) and consume 24.77 and 31.87 mg of the anode for DC electricity and solar energy system, respectively. The weight of the submerged part of the selected anode in this reactor was measured as 32,000 mg. Assuming that the anode can be effectively used until 50% of it is dissolved, the anode could be used for 645 (32,000/24.785 x 50%) days using DC electricity source (at U = 7.5 V) or 502 (32,000/31.866 x 50%) days using solar energy (at U = 12 V). The total volume of treated water produced per lifetime of the anode is calculated as 31.0 m^3 (645 days/20.83 days/m^3 water) using the DC electricity source and 24.1 m^3 (502 days/20.83 days/m^3 water) using a solar panel source.

Table 6.1. Cost calculation for EC system operation using DC electricity and solar energy (based on flow rate 12 L/h, operation time 4 h/day, and treatment capacity 0.048 m^3 water/system.day or 20.8 day/m^3 water)

	Formula	EC system	Solar system
Voltage (V)	U	7.5	12
Current (A)	I	0.03	0.08
Power (W)	U x I	0.225	0.960
Operation time in 1 day (h)	h	4	4
Energy consumption in 1 day (kWh)	W x h x 10^{-3}	0.0009	0
Energy cost in 1 day (A$)	A$0.30/kWh x kWh	0.00027	0
Energy cost for 1 m^3 treated water ($/$m^3$)	A$0.30 x kWh x 20.8 d/$m^3$	0.00563 **(1)**	0 **(1)**
Electrodes cost (A$)		3	3
Mass of electrode dissolved ($C_{electrode}$, mg/day)		24.77	31.87
Electrodes lifespan (day) (up to 50% dissolution)	= 32,000 mg/ ($C_{electrode}$ mg/m^3) x 50/100	645	502
Electrode cost/m^3 treated water ($/$m^3$)	= A$3/(lifespan d * 0.048 m^3/d)	0.097 **(2)**	0.125 **(2)**
Capital cost (Power supply and accessory in a reactor) (A$)*		12	12
Lifetime of power supply (year)**		5	5
Reactor/m^3 treated water ($/$m^3$)	= A12$/(lifetime y x 365 d x 0.048 m^3/d)	0.137 **(3)**	0.137 **(3)**
Treatment cost ($/$m^3$): (1) + (2) + (3)		0.240	0.262

Note: * Cost of the EC reactor, including power supply system DC or solar panel and accessory like buckets, is A$12.

** Assuming that the lifetime of the power supply is 5 years. According to the supplier, the lifetime of the solar panel could be as long as 20 years, and at least 10 years for power supply system DC.

The calculation shows that the DC electricity cost in this study is considerably low, 0.00563 A$/m^3 of treated water while the cost of the solar energy system is zero. The cost for the treatment of As-contaminated water is 0.240 A$/m^3 water for the electrical EC system and 0.262 A$/m^3 for the solar EC system. The slightly higher cost of the solar energy system is due to its higher voltage, which dissolved larger amounts of the anode. This resulted in a higher percentage of As being removed. Such a high percentage is not required for the solution of As concentration 0.1 mg/L used here because the final As concentration is well below the WHO limit. However, for waters containing higher As concentrations, this is an advantage.

In comparison with the estimated cost reported in other EC studies, the cost estimated in this study is lower. For example, Şık et al. (2017) and Thakur & Mondal (2017) reported treatment costs of $0.546 US$/m^3 (A$0.746/m^3) and 0.357 US$/m^3 (A$0.488/m^3), respectively. However, the expense calculated from most of these studies only included operating cost (energy cost and electrode cost). In this study, in addition to the operation cost the capital cost is included.

6.4. Conclusions

The new small-scale (household) EC system with DC power supply using stainless steel electrodes could successfully remove As(V) from contaminated water and maintain the As concentration below the WHO recommended safety level. In the batch study, the ideal scenario for the EC system's operation was determined as pH 7.0, electrodes distance apart of 1 cm, voltage of 7.5 V and current intensity of 0.030 A for initial As(V) concentration amounting to 0.1 mg/L. The batch study using a rechargeable battery and

solar energy, which also confirmed that these renewable energy sources could be used instead of the DC source to remove As(V) effectively in the EC system.

In the continuous water flow study, both DC electricity source and solar energy were able to supply the required power for the successful operation of the EC system with a low capital cost of A$15 and running cost of 0.240 - 0.262 A$/$m^3$ treated water. The system with all three power sources could remove As(V) from water at very high rate of efficiency, more than 91 – 96%. A small volume EC reactor of 1 L could supply enough drinking water daily for a household, and the anode replacement only needs to be done after more than 55 days at 4 h/day of operation. The low-cost EC system can be used with or without a DC electricity source, so it can be implemented in all areas.

CHAPTER 7

Conclusion and recommendation

Chapter 7. Conclusion and recommendation

7.1 Conclusion

Due to the high toxicity of As and the wide distribution of As in groundwater in many countries, the health of more than two hundred million people around the world is being harmfully affected by using As-contaminated drinking water. There are high demands on simple and cost-effective As removal water filters since most of the affected people are living in developing countries' rural areas. This study concentrates on two simple and cost-effective technologies that can remove As (V) effectively from water. The results from adsorption studies using new low-cost manganese oxide ore (VMO), bioadsorbent *luffa* fibre (LF) and their modified forms show that the modified VMOs and LFs have high adsorption performance on As(V) removal. The exhausted media generated from the above adsorption process could also be safely managed by encapsulation into cement and phytoremediation methods. These management approaches could reduce the risks of releasing toxic wastes back into the environment. A novel EC method developed in this study could also successfully reduce As(V) level in the water below the permeable level in a short time. The novel EC system could operate effectively with an alternative electricity source and generate less toxic waste.

A summary of the results of this study is presented in detail below.

7.1.1 Removal As(V) from water using original and modified natural manganese oxide ore (VMO, Fe^a-VMO, and Zr^a-VMO)

- Natural VMO originating from mines in northern Vietnam contains minerals, i.e. 25.6% Mn and 16.1% Fe. It was coated successfully by Fe or Zr separately to produce novel adsorption media, namely Fe^a-VMO and Zr^a-VMO. The ratio of Fe and Zr on Fe^a-VMO and Zr^a-VMO were 6.0% and 9.8% higher than that of VMO, respectively.
- The characteristics of VMO changed significantly after modification. Fe^a-VMO and Zr^a-VMO possessed more porous layers/channels, higher BET surface area, and larger pore volume than the original VMO. The surface charge of the modified VMOs was also more positive than that of the original VMO at all studied pH levels. Thus the modified forms have more affinity to As(V) than VMO.
- The As(V) adsorption capacity of modified VMOs was much higher than that of unmodified VMO. At pH 7.0 and As(V) initial concentration of 0.5 mg/L, the Langmuir adsorption capacities of Fe^a-VMO (2.19 mg/g) and Zr^a-VMO (1.94 mg/g) were nearly 20 times higher than that of VMO (0.11 mg/g).
- All types of VMOs could adsorb As(V) rapidly in the first 30 min. The adsorption rate then slowed down due to the reduction of adsorption sites. In addition to PFO and PSO models, the Elovich model fitted well to the data of adsorption kinetics. This outcome indicates that the main mechanism adsorption of these adsorbents is chemisorption.
- The As(V) adsorption was significantly influenced by solution pH and coexisting ions. The optimal pH for the As(V) adsorption of VMO and its modified forms was 3.0. The As(V) removal efficiency was observed to decrease with the increase

in pH. The existence of other anions such as PO_4^{3-}, SO_4^{2-}, SiO_3^{2-} and CO_3^{2-} in solution reduced the adsorption ability of these adsorbents through competition. The sequence was as follows: $PO_4^{3-} > SiO_3^{2-} > CO_3^{2-} > SO_4^{2-}$.

- The bed volumes of water (As (V) concentration 0.1 mg/L) treated to maintain the As(V) concentration below the WHO guideline concentration were 8 and 16 times higher for Fe^a-VMO, 6 and 12 times higher for Zr^a-VMO than for unmodified VMO at flow rates of 0.15 and 0.5 L/h, respectively.
- In the column study, an increase in influent As concentration increased the adsorption capacity, but increasing the flow rate reduced the adsorption capacity.
- The maximum adsorption capacities derived from the Thomas model for VMO, Fe^a-VMO, and Zr^a-VMO at an influent concentration of 0.25 mg As(V)/L, and flow rate of 0.15 L/h were 0.151, 1.145, and 0.925 mg/g, respectively. These values dropped when influent As(V) concentration decreased or the flow rate increased.
- The cost of VMO, Fe^a-VMO and Zr^a-VMO were estimated to be A$0.40/kg, A$0.80/kg and A$1.67/kg, respectively. At the flow rate 0.15 L/h and initial As(V) concentration of 0.1 mg/L, the cost to produce safe drinking water (< 0.01 mg As/L) by VMO, Zr^a-VMO, and Fe^a-VMO are estimated to be A$1.111/$m^3$, A$0.742/m^3, and A$0.278/$m^3$, respectively. At the same operation conditions, the costs of modified VMOs are lower whereas the adsorption capacities of modified VMOs are higher than that of commercial GAC.

7.1.2 Removal As(V) from water using original and modified *luffa* fibre (LF, FLF-3, ZLF-3)

- LF is a bio-material that originates from the *luffa* plant, and it belongs to the family of *Cucurbitaceae*. The major components of LF are cellulose (60 – 66%), hemicellulose (17 – 22%), and lignin (11 – 15%). It served as an adsorbent to remove methylene blue dye, phenol, and lead from water. However, to the best of the author's knowledge, it is the first time LF was used for removing As(V) from water.
- LF was grafted three times by $FeCl_2.4H_2O$ or $ZrOCl_2.8H_2O$ at pH 4.2 – 4.5 and dried at 70 ^oC in 24 h to produce new adsorbents, namely FLF-3 and ZLF-3, respectively.
- The grafting process significantly changed the characteristics of pristine LF. The surface morphology of LF changed from flat, smooth, homogeneous to irregular and porous. The ratios of Fe and Zr in grafted LFs were 6.09 and 4.95%, respectively. The BET surface area of the original LF also rose 11– and 18– fold after modification by Fe and Zr, respectively.
- The modification also changed the zeta potential of LF from negative to positive for FLF-3 and ZLF-3 at all pHs, which facilitated the As(V) adsorption.
- The Langmuir maximum adsorption capacity of LF (0.035 mg/g) at an initial concentration of As of 0.5 mg/L increased 70 – 80 times after grafting LF with Fe (2.55 mg/g) and Zr (2.89 mg/g).
- The adsorption capacity of pristine LF was slightly lower than that of other natural plants. However, the adsorption capacity of modified LFs was higher than that of

many modified adsorbents, such as iron hydroxide modified activated carbon, manganese oxide-modified pine biochar, and iron oxide-coated *A. niger* biomass.

- The modification also shortened the saturation time of LF in kinetic adsorption, from 6 h to 4 h for FLF-3 and only 1 h for ZLF-3.
- The adsorption efficiency of LF and its modified forms was also affected by pH and co-existing anions. The optimal solution pH was 3.0 for three adsorbents. With the co-existing anions, a similar order of competition for adsorption was observed to be $PO_4^{3-} > SiO_3^{2-} > CO_3^{2-} > SO_4^{2-}$. The As(V) adsorption efficiency was reduced by up to 90% when the mixed anions with a concentration of 10 mg/L of each ion were present in the solution.
- In the column study, at the same operating conditions, the breakthrough curves of LF were always steeper than those of FLF-3 and ZLF-3. Therefore, LF always saturated faster than the others did. The Thomas adsorption capacity of ZLF-3 was the highest (2.7 and 2.2 mg/g for 15 cm and 30 cm height columns, respectively), followed by FLF-3 (1.26 mg/g and 1.10 mg/g, respectively) and LF (0.06 mg/g for both column heights).
- The cost of LF, FLF-3 and ZLF-3 were estimated to be A$0.2/kg, A$1.02/kg and A$1.81/kg, respectively. At the initial As(V) concentration of 0.1 mg/L, the cost to produce 1 m^3 water containing less than 0.01 mg As/L by LF, FLF-3, and ZLF-3 is estimated to be A$3.9, A$0.26, and A$0.21, respectively. The cost of LF increased considerably after modification but the water treatment costs reduced due to the larger volume of treated water. The treatment cost was competitive with commercial GAC.

7.1.3 Waste management

The exhausted adsorbents from the adsorption process were managed by different methods. The solidification/stabilisation method with the encapsulation in concrete helped to manage the exhausted VMO and modified VMOs. The exhausted LF and modified LFs were managed by the phytoremediation method.

7.1.3.1 Exhausted VMO and modified VMOs

- The solidification/stabilisation method was applied to immobilise As(V) in the exhausted absorbent wastes. The used VMO and modified VMOs were incorporated into the monolithic concrete samples. Here, different ratios of sand (5, 10, 15, and 20%) in a sand/cement concrete mixture were replaced by exhausted VMO and modified VMOs.
- The value of compressive strength, rapid chloride penetrability, and volume of permeable voids of concrete samples at 28 days were 31.2 – 33.2 MPa, 1175 – 1281 coulombs, and 12.6 – 14.7 %, respectively. These concrete samples had good stability, making them suitable for use as a building material in construction work.
- The As(V) leaching from these materials, as measured by Method 1313 of the LEAF of USEPA, was much lower than regulation limit of 5 mg/L. Thus, the concrete was safely disposed of or reused for other purposes, such as driveways, pavements, where humans will not have direct contact.

7.1.3.2 Exhausted LF and modified LFs

- The exhausted original and modified LFs were managed by the phytoremediation method using the plant *Pityrogramma calomelanos*, a species of fern. The plants were grown in a potting mix, which was created by mixing waste LFs and garden soil at a ratio of 1 g of waste LFs: 30 g of garden soil.
- The plants were grown normally for six months without any visual signs of As toxicity. Most As(V) transferred to the plants was present in the shoot (69-77%), and a smaller amount stayed in the root (23 – 31%) of the plants. The average concentration of As(V) was 2286 mg As/kg dry plant**]**.
- After six months, 73.6 – 74.3% of the As(V) in the potting mix has transferred to the plant. The amount of dried plant was only 38 – 40% in comparison with the initial amount of waste LFs. The As(V) concentration remaining in mixed soil was 9.92 – 10.20 mg As/kg. This value was well below the recommended permissible soil As concentration as specified by the United States Environmental Protection Agency (USEPA) (24 mg/kg) and the ecological investigation level (EIL) limit of As in soil in Australia (20 mg/kg). Therefore, the soil containing waste LFs can also be safely disposed of or reused.

7.1.4 EC

- The small-scale EC system was designed using 1 L volume reactor. A couple of stainless steel plates (11 x 6 x 0.09 cm) were used as electrodes, and the system was operated in a monopolar parallel connection mode.
- In a batch study, for a solution with an As(V) initial concentration of 0.1 mg/L, DC electric potential difference of 7.5 V (corresponding to a current density of 0.030 A), electrodes distance of 1 cm and solution pH of 7.0 were found to be the optimal condition for EC process. At this condition, the As(V) removal efficiency was 92% after a short operation time of 5 min.
- By replacing DC electricity with a 9V rechargeable battery or small 12V solar panel, the EC system could remove 93% and 98% of As(V) from 0.1 mg As(V)/L solution, respectively. As(V) concentration in treated water was found to be lower than that of the WHO drinking water guidelines.
- In the continuous study, a small, cost-effective system (reactor volume of 1 L, capital cost $15AUD) using DC electricity or small 12V solar panel as the power source could successfully treat 12L As(V)-contaminated water per hour. During 4 hours of continuous testing, the As(V) removal efficiency of the continuous system was maintained continuously at more than 91% for the DC electrical system and 96% for the solar system, respectively. The lifespan of the sacrificial anode was more than 410 days for DC electrical system and 330 days for solar energy system in the continuous flow mode. The cost for the treatment of As(V)-contaminated water, including both operating cost and capital cost, is 0.240 A$/$m^3$ water for the electrical EC system and 0.262 A$/$m^3$ for the solar EC system.

7.2 Recommendation

- The novel adsorbents in the present study performed well in removing As(V) from synthetic water. It is recommended to carry out field trials of these adsorbents with real contaminated water sources (including both As(III) and As(V)) under various operational conditions. The field trials will provide comprehensive information to evaluate the practical applicability (including the technical and economic aspects) of the adsorbents in the future.
- The modification procedure of adsorbents is relatively complicated and poses chemical safety issues. In addition, only a small amount of adsorbents was prepared in the laboratory. A future study on a simpler modification process should facilitate the possibility of adsorbent production in an industrial process. In this case, the new adsorbents will become marketable products at affordable prices.
- Desorption/regeneration of adsorbents is important as it relates to the economic aspect of application. It is recommended to study simple desorption/regeneration methods for the exhausted VMOs and LFs.
- EC method could successfully remove As(V) from water using renewable energy. This is a promising method for application in rural and isolated areas. A future study should be carried out in the field to evaluate the practicality of this method.
- Hazardous waste management is very important for sustainable treatment. The methods applied in this study have demonstrated their ability to manage waste safely. More studies should be carried out in the future at different mixing ratios, different ages of concrete and plants, types of plants to establish guidelines on safe waste management.

- A comprehensive water treatment cost should be calculated in future studies at the field trial to evaluate exactly the economic efficiency of these methods.
- The research on applying simple, low-cost, and environmentally friendly methods to remove As in water will be continuously investigated in the future study.

Appendices

Appendix 1 (Chapter 3)

Pic. S3.1. As analytical instrument - Agilent Technologies 7900 ICP-MS

(a) (b)

Pic. S3.2. Batch (a) and column (b) adsorption

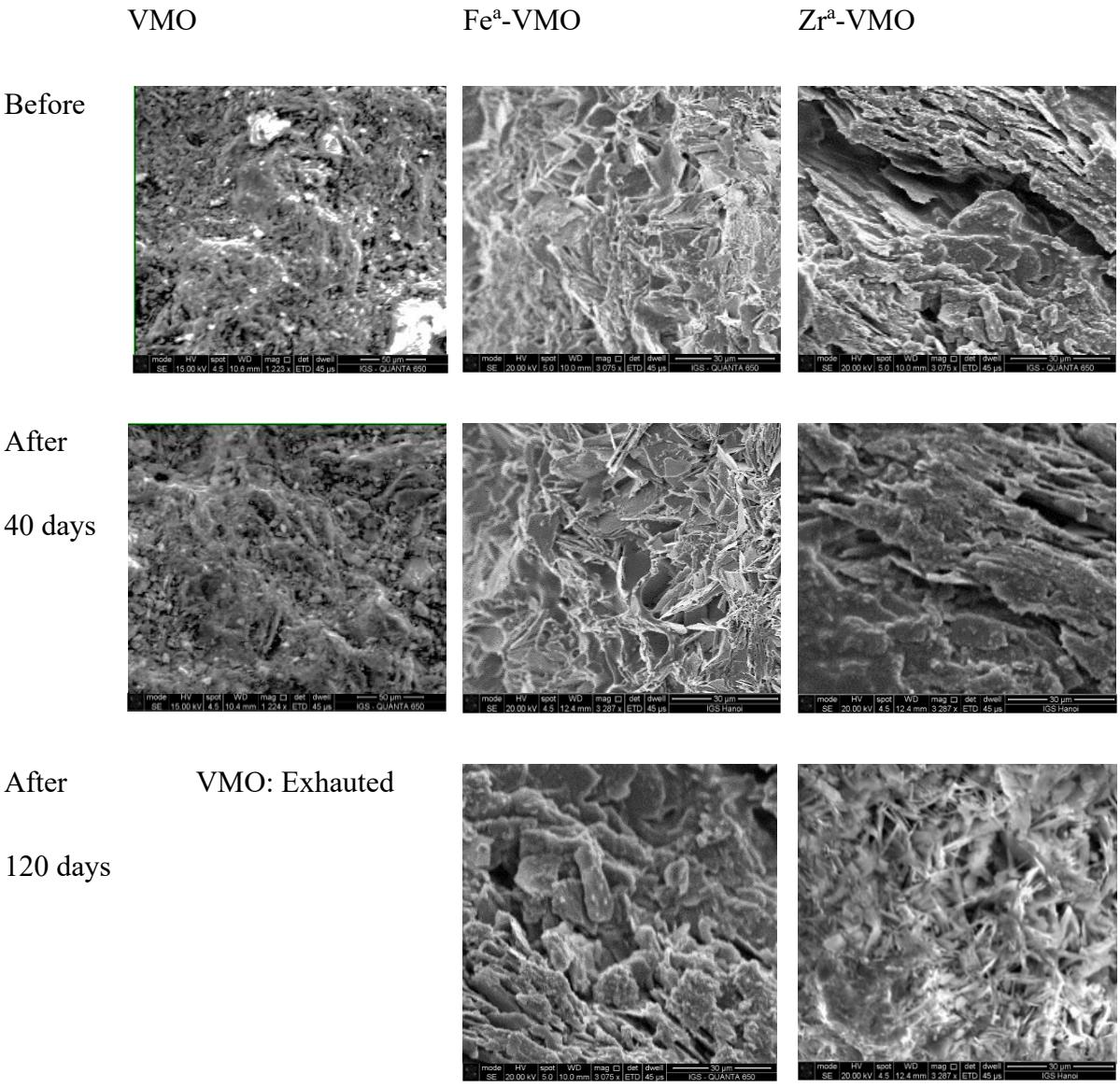

Fig. S3.1. SEM image of VMO, Fe[a]-VMO and Zr[a]-VMO before and after As(V) adsorption in column study

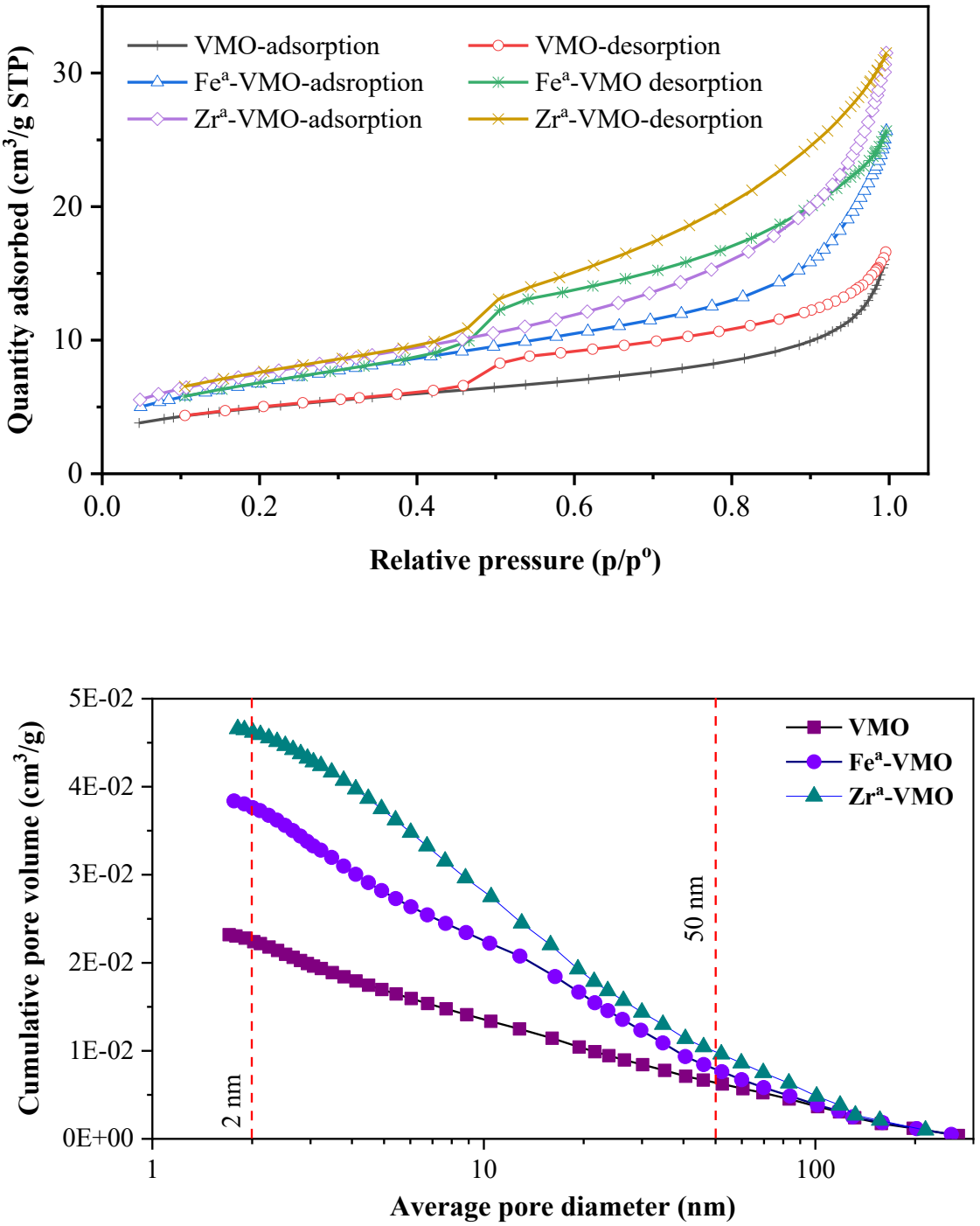

Fig. S3.2. BET N_2 adsorption/desorption isotherm plot (a) and BJH adsorption pore-size distribution graph (b) for VMO, Fe^a-VMO and Zr^a-VMO

Appendix 2 (Chapter 4)

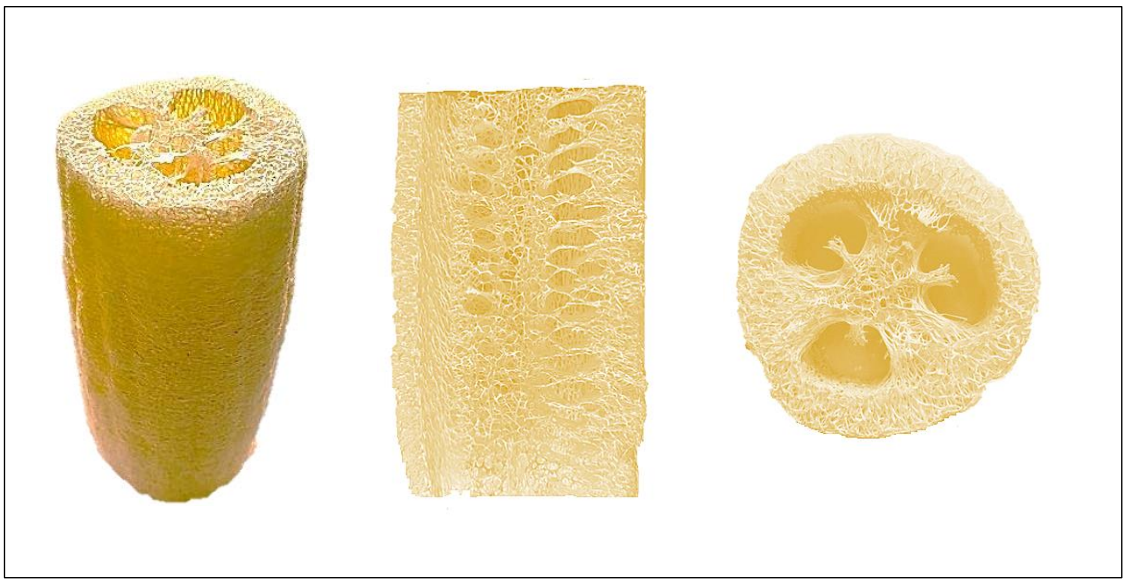

Fig. S4.1 Cylindrical *luffa* porous structure

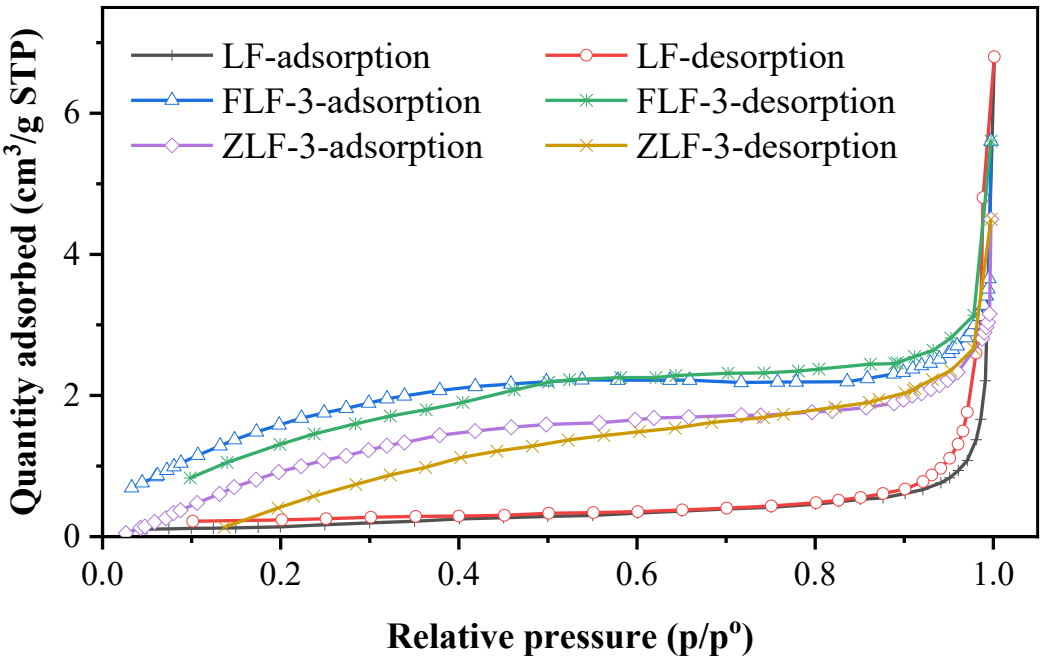

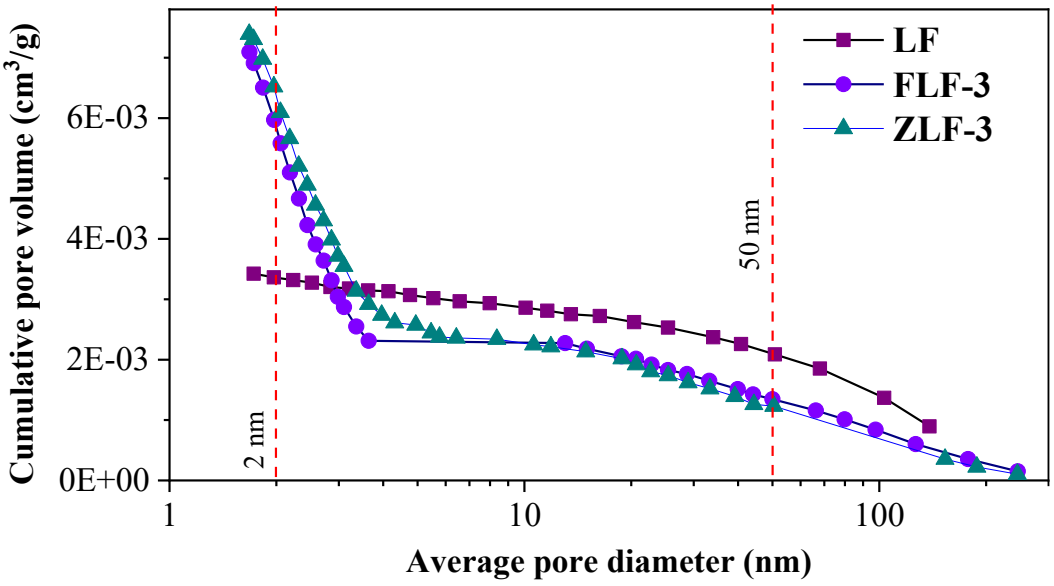

Fig S4.2. BET N_2 adsorption/desorption isotherm plot (a) and BJH adsorption pore-size distribution graph (b) for LF, FLF-3 and ZLF-3

Table S4.1. BET surface area and pore size distribution of LF, FLF-3 and ZLF-3

Parameter (unit)	LF	FLF-3	ZLF-3
BET surface area (cm^2/g)	0.61	6.70	10.69
BJH Adsorption cumulative volume of pores (cm^3/g)	0.0034	0.0071	0.0074
BJH Desorption cumulative volume of pores (cm^3/g)	0.0041	0.0059	0.0069
BJH Adsorption average pore width (nm)	15.5	3.3	3.5
BJH Desorption average pore width (nm)	27.3	4.9	5.0

Appendix 3 (Chapter 5)

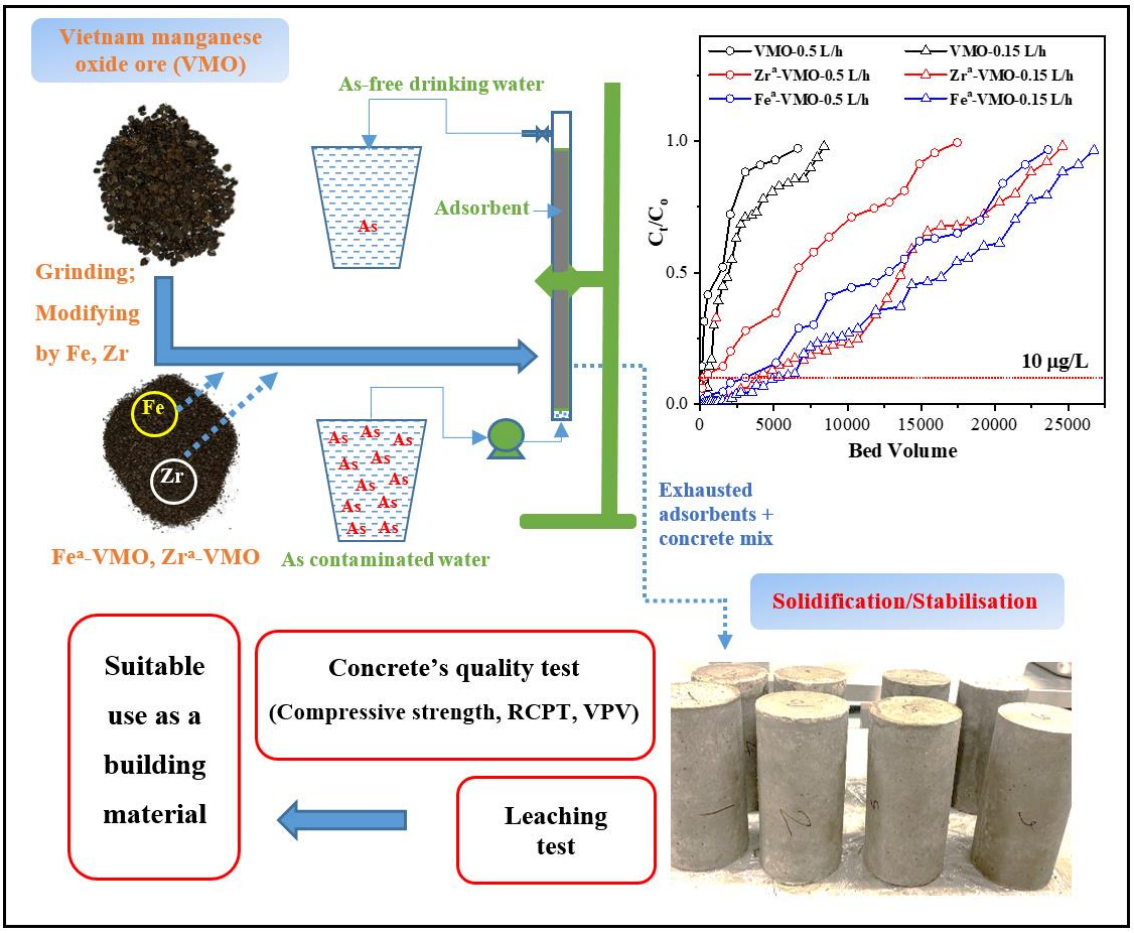

Fig. S5.1 As(V) removal from water using original and modified VMOs, followed by solidification/stabilisation

Pic. S5.1. Concrete casting and slicing

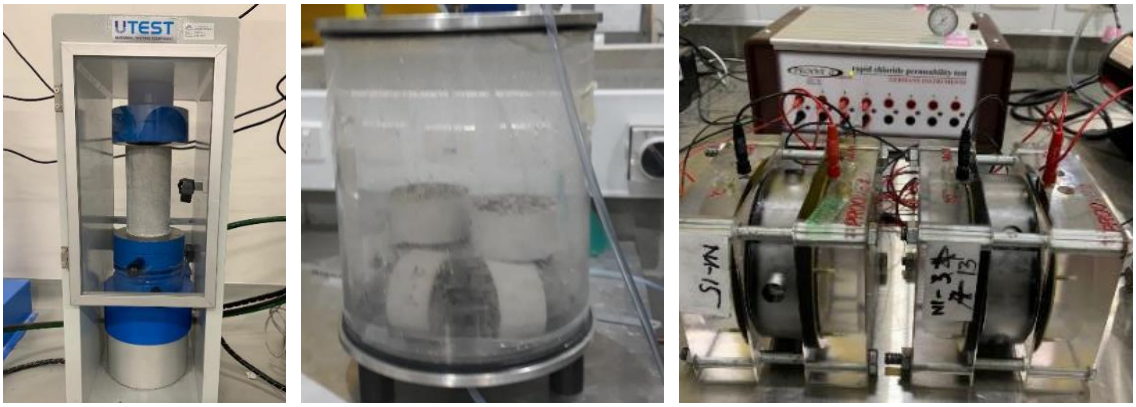

(a) (b) (c)

Pic. S5.2. Concrete characteristic measurement: (a) compressive strength, (b) VPV, and (c) RCPT

Pic. S5.3. As-extracted solutions from plant’s sections in the phytoremediation method

Appendix 4 (Chapter 6)

Video of the operation of EC system:

https://studentutsedu-my.sharepoint.com/:v:/g/personal/12671451_student_uts_edu_au/EcVR3xz8-OpDnZJ5aC6rtkYBAvh1Vy61OfgiBWVa5SPXLg?e=kPl75k

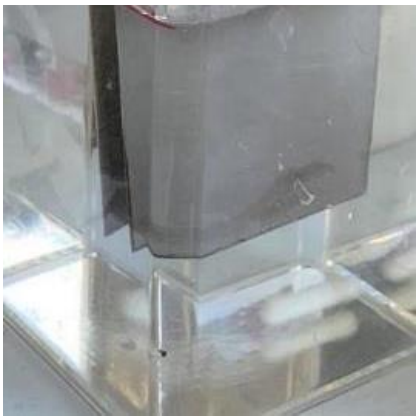

(a) 5 min

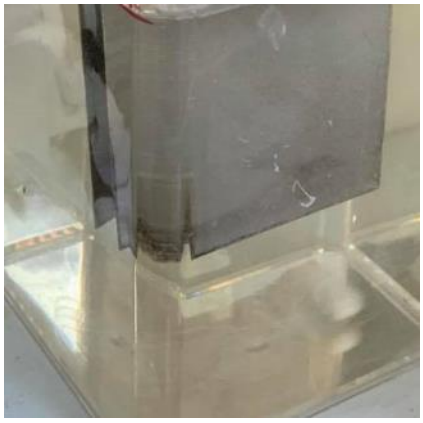

(b) 15 min

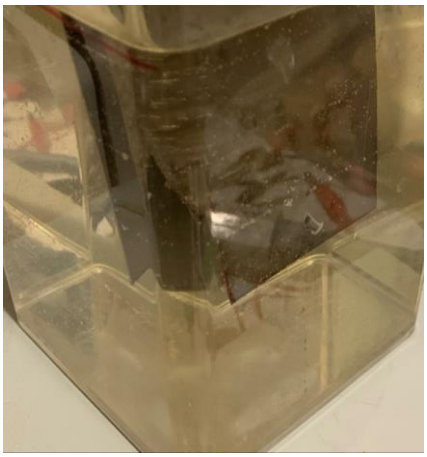

(c) 30min

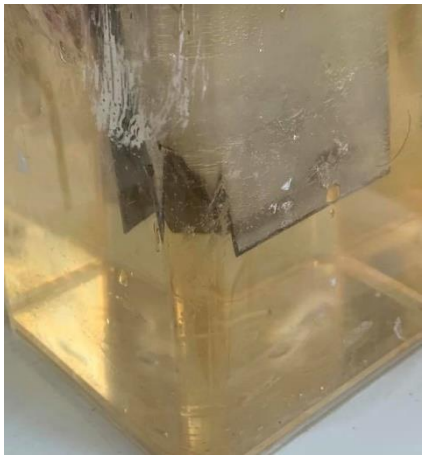

(d) 45 min

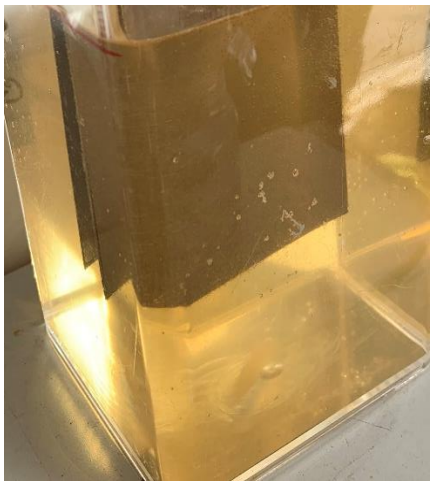

(e) 60 min

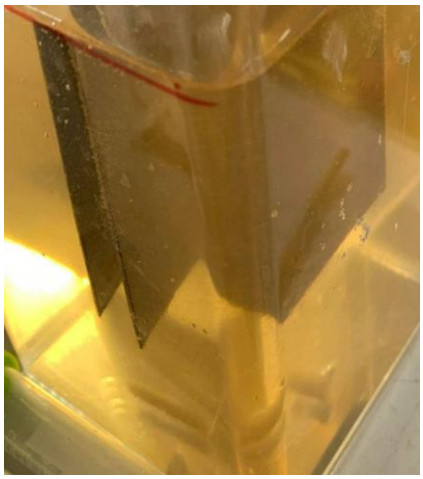

(f) 120 min

Pic. S6.1. The change of water colour in EC system with operation time

Pic. S6.2. Treated water after microfilter in EC system

REFERENCES

Abbas, G., Murtaza, B., Bibi, I., Shahid, M., Niazi, N.K., Khan, M.I., Amjad, M., Hussain, M. & Natasha 2018, 'Arsenic Uptake, Toxicity, Detoxification, and Speciation in Plants: Physiological, Biochemical, and Molecular Aspects', *International journal of environmental research and public health*, vol. 15, no. 1, p. 59.

Abdelwahab, O. & Amin, N.K. 2013, 'Adsorption of phenol from aqueous solutions by Luffa cylindrica fibers: Kinetics, isotherm and thermodynamic studies', *The Egyptian Journal of Aquatic Research*, vol. 39, no. 4, pp. 215-23.

Abu-El-Halawa, R., Quora, R. & Salim, R. 2003, 'Efficiency of removal of lead, cadmium, copper and zinc from aqueous solutions using six common types of plant leaves', *Journal of Applied Sciences*, vol. 3, pp. 79-84.

Adeogun, A.I. & Babu, R.B. 2015, 'One-step synthesized calcium phosphate-based material for the removal of alizarin S dye from aqueous solutions: isothermal, kinetics, and thermodynamics studies', *Applied Nanoscience*, pp. 1-13.

Adewuyi, A. & Pereira, F.V. 2017, 'Underutilized Luffa cylindrica sponge: A local bio-adsorbent for the removal of Pb(II) pollutant from water system', *Beni-Suef University Journal of Basic and Applied Sciences*, vol. 6, no. 2, pp. 118-26.

Ahmed, M.F. 2001, 'An overview of arsenic removal technologies in Bangladesh and India', pp. 5-7.

Aksu, Z. & Gönen, F. 2004, 'Biosorption of phenol by immobilized activated sludge in a continuous packed bed: prediction of breakthrough curves', *Process biochemistry*, vol. 39, no. 5, pp. 599-613.

Ali, I. 2018, 'Microwave assisted economic synthesis of multi walled carbon nanotubes for arsenic species removal in water: Batch and column operations', *Journal of Molecular Liquids*, vol. 271, pp. 677-85.

Alka, S., Shahir, S., Ibrahim, N., Ndejiko, M.J., Vo, D.-V.N. & Abd Manan, F. 2020, 'Arsenic Removal Technologies And Future Trends: A Mini Review', *Journal of Cleaner Production*, p. 123805.

Altundoğan, H.S., Altundoğan, S., Tümen, F. & Bildik, M. 2002, 'Arsenic adsorption from aqueous solutions by activated red mud', *Waste management*, vol. 22, no. 3, pp. 357-63.

Amini, M., Abbaspour, K.C., Berg, M., Winkel, L., Hug, S.J., Hoehn, E., Yang, H. & Johnson, C.A. 2008, 'Statistical modeling of global geogenic arsenic contamination in groundwater', *Environmental science & technology*, vol. 42, no. 10, pp. 3669-75.

Amrose, S., Gadgil, A., Srinivasan, V., Kowolik, K., Muller, M., Huang, J. & Kostecki, R. 2013, 'Arsenic removal from groundwater using iron electrocoagulation: effect of charge dosage rate', *Journal of Environmental Science and Health, Part A*, vol. 48, no. 9, pp. 1019-30.

Asere, T.G., Stevens, C.V. & Du Laing, G. 2019, 'Use of (modified) natural adsorbents for arsenic remediation: A review', *Science of The Total Environment*, vol. 676, pp. 706-20.

Asif, Z. & Chen, Z. 2017, 'Removal of arsenic from drinking water using rice husk', *Applied Water Science*, vol. 7, no. 3, pp. 1449-58.

Ayawei, N., Ebelegi, A.N. & Wankasi, D. 2017, 'Modelling and Interpretation of Adsorption Isotherms', *Journal of Chemistry*, vol. 2017, p. 3039817.

Balasubramanian, N., Kojima, T., Basha, C.A. & Srinivasakannan, C. 2009, 'Removal of arsenic from aqueous solution using electrocoagulation', *Journal of Hazardous Materials*, vol. 167, no. 1, pp. 966-9.

Baweja, D., Roper, H. & Sirivivatnanon, V. 2003, 'Improved electrochemical determinations of chloride-induced steel corrosion in concrete', *Materials Journal*, vol. 100, no. 3, pp. 228-38.

Berg, M. 2007, 'Arsenic contamination of groundwater and drinking water in the Red river delta, Vietnam: Geochemical investigations and mitigation measures: dis. dok. natur', *Zurich, Schweiz*.

Berg, M., Stengel, C., Trang, P.T.K., Viet, P.H., Sampson, M.L., Leng, M., Samreth, S. & Fredericks, D. 2007, 'Magnitude of arsenic pollution in the Mekong and Red River Deltas—Cambodia and Vietnam', *Science of the Total Environment*, vol. 372, no. 2-3, pp. 413-25.

Berg, M., Tran, H.C., Nguyen, T.C., Pham, H.V., Schertenleib, R. & Giger, W. 2001, 'Arsenic contamination of groundwater and drinking water in Vietnam: a human health threat', *Environmental science & technology*, vol. 35, no. 13, pp. 2621-6.

Brinkel, J., Khan, M.H. & Kraemer, A. 2009, 'A systematic review of arsenic exposure and its social and mental health effects with special reference to Bangladesh', *International journal of environmental research and public health*, vol. 6, no. 5, pp. 1609-19.

Buschmann, J., Berg, M., Stengel, C. & Sampson, M.L. 2007, 'Arsenic and manganese contamination of drinking water resources in Cambodia: coincidence of risk areas with low relief topography', *Environmental science & technology*, vol. 41, no. 7, pp. 2146-52.

Camacho, L.M., Parra, R.R. & Deng, S. 2011, 'Arsenic removal from groundwater by MnO2-modified natural clinoptilolite zeolite: Effects of pH and initial feed concentration', *Journal of Hazardous Materials*, vol. 189, no. 1, pp. 286-93.

Chakraborti, D., Rahman, M.M., Paul, K., Chowdhury, U.K., Sengupta, M.K., Lodh, D., Chanda, C.R., Saha, K.C. & Mukherjee, S.C. 2002, 'Arsenic calamity in the Indian subcontinent: what lessons have been learned?', *Talanta*, vol. 58, no. 1, pp. 3-22.

Chakravarty, S., Dureja, V., Bhattacharyya, G., Maity, S. & Bhattacharjee, S. 2002, 'Removal of arsenic from groundwater using low cost ferruginous manganese ore', *Water research*, vol. 36, no. 3, pp. 625-32.

Chaudhry, S.A., Zaidi, Z. & Siddiqui, S.I. 2017, 'Isotherm, kinetic and thermodynamics of arsenic adsorption onto Iron-Zirconium Binary Oxide-Coated Sand (IZBOCS):

Modelling and process optimization', *Journal of Molecular Liquids*, vol. 229, pp. 230-40.

Chen, Q., Shi, Q., Gorb, S.N. & Li, Z. 2014, 'A multiscale study on the structural and mechanical properties of the luffa sponge from Luffa cylindrica plant', *Journal of Biomechanics*, vol. 47, no. 6, pp. 1332-9.

Chiban, M., Zerbet, M., Carja, G. & Sinan, F. 2012, 'Application of low-cost adsorbents for arsenic removal: A review', *Journal of Environmental Chemistry and Ecotoxicology*, vol. 4, no. 5, pp. 91-102.

Chou, W.-L. & Huang, Y.-H. 2009, 'Electrochemical removal of indium ions from aqueous solution using iron electrodes', *Journal of Hazardous Materials*, vol. 172, no. 1, pp. 46-53.

Chowdhury, M.R.I. & Mulligan, C.N. 2011, 'Biosorption of arsenic from contaminated water by anaerobic biomass', *Journal of Hazardous Materials*, vol. 190, no. 1, pp. 486-92.

Ciardelli, M.C., Xu, H. & Sahai, N. 2008, 'Role of Fe (II), phosphate, silicate, sulfate, and carbonate in arsenic uptake by coprecipitation in synthetic and natural groundwater', *Water Research*, vol. 42, no. 3, pp. 615-24.

Criscuoli, A. & Figoli, A. 2019, 'Pressure-driven and thermally-driven membrane operations for the treatment of arsenic-contaminated waters: A comparison', *Journal of Hazardous Materials*, vol. 370, pp. 147-55.

Dabrowska, B.B., Vithanage, M., Gunaratna, K.R., Mukherjee, A.B. & Bhattacharya, P. 2012, 'Bioremediation of arsenic in contaminated terrestrial and aquatic environments', *Environmental chemistry for a sustainable world*, Springer, pp. 475-509.

Dada, A., Olalekan, A., Olatunya, A. & Dada, O. 2012, 'Langmuir, Freundlich, Temkin and Dubinin–Radushkevich isotherms studies of equilibrium sorption of Zn2+ unto phosphoric acid modified rice husk', *IOSR Journal of Applied Chemistry*, vol. 3, no. 1, pp. 38-45.

Daus, B., Wennrich, R. & Weiss, H. 2004, 'Sorption materials for arsenic removal from water:: a comparative study', *Water research*, vol. 38, no. 12, pp. 2948-54.

Delva, L., Verberckmoes, A., Cardon, L. & Ragaert, K. 2013, 'The use of rubber as a compatibilizer for injection moulding of recycled post-consumer mixed polyolefines', vol. 689.

Demir, H., Top, A., Balköse, D. & Ülkü, S. 2008, 'Dye adsorption behavior of Luffa cylindrica fibers', *Journal of Hazardous Materials*, vol. 153, no. 1, pp. 389-94.

Du, W., Li, Z.a., Zou, B. & Peng, S. 2005, 'Pteris multifida Poir., a new arsenic hyperaccumulator: characteristics and potential', *International journal of environment and pollution*, vol. 23, no. 4, pp. 388-96.

Dura, A. & Breslin, C.B. 2019, 'Electrocoagulation using stainless steel anodes: Simultaneous removal of phosphates, Orange II and zinc ions', *Journal of hazardous materials*, vol. 374, pp. 152-8.

El-Zohairy, A., Hammontree, H., Oh, E. & Moler, P. 2020, 'Temperature Effect on the Compressive Behavior and Constitutive Model of Plain Hardened Concrete', *Materials*, vol. 13, no. 12, p. 2801.

Elcik, H., Celik, S.O., Cakmakci, M. & Özkaya, B. 2016, 'Performance of nanofiltration and reverse osmosis membranes for arsenic removal from drinking water', *Desalination and Water Treatment*, vol. 57, no. 43, pp. 20422-9.

Elias, M., Wellner, A., Goldin Azulay, K., Chabriere, E., Vorholt, J., Erb, T. & Tawfik, D. 2012, 'The molecular basis of phosphate discrimination in arsenate-rich environments', *Nature*, vol. 491.

Erhayem, M., Al-Tohami, F., Mohamed, R. & Ahmida, K. 2015, 'Isotherm, kinetic and thermodynamic studies for the sorption of mercury (II) onto activated carbon from Rosmarinus officinalis leaves', *American Journal of Analytical Chemistry*, vol. 6, no. 01, p. 1.

Fang, Q., Chen, B., Lin, Y. & Guan, Y. 2014, 'Aromatic and hydrophobic surfaces of wood-derived biochar enhance perchlorate adsorption via hydrogen bonding to oxygen-containing organic groups', *Environmental science & technology*, vol. 48, no. 1, pp. 279-88.

Firdaous, L., Fertin, B., Khelissa, O., Dhainaut, M., Nedjar, N., Chataigné, G., Ouhoud, L., Lutin, F. & Dhulster, P. 2017, 'Adsorptive removal of polyphenols from an alfalfa white proteins concentrate: Adsorbent screening, adsorption kinetics and equilibrium study', *Separation and Purification Technology*, vol. 178, pp. 29-39.

Fisher, A.T., López-Carrillo, L., Gamboa-Loira, B. & Cebrián, M.E. 2017, 'Standards for arsenic in drinking water: Implications for policy in Mexico', *Journal of public health policy*, vol. 38, no. 4, pp. 395-406.

Flores, O.J., Nava, J.L. & Carreño, G. 2014, 'Arsenic removal from groundwater by electrocoagulation process in a filter-press-type FM01-LC reactor', *International Journal of Electrochemical Science*, vol. 9, no. 11, pp. 6658-67.

Fu, F. & Wang, Q. 2011, 'Removal of heavy metal ions from wastewaters: a review', *Journal of environmental management*, vol. 92, no. 3, pp. 407-18.

Ge, J., Guha, B., Lippincott, L., Cach, S., Wei, J., Su, T.-L. & Meng, X. 2020, 'Challenges of arsenic removal from municipal wastewater by coagulation with ferric chloride and alum', *Science of The Total Environment*, vol. 725, p. 138351.

Gilhotra, V., Das, L., Sharma, A., Kang, T.S., Singh, P., Dhuria, R.S. & Bhatti, M.S. 2018, 'Electrocoagulation technology for high strength arsenic wastewater: Process optimization and mechanistic study', *Journal of Cleaner Production*, vol. 198, pp. 693-703.

Gu, Z., Fang, J. & Deng, B. 2005, 'Preparation and evaluation of GAC-based iron-containing adsorbents for arsenic removal', *Environmental science & technology*, vol. 39, no. 10, pp. 3833-43.

Guo, H., Wen, D., Liu, Z., Jia, Y. & Guo, Q. 2014, 'A review of high arsenic groundwater in Mainland and Taiwan, China: Distribution, characteristics and geochemical processes', *Applied Geochemistry*, vol. 41, pp. 196-217.

Guo, X. & Chen, F. 2005, 'Removal of arsenic by bead cellulose loaded with iron oxyhydroxide from groundwater', *Environmental science & technology*, vol. 39, no. 17, pp. 6808-18.

Guo, X. & Wang, J. 2019, 'A general kinetic model for adsorption: Theoretical analysis and modeling', *Journal of Molecular Liquids*, vol. 288, p. 111100.

Gupta, D.K. & Chatterjee, S. 2017, *Arsenic contamination in the environment: the issues and solutions*, Springer.

Hammud, H., Shmait, A. & Hourani, N. 2014, 'Removal of Malachite Green from Water using Hydrothermally Carbonized Pine Needles', *RSC Adv.*, vol. 5.

Han, B., Runnells, T., Zimbron, J. & Wickramasinghe, R. 2002, 'Arsenic removal from drinking water by flocculation and microfiltration', *Desalination*, vol. 145, no. 1, pp. 293-8.

Han, R., Wang, Y., Zhao, X., Wang, Y., Xie, F., Cheng, J. & Tang, M. 2009, 'Adsorption of methylene blue by phoenix tree leaf powder in a fixed-bed column: Experiments and prediction of breakthrough curves', *Desalination*, vol. 245, pp. 284-97.

Hao, L., Liu, M., Wang, N. & Li, G. 2018, 'A critical review on arsenic removal from water using iron-based adsorbents', *RSC advances*, vol. 8, no. 69, pp. 39545-60.

Harfoush, M., Mirbagheri, S., Ehteshami, M. & Nejati, S. 2018, 'Arsenic removal from drinking water using low-pressure nanofiltration under various operating conditions', *Water Practice & Technology*, vol. 13, no. 2, pp. 295-302.

Hideno, A. 2016, 'Comparison of the thermal degradation properties of crystalline and amorphous cellulose, as well as treated lignocellulosic biomass', *Bioresources*, vol. 11, no. 3, pp. 6309-19.

Hu, X., Ding, Z., Zimmerman, A.R., Wang, S. & Gao, B. 2015, 'Batch and column sorption of arsenic onto iron-impregnated biochar synthesized through hydrolysis', *Water Research*, vol. 68, pp. 206-16.

Hussin, F., Abnisa, F., Issabayeva, G. & Aroua, M.K. 2017, 'Removal of lead by solar-photovoltaic electrocoagulation using novel perforated zinc electrode', *Journal of Cleaner Production*, vol. 147, pp. 206-16.

Jahin, A., Aziz, S., Tasnim, Z. & Ali, M.A. 2017, 'Effect of Bicarbonate on Arsenic Removal by Coagulation', vol. 3, p. 4.

Järup, L. 2003, 'Hazards of heavy metal contamination', *British medical bulletin*, vol. 68, no. 1, pp. 167-82.

Jia, Y., Xu, L., Wang, X. & Demopoulos, G.P. 2007, 'Infrared spectroscopic and X-ray diffraction characterization of the nature of adsorbed arsenate on ferrihydrite', *Geochimica et Cosmochimica Acta*, vol. 71, no. 7, pp. 1643-54.

Jiang, J.-Q., Ashekuzzaman, S., Jiang, A., Sharifuzzaman, S. & Chowdhury, S.R. 2013, 'Arsenic contaminated groundwater and its treatment options in Bangladesh', *International journal of environmental research and public health*, vol. 10, no. 1, pp. 18-46.

Jing, C., Liu, S. & Meng, X. 2005, 'Arsenic leachability and speciation in cement immobilized water treatment sludge', *Chemosphere*, vol. 59, no. 9, pp. 1241-7.

Jiuhui, Q. 2008, 'Research progress of novel adsorption processes in water purification: a review', *Journal of Environmental Sciences*, vol. 20, no. 1, pp. 1-13.

Jochem, M., Ende, L., Isasa, M., Ang, J., Schnell, H., Guerra-Moreno, A., Micoogullari, Y., Bhanu, M., Gygi, S.P. & Hanna, J. 2019, 'Targeted Degradation of Glucose Transporters Protects against Arsenic Toxicity', *Molecular and Cellular Biology*, vol. 39, no. 10, pp. e00559-18.

Jones, F. 2007, 'A broad view of arsenic', *Poultry science*, vol. 86, no. 1, pp. 2-14.

Kabir, F. & Chowdhury, S. 2017, 'Arsenic removal methods for drinking water in the developing countries: technological developments and research needs', *Environmental Science and Pollution Research*, vol. 24.

Kalaruban, M. 2017, 'Nitrate removal from water using surface-modified adsorbents'.

Kalaruban, M., Loganathan, P., Kandasamy, J., Naidu, R. & Vigneswaran, S. 2017, 'Enhanced removal of nitrate in an integrated electrochemical-adsorption system', *Separation and Purification Technology*, vol. 189, pp. 260-6.

Kalaruban, M., Loganathan, P., Nguyen, T.V., Nur, T., Hasan Johir, M.A., Nguyen, T.H., Trinh, M.V. & Vigneswaran, S. 2019, 'Iron-impregnated granular activated carbon for arsenic removal: Application to practical column filters', *Journal of Environmental Management*, vol. 239, pp. 235-43.

Kalaruban, M., Loganathan, P., Shim, W., Kandasamy, J., Naidu, G., Nguyen, T.V. & Vigneswaran, S. 2016, 'Removing nitrate from water using iron-modified Dowex 21K XLT ion exchange resin: Batch and fluidised-bed adsorption studies', *Separation and Purification Technology*, vol. 158, pp. 62-70.

Karanac, M., Đolić, M., Veljović, Đ., Rajaković-Ognjanović, V., Veličković, Z., Pavićević, V. & Marinković, A. 2018, 'The removal of Zn2+, Pb2+, and As (V) ions by lime activated fly ash and valorization of the exhausted adsorbent', *Waste Management*, vol. 78, pp. 366-78.

Kaur, H., Siddique, R. & Rajor, A. 2019, 'Influence of incinerated biomedical waste ash on the properties of concrete', *Construction and Building Materials*, vol. 226, pp. 428-41.

Khalajestani, M.K., Parvez, A., Foster, S.J., Valipour, H. & McGregor, G. 2018, 'Strength and Ductility of High-Strength Concrete Columns Reinforced with High-Strength Steel'.

Khan, T.A., Chaudhry, S.A. & Ali, I. 2013, 'Thermodynamic and kinetic studies of As (V) removal from water by zirconium oxide-coated marine sand', *Environmental Science and Pollution Research*, vol. 20, no. 8, pp. 5425-40.

Kobya, M., Demirbas, E. & Ulu, F. 2016, 'Evaluation of operating parameters with respect to charge loading on the removal efficiency of arsenic from potable water by electrocoagulation', *Journal of environmental chemical engineering*, vol. 4, no. 2, pp. 1484-94.

Kobya, M., Soltani, R.D.C., Omwene, P.I. & Khataee, A. 2020, 'A review on decontamination of arsenic-contained water by electrocoagulation: Reactor configurations and operating cost along with removal mechanisms', *Environmental Technology & Innovation*, vol. 17, p. 100519.

Kocherbitov, V. & Arnebrant, T. 2010, 'Hydration of lysozyme: The protein− protein interface and the enthalpy− entropy compensation', *Langmuir*, vol. 26, no. 6, pp. 3918-22.

Kofa, G.P., NdiKoungou, S., Kayem, G.J. & Kamga, R. 2015, 'Adsorption of arsenic by natural pozzolan in a fixed bed: Determination of operating conditions and modeling', *Journal of Water Process Engineering*, vol. 6, pp. 166-73.

Kosson, D.S., Garrabrants, A.C., DeLapp, R. & van der Sloot, H.A. 2014, 'pH-dependent leaching of constituents of potential concern from concrete materials containing coal combustion fly ash', *Chemosphere*, vol. 103, pp. 140-7.

Kumar, P.R., Chaudhari, S., Khilar, K.C. & Mahajan, S.P. 2004a, 'Removal of arsenic from water by electrocoagulation', *Chemosphere*, vol. 55, no. 9, pp. 1245-52.

Kumar, R.P., Chaudhari, S., Khilar, K.C. & Mahajan, S.P. 2004b, 'Removal of arsenic from water by electrocoagulation', *Chemosphere*, vol. 55, no. 9, pp. 1245-52.

Kumendong, E.E., Supit, S.W. & Mantiri, H. 2019, 'Effects of Coconut Sawdust on Mechanical Properties and Porosity of Concrete Mixtures', *Journal of Sustainable Engineering: Proceedings Series*, vol. 1, no. 2, pp. 187-93.

Lakshmanan, D., Clifford, D.A. & Samanta, G. 2010, 'Comparative study of arsenic removal by iron using electrocoagulation and chemical coagulation', *Water Research*, vol. 44, no. 19, pp. 5641-52.

Le Luu, T. 2019, 'Remarks on the current quality of groundwater in Vietnam', *Environmental Science and Pollution Research*, vol. 26, no. 2, pp. 1163-9.

Lei, J., Peng, B., Min, X., Liang, Y., You, Y. & Chai, L. 2017, 'Modeling and optimization of lime-based stabilization in high alkaline arsenic-bearing sludges with a central composite design', *Journal of Environmental Science and Health, Part A*, vol. 52, no. 5, pp. 449-58.

Leist, M., Casey, R. & Caridi, D. 2000, 'The management of arsenic wastes: problems and prospects', *Journal of Hazardous Materials*, vol. 76, no. 1, pp. 125-38.

Lescano, M.R., Passalía, C., Zalazar, C.S. & Brandi, R.J. 2015, 'Arsenic sorption onto titanium dioxide, granular ferric hydroxide and activated alumina: batch and dynamic studies', *Journal of Environmental Science and Health, Part A*, vol. 50, no. 4, pp. 424-31.

Li, C., Xu, W., Jia, D. & Liu, X. 2013, 'Removal of Arsenic from Drinking Water by Using the Zr-Loaded Resin', *Journal of Chemical & Engineering Data*, vol. 58, no. 2, pp. 427-35.

Li, W.-G., Gong, X.-J., Wang, K., Zhang, X.-R. & Fan, W.-B. 2014, 'Adsorption characteristics of arsenic from micro-polluted water by an innovative coal-based mesoporous activated carbon', *Bioresource technology*, vol. 165, pp. 166-73.

Li, Y.-C., Min, X.-B., Chai, L.-Y., Shi, M.-Q., Tang, C.-J., Wang, Q.-W., Liang, Y.-j., Lei, J. & Liyang, W.-J. 2016, 'Co-treatment of gypsum sludge and Pb/Zn smelting slag for the solidification of sludge containing arsenic and heavy metals', *Journal of Environmental Management*, vol. 181, pp. 756-61.

Li, Y., Zhu, Y., Zhu, Z., Zhang, X., Wang, D. & Xie, L. 2018, 'Fixed-bed column adsorption of arsenic (V) by porous composite of magnetite/hematite/carbon with eucalyptus wood microstructure', *Journal of Environmental Engineering and Landscape Management*, vol. 26, no. 1, pp. 38-56.

Lincoln, J.D., Ogunseitan, O.A., Shapiro, A.A. & Saphores, J.-D.M. 2007, 'Leaching assessments of hazardous materials in cellular telephones', *Environmental Science & Technology*, vol. 41, no. 7, pp. 2572-8.

Litter, M.I., Ingallinella, A.M., Olmos, V., Savio, M., Difeo, G., Botto, L., Torres, E.M.F., Taylor, S., Frangie, S., Herkovits, J., Schalamuk, I., González, M.J., Berardozzi, E., García Einschlag, F.S., Bhattacharya, P. & Ahmad, A. 2019, 'Arsenic in Argentina: Technologies for arsenic removal from groundwater sources, investment costs and waste management practices', *Science of The Total Environment*, vol. 690, pp. 778-89.

Liu, D.-G., Min, X.-B., Ke, Y., Chai, L.-Y., Liang, Y.-j., Li, Y.-C., Yao, L.-W. & Wang, Z.-B. 2018, 'Co-treatment of flotation waste, neutralization sludge, and arsenic-containing gypsum sludge from copper smelting: solidification/stabilization of arsenic and heavy metals with minimal cement clinker', *Environmental Science and Pollution Research*, vol. 25, no. 8, pp. 7600-7.

Liu, S., Zhang, F., Chen, J. & Sun, G. 2011, 'Arsenic removal from contaminated soil via biovolatilization by genetically engineered bacteria under laboratory conditions', *Journal of Environmental Sciences*, vol. 23, no. 9, pp. 1544-50.

Loganathan, P., Vigneswaran, S., Kandasamy, J. & Bolan, N.S. 2014, 'Removal and recovery of phosphate from water using sorption', *Critical Reviews in Environmental Science and Technology*, vol. 44, no. 8, pp. 847-907.

Ma, L.Q., Komar, K.M., Tu, C., Zhang, W., Cai, Y. & Kennelley, E.D. 2001, 'A fern that hyperaccumulates arsenic', *Nature*, vol. 409, no. 6820, pp. 579-.

Maiti, A., Basu, J.K. & De, S. 2010, 'Development of a treated laterite for arsenic adsorption: effects of treatment parameters', *Industrial & Engineering Chemistry Research*, vol. 49, no. 10, pp. 4873-86.

Malakootian, M., Mansoorian, H.J. & Moosazadeh, M. 2010, 'Performance evaluation of electrocoagulation process using iron-rod electrodes for removing hardness from drinking water', *Desalination*, vol. 255, no. 1, pp. 67-71.

Mamindy-Pajany, Y., Hurel, C., Marmier, N. & Roméo, M. 2011, 'Arsenic (V) adsorption from aqueous solution onto goethite, hematite, magnetite and zero-valent iron: effects of pH, concentration and reversibility', *Desalination*, vol. 281, pp. 93-9.

Mandal, P., Debbarma, S., Saha, A. & Ruj, B. 2016, 'Disposal problem of arsenic sludge generated during arsenic removal from drinking water', *Procedia Environmental Sciences*, vol. 35, pp. 943-9.

Markovski, J.S., Marković, D.D., Đokić, V.R., Mitrić, M., Ristić, M.Đ., Onjia, A.E. & Marinković, A.D. 2014, 'Arsenate adsorption on waste eggshell modified by goethite, α-MnO2 and goethite/α-MnO2', *Chemical Engineering Journal*, vol. 237, pp. 430-42.

Meng, X., Korfiatis, G.P., Bang, S. & Bang, K.W. 2002, 'Combined effects of anions on arsenic removal by iron hydroxides', *Toxicology letters*, vol. 133, no. 1, pp. 103-11.

Michalke, K., Wickenheiser, E.B., Mehring, M., Hirner, A.V. & Hensel, R. 2000, 'Production of Volatile Derivatives of Metal(loid)s by Microflora Involved in Anaerobic Digestion of Sewage Sludge', *Applied and Environmental Microbiology*, vol. 66, no. 7, p. 2791.

Mohan, D. & Pittman Jr, C.U. 2007, 'Arsenic removal from water/wastewater using adsorbents—a critical review', *Journal of hazardous materials*, vol. 142, no. 1-2, pp. 1-53.

Mohanty, D. 2017, 'Conventional as well as Emerging Arsenic Removal Technologies—a Critical Review', *Water, Air, & Soil Pollution*, vol. 228, no. 10, p. 381.

Mohapatra, D., Mishra, D., Chaudhury, G.R. & Das, R.P. 2008, 'Removal of arsenic from arsenic rich sludge by volatilization using anaerobic microorganisms treated with cow dung', *Soil & Sediment Contamination*, vol. 17, no. 3, pp. 301-11.

Mohora, E., Rončević, S., Agbaba, J., Zrnić, K., Tubić, A. & Dalmacija, B. 2018, 'Arsenic removal from groundwater by horizontal-flow continuous electrocoagulation (EC) as a standalone process', *Journal of environmental chemical engineering*, vol. 6, no. 1, pp. 512-9.

Mollah, M.Y.A., Schennach, R., Parga, J.R. & Cocke, D.L. 2001, 'Electrocoagulation (EC) — science and applications', *Journal of Hazardous Materials*, vol. 84, no. 1, pp. 29-41.

Mondal, P., Balomajumder, C. & Mohanty, B. 2007, 'A laboratory study for the treatment of arsenic, iron, and manganese bearing ground water using Fe3+ impregnated activated carbon: effects of shaking time, pH and temperature', *Journal of hazardous materials*, vol. 144, no. 1-2, pp. 420-6.

Moreno-Jiménez, E., Manzano, R., Esteban, E. & Peñalosa, J. 2010, 'The fate of arsenic in soils adjacent to an old mine site (Bustarviejo, Spain): mobility and transfer to native flora', *Journal of Soils and Sediments*, vol. 10, no. 2, pp. 301-12.

Myneni, S.C., Traina, S.J., Waychunas, G.A. & Logan, T.J. 1998, 'Vibrational spectroscopy of functional group chemistry and arsenate coordination in ettringite', *Geochimica et Cosmochimica Acta*, vol. 62, no. 21-22, pp. 3499-514.

Nahar, N., Rahman, A., Nawani, N.N., Ghosh, S. & Mandal, A. 2017, 'Phytoremediation of arsenic from the contaminated soil using transgenic tobacco plants expressing ACR2 gene of Arabidopsis thaliana', *Journal of plant physiology*, vol. 218, pp. 121-6.

Nanseu-Njiki, C.P., Tchamango, S.R., Ngom, P.C., Darchen, A. & Ngameni, E. 2009, 'Mercury (II) removal from water by electrocoagulation using aluminium and iron electrodes', *Journal of Hazardous Materials*, vol. 168, no. 2-3, pp. 1430-6.

Nawarkar, C.J. & Salkar, V.D. 2019, 'Solar powered Electrocoagulation system for municipal wastewater treatment', *Fuel*, vol. 237, pp. 222-6.

Nayl, A., Ahmed, I., Abd-Elhamid, A., Aly, H. & Attallah, M. 2020, 'Selective sorption of 134Cs and 60Co radioisotopes using synthetic nanocopper ferrocyanide-SiO2 materials', *Separation and Purification Technology*, vol. 234, p. 116060.

Nazari, A.M., Radzinski, R. & Ghahreman, A. 2017, 'Review of arsenic metallurgy: Treatment of arsenical minerals and the immobilization of arsenic', *Hydrometallurgy*, vol. 174, pp. 258-81.

Nguyen, T.H., Tran, H.N., Vu, H.A., Trinh, M.V., Nguyen, T.V., Loganathan, P., Vigneswaran, S., Nguyen, T.M., Vu, D.L. & Nguyen, T.H.H. 2020, 'Laterite as a low-cost adsorbent in a sustainable decentralized filtration system to remove arsenic from groundwater in Vietnam', *Science of The Total Environment*, vol. 699, p. 134267.

Nguyen, T.T.Q., Loganathan, P., Nguyen, T.V. & Vigneswaran, S. 2020, 'Removing arsenic from water with an original and modified natural manganese oxide ore: batch kinetic and equilibrium adsorption studies', *Environmental Science and Pollution Research*, vol. 27, no. 5, pp. 5490-502.

Nguyen, T.T.Q., Loganathan, P., Nguyen, T.V., Vigneswaran, S. & Ngo, H.H. 2020, 'Iron and zirconium modified luffa fibre as an effective bioadsorbent to remove arsenic from drinking water', *Chemosphere*, p. 127370.

Nguyen, T.V., Loganathan, P., Vigneswaran, S., Krupanidhi, S., Pham, T.T.N. & Ngo, H.-H. 2014, 'Arsenic waste from water treatment systems: characteristics, treatments and its disposal', *Water Science and Technology: Water Supply*, vol. 14, no. 6, pp. 939-50.

Niazi, N.K., Bashir, S., Bibi, I., Murtaza, B., Shahid, M., Javed, M.T., Shakoor, M.B., Saqib, Z.A., Nawaz, M.F. & Aslam, Z. 2016, 'Phytoremediation of arsenic-contaminated soils using arsenic hyperaccumulating ferns', *Phytoremediation*, Springer, pp. 521-45.

Niazi, N.K., Bibi, I., Shahid, M., Ok, Y.S., Burton, E.D., Wang, H., Shaheen, S.M., Rinklebe, J. & Lüttge, A. 2018, 'Arsenic removal by perilla leaf biochar in aqueous solutions and groundwater: an integrated spectroscopic and microscopic examination', *Environmental Pollution*, vol. 232, pp. 31-41.

Niazi, N.K., Singh, B., Van Zwieten, L. & Kachenko, A.G. 2012, 'Phytoremediation of an arsenic-contaminated site using Pteris vittata L. and Pityrogramma calomelanos var. austroamericana: a long-term study', *Environmental Science and Pollution Research*, vol. 19, no. 8, pp. 3506-15.

Nicomel, N.R., Leus, K., Folens, K., Van Der Voort, P. & Du Laing, G. 2016, 'Technologies for arsenic removal from water: current status and future perspectives', *International journal of environmental research and public health*, vol. 13, no. 1, p. 62.

Nidheesh, P. & Singh, T.A. 2017, 'Arsenic removal by electrocoagulation process: recent trends and removal mechanism', *Chemosphere*, vol. 181, pp. 418-32.

Nur, T., Johir, M., Loganathan, P., Nguyen, T., Vigneswaran, S. & Kandasamy, J. 2014, 'Phosphate removal from water using an iron oxide impregnated strong base anion exchange resin', *Journal of Industrial and Engineering Chemistry*, vol. 20, no. 4, pp. 1301-7.

Nur, T., Loganathan, P., Ahmed, M.B., Johir, M.A.H., Nguyen, T.V. & Vigneswaran, S. 2019, 'Removing arsenic from water by coprecipitation with iron: effect of arsenic and iron concentrations and adsorbent incorporation', *Chemosphere*, vol. 226, pp. 431-8.

Nur, T., Loganathan, P., Nguyen, T., Vigneswaran, S., Singh, G. & Kandasamy, J. 2014, 'Batch and column adsorption and desorption of fluoride using hydrous ferric oxide: Solution chemistry and modeling', *Chemical Engineering Journal*, vol. 247, pp. 93-102.

Oh, C., Pak, S., Han, Y.-S., Ha, N.T.H., Hong, M. & Ji, S. 2019, 'Field demonstration of solar-powered electrocoagulation water treatment system for purifying groundwater contaminated by both total coliforms and arsenic', *Environmental Technology*, pp. 1-13.

Oladoja, N. & Helmreich, B. 2014, 'Batch defluoridation appraisal of aluminium oxide infused diatomaceous earth', *Chemical Engineering Journal*, vol. 258, pp. 51-61.

Önal, Y. 2006, 'Kinetics of adsorption of dyes from aqueous solution using activated carbon prepared from waste apricot', *Journal of hazardous materials*, vol. 137, no. 3, pp. 1719-28.

Ouvrard, S., Simonnot, M.-O. & Sardin, M. 2002, 'Reactive behavior of natural manganese oxides toward the adsorption of phosphate and arsenate', *Industrial & engineering chemistry research*, vol. 41, no. 11, pp. 2785-91.

Padmesh, T., Vijayaraghavan, K., Sekaran, G. & Velan, M. 2005, 'Batch and column studies on biosorption of acid dyes on fresh water macro alga Azolla filiculoides', *Journal of Hazardous Materials*, vol. 125, no. 1-3, pp. 121-9.

Petit, T. & Puskar, L. 2018, 'FTIR spectroscopy of nanodiamonds: Methods and interpretation', *Diamond and Related Materials*.

Pichhode, M. & Gaherwal, S. 2019, 'Toxic effect of arsenic trioxide on biochemical response in catfish, Clarias Batrachus', *Int J Recent Sci Res*, vol. 10, no. 08, pp. 34033-6.

Pokhrel, D. & Viraraghavan, T. 2008a, 'Arsenic removal from an aqueous solution by modified A. niger biomass: batch kinetic and isotherm studies', *Journal of Hazardous Materials*, vol. 150, no. 3, pp. 818-25.

Pokhrel, D. & Viraraghavan, T. 2008b, 'Arsenic removal from aqueous solution by iron oxide-coated biomass: common ion effects and thermodynamic analysis', *Separation Science and Technology*, vol. 43, no. 13, pp. 3545-62.

Polya, D., Gault, A., Diebe, N., Feldman, P., Rosenboom, J., Gilligan, E., Fredericks, D., Milton, A., Sampson, M. & Rowland, H. 2005, 'Arsenic hazard in shallow Cambodian groundwaters', *Mineralogical Magazine*, vol. 69, no. 5, pp. 807-23.

Postma, D., Larsen, F., Minh Hue, N.T., Duc, M.T., Viet, P.H., Nhan, P.Q. & Jessen, S. 2007, 'Arsenic in groundwater of the Red River floodplain, Vietnam: Controlling

geochemical processes and reactive transport modeling', *Geochimica et Cosmochimica Acta*, vol. 71, no. 21, pp. 5054-71.

Preece, D. 1982, 'Agricultural Experimentation: Design and Analysis', Series Agricultural Experimentation: Design and Analysis JSTOR.

Puttamat, S. & Pavarajarn, V. 2016, 'Adsorption study for removal of Mn (II) ion in aqueous solution by hydrated ferric (III) oxides', *International Journal of Chemical Engineering and Applications*, vol. 7, no. 4, pp. 239-43.

Qiu, Z., Zheng, T., Dai, Q. & Chen, J. 2019, 'Sulfide and arsenic compounds removal from liquid digestate by ferric coagulation and toxicity evaluation', *Water Environment Research*, vol. 91, no. 12, pp. 1613-23.

Rahaman, M., Basu, A. & Islam, M. 2008, 'The removal of As (III) and As (V) from aqueous solutions by waste materials', *Bioresource technology*, vol. 99, no. 8, pp. 2815-23.

Raj, A. & Singh, N. 2015, 'Phytoremediation of arsenic contaminated soil by arsenic accumulators: a three year study', *Bulletin of environmental contamination and toxicology*, vol. 94, no. 3, pp. 308-13.

Ranjan, D., Talat, M. & Hasan, S.H. 2009, 'Biosorption of arsenic from aqueous solution using agricultural residue 'rice polish'', *Journal of Hazardous Materials*, vol. 166, no. 2, pp. 1050-9.

Ren, Z., Zhang, G. & Paul Chen, J. 2011, 'Adsorptive removal of arsenic from water by an iron–zirconium binary oxide adsorbent', *Journal of Colloid and Interface Science*, vol. 358, no. 1, pp. 230-7.

Roy, P., Mondal, N.K., Bhattacharya, S., Das, B. & Das, K. 2013, 'Removal of arsenic (III) and arsenic (V) on chemically modified low-cost adsorbent: batch and column operations', *Applied Water Science*, vol. 3, no. 1, pp. 293-309.

Sarntanayoot, P., Fuangswasdi, S. & Imyim, A. 2019, 'Iron nanoparticle-modified water treatment residues for adsorption of As (III) and As (V) and their cement-based solidification/stabilization', *International Journal of Environmental Science and Technology*, vol. 16, no. 8, pp. 4285-92.

Sekar, A. & Kandasamy, G. 2019, 'Study on Durability Properties of Coconut Shell Concrete with Coconut Fiber', *Buildings*, vol. 9, no. 5, p. 107.

Shahmohammadi-Kalalagh, S. 2011, 'Isotherm and kinetic studies on adsorption of Pb, Zn and Cu by kaolinite', *Caspian Journal of Environmental Sciences*, vol. 9, no. 2, pp. 243-55.

Sharma, V.K., Dutta, P.K. & Ray, A.K. 2007, 'Review of kinetics of chemical and photocatalytical oxidation of arsenic (III) as influenced by pH', *Journal of Environmental Science and Health Part A*, vol. 42, no. 7, pp. 997-1004.

Siddique, T., Dutta, N.K. & Roy Choudhury, N. 2020, 'Nanofiltration for Arsenic Removal: Challenges, Recent Developments, and Perspectives', *Nanomaterials*, vol. 10, no. 7, p. 1323.

Sigrist, M.E., Brusa, L., Beldomenico, H.R., Dosso, L., Tsendra, O.M., González, M.B., Pieck, C.L. & Vera, C.R. 2014, 'Influence of the iron content on the arsenic

adsorption capacity of Fe/GAC adsorbents', *Journal of Environmental Chemical Engineering*, vol. 2, no. 2, pp. 927-34.

Şık, E., Demirbas, E., Goren, A.Y., Oncel, M.S. & Kobya, M. 2017, 'Arsenite and arsenate removals from groundwater by electrocoagulation using iron ball anodes: Influence of operating parameters', *Journal of Water Process Engineering*, vol. 18, pp. 83-91.

Silva Gonzaga, M.I., Santos, J.A.G. & Ma, L.Q. 2006, 'Arsenic chemistry in the rhizosphere of Pteris vittata L. and Nephrolepis exaltata L', *Environmental Pollution*, vol. 143, no. 2, pp. 254-60.

Singh, S.K. 2017, 'Conceptual framework of a cloud-based decision support system for arsenic health risk assessment', *Environment Systems and Decisions*, vol. 37, no. 4, pp. 435-50.

Singh, S.K. & Stern, E.A. 2017, 'Global arsenic contamination: living with the poison nectar', *Environment: Science and Policy for Sustainable Development*, vol. 59, no. 2, pp. 24-8.

Singh, T.S. & Pant, K.K. 2006, 'Solidification/stabilization of arsenic containing solid wastes using portland cement, fly ash and polymeric materials', *Journal of Hazardous Materials*, vol. 131, no. 1, pp. 29-36.

Siqueira, G., Bras, J. & Dufresne, A. 2010, 'Luffa cylindrica as a lignocellulosic source of fiber, microfibrillated cellulose and cellulose nanocrystals', *BioResources*, vol. 5, no. 2, pp. 727-40.

Smedley, P.L. & Kinniburgh, D. 2002a, 'A review of the source, behaviour and distribution of arsenic in natural waters', *Applied geochemistry*, vol. 17, no. 5, pp. 517-68.

Smedley, P.L. & Kinniburgh, D.G. 2002b, 'A review of the source, behaviour and distribution of arsenic in natural waters', *Applied geochemistry*, vol. 17, no. 5, pp. 517-68.

Smith, P.G., Koch, I. & Reimer, K.J. 2008, 'Uptake, transport and transformation of arsenate in radishes (Raphanus sativus)', *Science of the total environment*, vol. 390, no. 1, pp. 188-97.

Sogaard, E. 2014, *Chemistry of advanced environmental purification processes of water: Fundamentals and applications*, Newnes.

Song, P., Yang, Z., Xu, H., Huang, J., Yang, X. & Wang, L. 2014, 'Investigation of Influencing Factors and Mechanism of Antimony and Arsenic Removal by Electrocoagulation Using Fe–Al Electrodes', *Industrial & Engineering Chemistry Research*, vol. 53, no. 33, pp. 12911-9.

Song, P., Yang, Z., Zeng, G., Yang, X., Xu, H., Wang, L., Xu, R., Xiong, W. & Ahmad, K. 2017, 'Electrocoagulation treatment of arsenic in wastewaters: a comprehensive review', *Chemical Engineering Journal*, vol. 317, pp. 707-25.

Sorg, T.J., Chen, A.S. & Wang, L. 2014, 'Arsenic species in drinking water wells in the USA with high arsenic concentrations', *Water Research*, vol. 48, pp. 156-69.

Stella, S.M. & Vijayalakshmi, U. 2019, 'Influence of chemically modified Luffa on the preparation of nanofiber and its biological evaluation for biomedical applications', *Journal of Biomedical Materials Research Part A*, vol. 107, no. 3, pp. 610-20.

Sullivan, C., Tyrer, M., Cheeseman, C.R. & Graham, N.J. 2010, 'Disposal of water treatment wastes containing arsenic—a review', *Science of the Total Environment*, vol. 408, no. 8, pp. 1770-8.

Thakur, L.S. & Mondal, P. 2017, 'Simultaneous arsenic and fluoride removal from synthetic and real groundwater by electrocoagulation process: Parametric and cost evaluation', *Journal of Environmental Management*, vol. 190, pp. 102-12.

Thirunavukkarasu, O., Viraraghavan, T. & Subramanian, K. 2001, 'Removal of arsenic in drinking water by iron oxide-coated sand and ferrihydrite—batch studies', *Water Quality Research Journal*, vol. 36, no. 1, pp. 55-70.

Thirunavukkarasu, O., Viraraghavan, T. & Subramanian, K. 2003, 'Arsenic removal from drinking water using iron oxide-coated sand', *Water, air, and soil pollution*, vol. 142, no. 1-4, pp. 95-111.

Thirunavukkarasu, O.S., Viraraghavan, T., Subramanian, K.S. & Tanjore, S. 2002, 'Organic arsenic removal from drinking water', *Urban Water*, vol. 4, no. 4, pp. 415-21.

Titah, H.S., Halmi, M.I.E.B., Abdullah, S.R.S., Hasan, H.A., Idris, M. & Anuar, N. 2018, 'Statistical optimization of the phytoremediation of arsenic by Ludwigia octovalvis-in a pilot reed bed using response surface methodology (RSM) versus an artificial neural network (ANN)', *International journal of phytoremediation*, vol. 20, no. 7, pp. 721-9.

Tomić, Z.P., Antić-Mladenović, S.B., Babić, B.M., Poharc-Logar, V.A., Đorđević, A.R. & Cupać, S.B. 2011, 'Modification of smectite structure by sulfuric acid and characteristics of the modified smectite', *Journal of Agricultural Sciences*, vol. 56, no. 1, pp. 25-35.

Tuna, A.Ö.A., Özdemir, E., Şimşek, E.B. & Beker, U. 2013, 'Removal of As (V) from aqueous solution by activated carbon-based hybrid adsorbents: Impact of experimental conditions', *Chemical Engineering Journal*, vol. 223, pp. 116-28.

Tuutijärvi, T., Repo, E., Vahala, R., Sillanpää, M. & Chen, G. 2012, 'Effect of competing anions on arsenate adsorption onto maghemite nanoparticles', *Chinese Journal of Chemical Engineering*, vol. 20, no. 3, pp. 505-14.

Ucar, C., Baskan, M.B. & Pala, A. 2013, 'Arsenic removal from drinking water by electrocoagulation using iron electrodes', *Korean Journal of Chemical Engineering*, vol. 30, no. 10, pp. 1889-95.

Vasudevan, S., Lakshmi, J. & Sozhan, G. 2010, 'Studies on the Removal of Arsenate by Electrochemical Coagulation Using Aluminum Alloy Anode', *CLEAN – Soil, Air, Water*, vol. 38, no. 5-6, pp. 506-15.

Velazquez-Jimenez, L.H., Arcibar-Orozco, J.A. & Rangel-Mendez, J.R. 2018, 'Overview of As(V) adsorption on Zr-functionalized activated carbon for aqueous streams remediation', *Journal of Environmental Management*, vol. 212, pp. 121-30.

Velazquez-Jimenez, L.H., Hurt, R.H., Matos, J. & Rangel-Mendez, J.R. 2014, 'Zirconium–Carbon Hybrid Sorbent for Removal of Fluoride from Water: Oxalic Acid Mediated Zr(IV) Assembly and Adsorption Mechanism', *Environmental Science & Technology*, vol. 48, no. 2, pp. 1166-74.

Vitela-Rodriguez, A.V. & Rangel-Mendez, J.R. 2013, 'Arsenic removal by modified activated carbons with iron hydro(oxide) nanoparticles', *Journal of Environmental Management*, vol. 114, pp. 225-31.

Vithanage, M., Dabrowska, B.B., Mukherjee, A.B., Sandhi, A. & Bhattacharya, P. 2012, 'Arsenic uptake by plants and possible phytoremediation applications: a brief overview', *Environmental chemistry letters*, vol. 10, no. 3, pp. 217-24.

Wan, W., Pepping, T.J., Banerji, T., Chaudhari, S. & Giammar, D.E. 2011, 'Effects of water chemistry on arsenic removal from drinking water by electrocoagulation', *Water research*, vol. 45, no. 1, pp. 384-92.

Wang, S., Gao, B., Li, Y., Mosa, A., Zimmerman, A.R., Ma, L.Q., Harris, W.G. & Migliaccio, K.W. 2015, 'Manganese oxide-modified biochars: preparation, characterization, and sorption of arsenate and lead', *Bioresource technology*, vol. 181, pp. 13-7.

Wang, Y., Liu, H., Wang, S., Li, X., Wang, X. & Jia, Y. 2020, 'Simultaneous removal and oxidation of arsenic from water by δ-MnO2 modified activated carbon', *Journal of Environmental Sciences*, vol. 94, pp. 147-60.

Wang, Z., Ma, H., Chu, B. & Hsiao, B.S. 2017, 'Super-hydrophobic modification of porous natural polymer “luffa sponge” for oil absorption', *Polymer*, vol. 126, pp. 470-6.

WHO 2001, 'Arsenic and arsenic compounds. Environmental Health Criteria', *WHO, Geneva*, p. 224.

Worch, E. 2012, *Adsorption technology in water treatment: fundamentals, processes, and modeling*, Walter de Gruyter.

Wu, F.-C., Tseng, R.-L., Huang, S.-C. & Juang, R.-S. 2009, 'Characteristics of pseudo-second-order kinetic model for liquid-phase adsorption: A mini-review', *Chemical Engineering Journal*, vol. 151, no. 1, pp. 1-9.

Xuan, H.N., Van, L.T., Bulgakov, B. & Alexandrova, O. 2019, 'Strength, chloride resistance and corrosion reinforced of High-strength concrete', vol. 1425, IOP Publishing, p. 012193.

Yadav, R.S., Shukla, R.K., Sankhwar, M.L., Patel, D.K., Ansari, R.W., Pant, A.B., Islam, F. & Khanna, V.K. 2010, 'Neuroprotective effect of curcumin in arsenic-induced neurotoxicity in rats', *Neurotoxicology*, vol. 31, no. 5, pp. 533-9.

Yang, C., Ho, Y.-N., Makita, R., Inoue, C. & Chien, M.-F. 2020, 'A multifunctional rhizobacterial strain with wide application in different ferns facilitates arsenic phytoremediation', *Science of The Total Environment*, vol. 712, p. 134504.

Yoon, I.-H., Moon, D.H., Kim, K.-W., Lee, K.-Y., Lee, J.-H. & Kim, M.G. 2010, 'Mechanism for the stabilization/solidification of arsenic-contaminated soils with Portland cement and cement kiln dust', *Journal of Environmental Management*, vol. 91, no. 11, pp. 2322-8.

Zhang, G., Liu, H., Liu, R. & Qu, J. 2009, 'Adsorption behavior and mechanism of arsenate at Fe–Mn binary oxide/water interface', *Journal of Hazardous Materials*, vol. 168, no. 2-3, pp. 820-5.

Zhang, M., Gao, B., Varnoosfaderani, S., Hebard, A., Yao, Y. & Inyang, M. 2013, 'Preparation and characterization of a novel magnetic biochar for arsenic removal', *Bioresource technology*, vol. 130, pp. 457-62.

Zhou, Z., Liu, Y.-g., Liu, S.-b., Liu, H.-y., Zeng, G.-m., Tan, X.-f., Yang, C.-p., Ding, Y., Yan, Z.-l. & Cai, X.-x. 2017, 'Sorption performance and mechanisms of arsenic(V) removal by magnetic gelatin-modified biochar', *Chemical Engineering Journal*, vol. 314, pp. 223-31.

https://www.epa.nsw.gov.au/~/media/EPA/Corporate%20Site/resources/wasteregulation/140796-classify-waste.ashxhttps://www.energyaustralia.com.au/home/electricity-and-gas/plans